

LOCALIZED MODEL REDUCTION FOR PARAMETERIZED PROBLEMS

ANDREAS BUHR, LAURA IAPICHINO, MARIO OHLBERGER, STEPHAN RAVE,
FELIX SCHINDLER, AND KATHRIN SMETANA

ABSTRACT. In this contribution we present a survey of concepts in localized model order reduction methods for parameterized partial differential equations. The key concept of localized model order reduction is to construct local reduced spaces that have only support on part of the domain and compute a global approximation by a suitable coupling of the local spaces. In detail, we show how optimal local approximation spaces can be constructed and approximated by random sampling. An overview of possible conforming and non-conforming couplings of the local spaces is provided and corresponding localized a posteriori error estimates are derived. We introduce concepts of local basis enrichment, which includes a discussion of adaptivity. Implementational aspects of localized model reduction methods are addressed. Finally, we illustrate the presented concepts for multiscale, linear elasticity and fluid-flow problems, providing several numerical experiments.

This work has been accepted as a chapter in P. Benner, S. Grivet-Talocia, A. Quarteroni, G. Rozza, W.H.A. Schilders, L.M. Sileira. Handbook on Model Order Reduction. Walter De Gruyter GmbH, Berlin, 2019+.

1. INTRODUCTION

Projection based model order reduction has become a mature technique for simulations of large classes of parameterized systems; for an introduction, we refer to the text books and survey [BCOW17, HRS16, QN16, BGW15]. However, especially for large-scale and multi-scale problems the “standard” model order reduction approach exhibits several limitations: Curse of parameter dimensionality in the sense that many parameters require prohibitively large reduced spaces, no topological flexibility, and possibly high computational costs and storage requirements in the offline stage for instance due to large computational domains. Localized model order reduction methods, which combine approaches from model order reduction, multiscale methods and/or domain decomposition techniques, overcome or significantly mitigate those limitations. As an further advantage, they allow using reduced spaces of different dimensions in different parts of the computational domain and accommodate (local)

Date: October 29, 2019.

2010 Mathematics Subject Classification. 65Y15, 65N30, 65N55, 65N15, 35J20, 35J25 .

Key words and phrases. localized model reduction, reduced basis method, randomized training, a posteriori error estimation, basis enrichment, online adaptivity, parameterized systems, multi-scale problems.

The authors from Mathematics Münster are funded by the Deutsche Forschungsgemeinschaft (DFG, German Research Foundation) under Germany’s Excellence Strategy – EXC 2044 – 390685587, Mathematics Münster: Dynamics – Geometry - Structure. F. Schindler acknowledges funding by the Deutsche Forschungsgemeinschaft (DFG, German Research Foundation) under contract SCHI 1493/1-1.

changes of the geometry and the partial differential equation (PDE) in the online stage. The key idea of localized model order reduction is to construct local reduced spaces on (unions of) subdomains of the decomposed computational domain and couple the local reduced spaces across interfaces either in a conforming or non-conforming manner. In this chapter we investigate localized model order reduction for linear coercive elliptic parameterized problems; inf-sup stable problems have for instance been considered in [HKP13a] and parabolic and nonlinear problems will be briefly discussed at the end of this chapter.

We discuss both conforming and non-conforming localized approximations. Prominent examples for a conforming localization for non-parametric PDEs are the partition of unity method [BM97], the generalized finite element method (GFEM) [BCO94, BBO04, BM97, BL11] as well as component mode synthesis (CMS) [Hur65, BC68, Bou92], [HL10, JBL11].

A combination of domain decomposition and reduced basis (RB) methods has first been considered in the reduced basis element method (RBEM) [MR02, MR04, LMR06], where the local RB approximations are coupled by Lagrange multipliers in a non-conforming manner. The reduced basis hybrid method [IQR12] extends the RBEM by additionally considering a coarse FE discretization on the whole domain to account for continuity of normal stresses in the context of Stokes equations. Alternatively, a non-conforming coupling can be realized say by penalization as in the local reduced basis discontinuous Galerkin approach [KOH11], the localized reduced basis multiscale method (LRBMS) [AHKO12, OS15, ORS17], the discontinuous Galerkin reduced basis element method [APQ16], or the generalized multiscale discontinuous Galerkin method [CEL17a]. The static condensation reduced basis element (scRBEM) method [HKP13b, HKP13a, EP13, SP16] combines intra-element RB approximations similar to the RBEM with coupling techniques from CMS resulting in a conforming approximation. A similar approach is pursued by the ArbiLoMod [BEOR17] that also allows for arbitrary (non-parametric) local changes of the underlying equations and/or the geometry.

In the context of the proper generalized decomposition (PGD) method (for a review see for instance [CA10, CLC11, CKL14]) a domain decomposition strategy has been proposed in [HNC18] and in [PEV10] hierarchical model reduction [VB81, PEV10, OS14b, SO17] has been combined with an iterative substructuring method.

Concerning the generation of local approximation spaces we focus on empirical training (see for instance [EP13, BL11, SP16]), i.e. local reduced spaces generated from local solutions of the PDE, and adaptive basis enrichment. In detail, we present local approximation spaces that are optimal in the sense of Kolmogorov and can be constructed by solving a local so-called transfer eigenvalue problem on the space of local solutions of the PDE. Optimal local approximation spaces for subdomains have first been proposed in [BL11] and for interfaces and parametrized PDEs in [SP16]. We will also show how those optimal approximation spaces can be approximated by random sampling [BS18].

A localizable a posteriori error estimator is crucial for an adaptive enrichment of the local reduced spaces where the reduced approximation is not accurate enough. Such an adaptive basis enrichment is one way to approach “optimal” computational complexity within outer-loop applications such as optimal control, inverse problems or Monte Carlo methods. With this respect, we will also present a framework

for localized residual based error control [BEOR17, Sme15] as well as localized a posteriori error estimation based on flux reconstruction [ESV10, OS15].

Naturally, the presented methods for localized model reduction share a lot of features with domain decomposition techniques and multiscale methods. We particularly refer to domain decomposition and preconditioning techniques with multiscale coarse spaces such as [AH02, GLS07, GE10] or the more recent contributions [SDH⁺14, GL17, HKKR18]. In the context of the FETI-DP iterative substructuring method we refer to [MS07, KRR16]. For multiscale problems there has been a tremendous development of suitable numerical methods in the last two decades including the multiscale finite element method (MsFEM) [HW97, EHG04, EH09, HOS14], the heterogeneous multiscale method (HMM) [EE03, EE05, Ohl05, Abd05], the variational multiscale method (VMM) [Hug95, HFMQ98, LM05] or the more recent local orthogonal decomposition (LOD) [MP14, HMP14]. Model reduction can be used to accelerate the solution of localized problems which occur in multiscale methods, see e.g. [AB12, Abd15]. Similar to the methods presented in this chapter the generalized multiscale finite element method (GMsFEM) [EGH13, CEL14b, CEL18a] relies on a Galerkin projection on local subspaces, but in contrast uses ideas from multiscale methods to construct the local bases. A connection between multiscale methods and domain decomposition has recently been investigated in [KPY18, KPY17, KY16].

This chapter is organized as follows. In Sec. 2 we introduce the problem setting and basic notation for localized model order reduction of coercive variational problems. Concepts for conforming and non-conforming coupling of approximation spaces are presented in Sec. 3. Sec. 4 deals with the preparation of local approximation spaces. Particularly, the construction of optimal local approximation spaces and their approximation via random sampling is presented and illustrated with numerical experiments for linear elasticity. In Sec. 5 we present two abstract frameworks for localized a posteriori error estimation and give exemplifications for conforming and non-conforming localized model reduction approaches. Localized a posteriori error estimators are the key ingredient for basis enrichment strategies and online adaptivity that are presented in Sec. 6. Computational aspects are discussed in Sec. 7 and numerical experiments for multiscale problems and fluid flow are presented in Sec. 8. We conclude by showing possible extensions to parabolic and nonlinear problems in Sec. 9.

2. PARAMETERIZED PARTIAL DIFFERENTIAL EQUATIONS AND LOCALIZATION

Let $\Omega \subset \mathbb{R}^d$, $d = 1, 2, 3$, be a large, bounded domain with Lipschitz boundary. Let us further introduce a Hilbert space V such that $[H_0^1(\Omega)]^z \subset V \subset [H^1(\Omega)]^z$, $z = 1, \dots, d$ and denote by V' the dual space of V . Moreover, we introduce the compact set of admissible parameters $\mathcal{P} \subset \mathbb{R}^p$, $p \in \mathbb{N}$. We consider the following variational problem.

Definition 2.1 (Parameterized coercive problem in variational form). *For any parameter $\boldsymbol{\mu} \in \mathcal{P}$ find $u(\boldsymbol{\mu}) \in V$, such that*

$$(1) \quad a(u(\boldsymbol{\mu}), v; \boldsymbol{\mu}) = f(v; \boldsymbol{\mu}) \quad \text{for all } v \in V.$$

Here, $f(\cdot; \boldsymbol{\mu}) \in V'$ and $a(\cdot, \cdot; \boldsymbol{\mu}) : V \times V \rightarrow \mathbb{R}$ denote parametric linear and bilinear forms, the latter being continuous and coercive w.r.t. the norm $\|\cdot\|_V$ induced by the inner product $(\cdot, \cdot)_V : V \times V \rightarrow \mathbb{R}$. That is, there exist constants

$0 < \alpha \leq \alpha(\boldsymbol{\mu}) \leq \gamma(\boldsymbol{\mu}) \leq \gamma$, such that for any $\boldsymbol{\mu} \in \mathcal{P}$,

$$\begin{aligned} a(v, w; \boldsymbol{\mu}) &\leq \gamma(\boldsymbol{\mu}) \|v\|_V \|w\|_V && \text{for all } v, w \in V, \\ a(v, v; \boldsymbol{\mu}) &\geq \alpha(\boldsymbol{\mu}) \|v\|_V^2 && \text{for all } v \in V. \end{aligned}$$

Let us denote the energy norm of u for parameter $\boldsymbol{\mu}$ as $\|u\|_{\boldsymbol{\mu}} := a(u, u; \boldsymbol{\mu})^{1/2}$. Problem (1) thus admits a unique solution for all $\boldsymbol{\mu} \in \mathcal{P}$ owing to the Lax-Milgram theorem. Examples for (1) include elliptic multiscale problems, incompressible fluid flow or linear elasticity as detailed in the following. We will consider Neumann boundary conditions on Γ_N and Dirichlet boundary conditions on Γ_D , where Γ_N, Γ_D are non-overlapping and $\Gamma_N \cup \Gamma_D = \partial\Omega$. To simplify notations, homogenous boundary conditions on $\partial\Omega$ will be prescribed in most places.

Example 2.2 (Parametric elliptic multiscale problems). *With $V = H_0^1(\Omega)$, the pressure equation in the context of two-phase flow in porous media (obtained through Darcy's law) reads: given a collection of sources and sinks $q \in L^2(\Omega)$, a parametric and possibly highly heterogeneous permeability field $\kappa : \mathcal{P} \rightarrow L^\infty(\Omega)^{d \times d}$, find for each $\boldsymbol{\mu} \in \mathcal{P}$ the global pressure $u(\boldsymbol{\mu}) \in V$, such that*

$$(2) \quad -\nabla \cdot (\kappa(\boldsymbol{\mu}) \nabla u(\boldsymbol{\mu})) = q \quad \text{in a weak sense in } V'.$$

If the smallest eigenvalue of $\kappa(\boldsymbol{\mu})$ is bounded from below away from zero for all $\boldsymbol{\mu} \in \mathcal{P}$, we can consider this to be an example of Definition 2.1 by setting $a(u, v; \boldsymbol{\mu}) := \int_{\Omega} (\kappa(\boldsymbol{\mu}) \nabla u) \cdot \nabla v \, dx$ and $f(v; \boldsymbol{\mu}) := \int_{\Omega} qv \, dx$. In the context of instationary two-phase flow, (2) needs to be solved in each time step for varying total mobilities (modelled by the parametric nature of κ), while the permeability field κ typically resolves fine geological structures and thus requires a very fine computational grid compared to the size of Ω (see [OS15] and the references therein).

Example 2.3 (Incompressible fluid flow). *The Stokes and Navier-Stokes equations represent a model of the flow motion for a viscous Newtonian incompressible fluid. In the steady case it can be formulated as follows:*

$$(3) \quad \begin{cases} -\nu \Delta \mathbf{y} + \delta(\mathbf{y} \cdot \nabla) \mathbf{y} + \nabla p = \mathbf{f} & \text{in } \Omega \\ \nabla \cdot \mathbf{y} = 0 & \text{in } \Omega \\ \mathbf{y} = \mathbf{g}_D & \text{on } \Gamma_D \\ -p \mathbf{n} + \nu \frac{\partial \mathbf{y}}{\partial \mathbf{n}} = \mathbf{g}_N & \text{on } \Gamma_N, \end{cases}$$

where (\mathbf{y}, p) are the velocity and the pressure fields defined on the computational domain Ω . The first equation expresses the linear momentum conservation, the second one the mass conservation, which is also called the continuity equation. Here \mathbf{f} denotes a forcing term per unit mass, \mathbf{g}_D and \mathbf{g}_N are the functions addressing the Dirichlet and Neumann boundary conditions respectively on Γ_D and Γ_N . The parameter $\nu = \sigma/\rho$ denotes the kinematic viscosity, being ρ the density and σ the viscosity of the fluid. Navier-Stokes equations correspond to the case $\delta = 1$, here we consider only $\delta = 0$, the convective term is neglected, obtaining the steady Stokes equations, which provide a model in the case of slow motion of fluids with very high viscosity.

We denote the functional spaces for velocity and pressure fields by $X = (H_{0, \Gamma_D}^1(\Omega))^d$, $Q = L^2(\Omega)$, respectively, where $H_{0, \Gamma_D}^1(\Omega) = \{y \in H^1(\Omega) : y|_{\Gamma_D} = 0\}$. Moreover, for simplicity, we assume that $\mathbf{g}_D = 0$ (otherwise the lift function is required). The

corresponding weak form of the Stokes equations (3) reads: find $(\mathbf{y}, p) \in X \times Q$ such that

$$\begin{aligned} \nu \int_{\Omega} \nabla \mathbf{y} : \nabla \mathbf{w} \, d\Omega - \int_{\Omega} p \nabla \cdot \mathbf{w} \, d\Omega &= \int_{\Omega} \mathbf{f} \cdot \mathbf{w} \, d\Omega + \int_{\Gamma_N} \mathbf{g}_N \cdot \mathbf{w} \, d\Gamma, \quad \forall \mathbf{w} \in X \\ \int_{\Omega} q \nabla \cdot \mathbf{y} \, d\Omega &= 0, \quad \forall q \in Q. \end{aligned}$$

In a parameterized setting, the input-parameter vector $\boldsymbol{\mu}$ may characterize either the geometrical configuration or physical properties, boundary data and sources of the problem.

Denoting by V the product space given by $V = X \times Q$, defining by $u(\boldsymbol{\mu}) = (\mathbf{y}(\boldsymbol{\mu}), p(\boldsymbol{\mu})) \in V$ and $v = (\mathbf{w}, q)$, the parametrized abstract formulation (2.3) can be rewritten in the following form: find $u(\boldsymbol{\mu}) = (\mathbf{y}(\boldsymbol{\mu}), p(\boldsymbol{\mu})) \in V$ s.t.

$$(4) \quad a(u(\boldsymbol{\mu}), v; \boldsymbol{\mu}) = f(v; \boldsymbol{\mu}), \quad \forall v \in V$$

where

$$(5) \quad a(u, v; \boldsymbol{\mu}) = \nu \int_{\Omega} \nabla \mathbf{y} : \nabla \mathbf{w} \, d\Omega - \int_{\Omega} p \nabla \cdot \mathbf{w} \, d\Omega - \int_{\Omega} q \nabla \cdot \mathbf{y} \, d\Omega,$$

$$(6) \quad f(v; \boldsymbol{\mu}) = \int_{\Omega} \mathbf{f} \cdot \mathbf{w} \, d\Omega + \int_{\Gamma_N} \mathbf{g}_N \cdot \mathbf{w} \, d\Gamma.$$

Example 2.4 (Linear elasticity). We assume that $\Omega \subset \mathbb{R}^3$ represents an isotropic homogeneous material and we consider the following linear elastic boundary value problem: Find the displacement vector $u(\boldsymbol{\mu})$ and the Cauchy stress tensor $\boldsymbol{\sigma}(u(\boldsymbol{\mu}))$ such that

$$(7) \quad \begin{aligned} -\nabla \cdot \boldsymbol{\sigma}(u(\boldsymbol{\mu})) &= \mathbf{G}(\boldsymbol{\mu}) && \text{in } \Omega, \\ \boldsymbol{\sigma}(u(\boldsymbol{\mu})) \cdot \mathbf{n} &= 0 && \text{on } \Gamma_N, \\ u(\boldsymbol{\mu}) &= \mathbf{g}_D && \text{on } \Gamma_D, \end{aligned}$$

where the body force $\mathbf{G} : \mathcal{P} \rightarrow \mathbb{R}^3$ accounts for gravity. We can express for a linear elastic material the Cauchy stress tensor as $\boldsymbol{\sigma}(u(\boldsymbol{\mu})) = E(\boldsymbol{\mu}) \mathbf{C} : \boldsymbol{\varepsilon}(u(\boldsymbol{\mu}))$, where \mathbf{C} is the fourth-order stiffness tensor, $\boldsymbol{\varepsilon}(u(\boldsymbol{\mu})) = 0.5(\nabla u(\boldsymbol{\mu}) + (\nabla u(\boldsymbol{\mu}))^T)$ is the infinitesimal strain tensor, and the colon operator $:$ is defined as $\mathbf{C} : \boldsymbol{\varepsilon}(u(\boldsymbol{\mu})) = \sum_{k,l=1}^3 \mathbf{C}_{ijkl} \varepsilon_{kl}(u(\boldsymbol{\mu}))$. Moreover, $E : \mathcal{P} \rightarrow L^\infty(\Omega)$ denotes Young's modulus, which is assumed to be piecewise constant on Ω and satisfy $E(\boldsymbol{\mu}) \geq E_0 > 0$ for a constant $E_0 \in \mathbb{R}^+$. Therefore, the stiffness tensor can be written as

$$\mathbf{C}_{ijkl} = \frac{\nu}{(1+\nu)(1-2\nu)} \delta_{ij} \delta_{kl} + \frac{1}{2(1+\nu)} (\delta_{ik} \delta_{jl} + \delta_{il} \delta_{jk}), \quad 1 \leq i, j, k, l \leq 3,$$

where δ_{ij} denotes the Kronecker delta; we choose Poisson's ratio $\nu = 0.3$. The corresponding variational formulation of (7) then reads as follows: For any $\boldsymbol{\mu} \in \mathcal{P}$ find $u(\boldsymbol{\mu}) \in V = \{\mathbf{v} \in [H^1(\Omega)]^3 : \mathbf{v} = 0 \text{ on } \Gamma_D\}$ such that

$$(8) \quad a(u(\boldsymbol{\mu}), \mathbf{v}; \boldsymbol{\mu}) = f(\mathbf{v}; \boldsymbol{\mu}) \quad \forall \mathbf{v} \in V.$$

Here, the bilinear and linear forms $a(\cdot, \cdot; \boldsymbol{\mu}) : [H^1(\Omega)]^3 \times [H^1(\Omega)]^3 \rightarrow \mathbb{R}$ and $f(\cdot; \boldsymbol{\mu}) : [H^1(\Omega)]^3 \rightarrow \mathbb{R}$ are defined as

$$a(w, v; \boldsymbol{\mu}) := \int_{\Omega} E(\boldsymbol{\mu}) \frac{\partial w^i}{\partial x_j} \mathbf{C}_{ijkl} \frac{\partial v^k}{\partial x_l} \, d\Omega \quad \text{and} \quad f(\mathbf{v}; \boldsymbol{\mu}) := \int_{\Omega} \mathbf{G}(\boldsymbol{\mu}) \cdot \mathbf{v} - a(\widehat{\mathbf{G}}(\boldsymbol{\mu}), \mathbf{v}; \boldsymbol{\mu}),$$

where $\widehat{\mathbf{G}}(\boldsymbol{\mu}) \in [H^1(\Omega)]^3$ denotes a suitable lifting function of the possibly non-homogeneous Dirichlet boundary conditions.

To obtain approximate solutions of (1) we presume we have an appropriate grid-based numerical method at hand (the full order model, FOM), yielding a high (but finite) dimensional approximation space V_h . We consider conforming continuous Galerkin finite elements (FE), where $V_h \subset V$, and nonconforming discontinuous Galerkin (DG) or finite volume (FV) schemes, where $V_h \not\subset V$ (in which case we require broken Sobolev spaces for our analysis, see Section 3.2.2). As a starting point for localized model reduction we require the FOM space to be decomposable into “local” spaces, which we will make more precise shortly. While a localizing space decomposition could in general stem from any clustering of the degrees of freedom (DoF) of V_h (see for instance [Car15]), we are particularly interested in local approximation spaces which are associated with a domain decomposition of the physical domain.

Definition 2.5 (Non overlapping domain decomposition). *We call a finite collection of $M \in \mathbb{N}$ open polygonal subdomains $\mathcal{T}_H := \{\Omega_1, \Omega_2, \dots, \Omega_M\}$ a non overlapping domain decomposition of the physical domain Ω , if $\bigcup_{m=1}^M \overline{\Omega}_m = \overline{\Omega}$ and $\Omega_m \cap \Omega_{m'} = \emptyset$ for $1 \leq m, m' \leq M$, $m \neq m'$. We collect in \mathcal{T}_H^v , \mathcal{T}_H^e and \mathcal{T}_H^γ , the set of all vertices, edges and facets (which we will denote interfaces from now on)¹, respectively, associated with the partition \mathcal{T}_H and define $H := \max_{m=1}^M \text{diam } \Omega_m$. Moreover, we denote by $\Gamma := \left(\bigcup_{m=1}^M \partial\Omega_m\right) \setminus \partial\Omega$ the whole interface of the decomposition \mathcal{T}_H . Note that $\mathcal{T}_H^e = \emptyset$ for $d = 2$ and $\mathcal{T}_H^e = \mathcal{T}_H^\gamma = \emptyset$ for $d = 1$. Each of the sets \mathcal{T}_H , \mathcal{T}_H^v , \mathcal{T}_H^e and \mathcal{T}_H^γ can be decomposed into elements associated with the domain boundary and inner elements, and we collect the latter in $\overset{\circ}{\mathcal{T}}_H$, $\overset{\circ}{\mathcal{T}}_H^v$, $\overset{\circ}{\mathcal{T}}_H^e$ and $\overset{\circ}{\mathcal{T}}_H^\gamma$, respectively. For instance, for each two adjacent subdomains $\Omega_m, \Omega_{m'} \in \mathcal{T}_H$, there exists a shared interface $\Gamma_{m,m'} \in \overset{\circ}{\mathcal{T}}_H^\gamma$, while for all boundary subdomains $\Omega_m \in \mathcal{T}_H$ there exists at least one boundary interface $\Gamma_{m,\partial\Omega} \in \overset{\circ}{\mathcal{T}}_H^\gamma \setminus \overset{\circ}{\mathcal{T}}_H^\gamma$.*

We can thus think of the domain decomposition as a usual grid, but without the requirements of \mathcal{T}_H to actually resolve any data functions of the PDE. Given such a domain decomposition, we can abstractly define a localizing space decomposition.

Definition 2.6 (Localizing space decomposition). *Let the FOM space V_h be a finite dimensional Hilbert space with inner product and induced norm $\|\cdot\|_{V_h}^2 = (\cdot, \cdot)_{V_h}$. We call the direct sum decomposition of V_h into subdomain spaces, interface spaces, edge spaces and vertex spaces,*

$$(9) \quad V_h = \bigoplus_{m=1}^M V_h^m \oplus \bigoplus_{\gamma \in \mathcal{T}_H^\gamma} V_h^\gamma \oplus \bigoplus_{e \in \mathcal{T}_H^e} V_h^e \oplus \bigoplus_{v \in \mathcal{T}_H^v} V_h^v,$$

a localizing space decomposition.

Note that such a decomposition is not unique and can always be found. Since the reduced space shall inherit this localizing decomposition, its purpose will be threefold: (i) offline, it allows for an independent and localized generation of the local reduced approximation spaces (compare Section 4), (ii) it allows to define

¹Note that to simplify notation we denote both the upper bound of the continuity constant and the local interfaces with γ , expecting that the respective meaning will be clear from the context.

and alter the physical domain Ω online, given that local approximation spaces for certain reference subdomains have been prepared offline, and (iii) it allows to adapt a local approximation space online (by adding basis functions or changing the local grid), while only requiring an update of local and neighboring prepared quantities (compare Section 6). For actual examples of space decompositions we refer to Section 3.

Abstractly, we do not impose any further assumptions on the FOM as well as the reduced order model (ROM). However, given the (bi-)linearity of a and f , the computational benefits of the localizing space decomposition are apparent (and are made more precise throughout the rest of this chapter). Since we allow for non conforming approximations, in general we need to consider discrete counterparts of a and f which are only defined on the FOM space V_h and not necessarily on V , where we again refer to the following sections for examples.

Definition 2.7 (Locally decomposed full order model (FOM)). *Let V_h be locally decomposable as in definition (9), and let $a_h(\cdot, \cdot; \boldsymbol{\mu}) : V_h \times V_h \rightarrow \mathbb{R}$ and $f_h(\cdot; \boldsymbol{\mu}) \in V_h'$ denote discrete variants of a and f , respectively, which are continuous and coercive w.r.t. the inner product of V_h . For each $\boldsymbol{\mu} \in \mathcal{P}$, find $u_h(\boldsymbol{\mu}) \in V_h$ such that*

$$(10) \quad a_h(u_h(\boldsymbol{\mu}), v_h; \boldsymbol{\mu}) = f_h(v_h; \boldsymbol{\mu}) \quad \text{for all } v_h \in V_h.$$

The idea of projection-based localized model order reduction is to consider a local reduced approximation space for each element of the localizing space decomposition (9), in order to obtain a similarly decomposed reduced space $V_N \subset V_h$:

$$(11) \quad V_N = \bigoplus_{m=1}^M V_N^m \oplus \bigoplus_{\gamma \in \mathcal{T}_H^\gamma} V_N^\gamma \oplus \bigoplus_{e \in \mathcal{T}_H^e} V_N^e \oplus \bigoplus_{v \in \mathcal{T}_H^v} V_N^v,$$

with reduced subdomain spaces $V_N^m \subset V_h^m$, reduced interface spaces $V_N^\gamma \subset V_h^\gamma$, reduced edge spaces $V_N^e \subset V_h^e$ and reduced vertex spaces $V_N^v \subset V_h^v$. Similar to standard projection based model order reduction, we obtain the ROM simply by Galerkin projection of the locally decomposed FOM (10) onto this locally decomposed reduced space.

Definition 2.8 (Locally decomposed reduced order model (ROM)). *Given a locally decomposed reduced space as in (11), for each $\boldsymbol{\mu} \in \mathcal{P}$, find $u_N(\boldsymbol{\mu}) \in V_N$ such that*

$$(12) \quad a_h(u_N(\boldsymbol{\mu}), v_N; \boldsymbol{\mu}) = f_h(v_N; \boldsymbol{\mu}) \quad \text{for all } v_N \in V_N.$$

The main questions remain: (i) how to choose good local reduced approximation spaces to guarantee accurate and at the same time efficient reduced order approximations, (ii) how to benefit from the localization of V_N , that is how to obtain an offline/online decomposed scheme and in particular how to couple these local reduced approximation spaces, and (iii) how to adaptively enrich these local reduced approximation spaces online, if required. These topics will be answered throughout the remainder of this chapter, starting with examples of how to obtain localized FOMs from standard discretization schemes and how to couple the resulting local reduced spaces.

Therefore, we introduce local grids $\tau_h(\Omega_m)$ on each subdomain $\Omega_m \subset \mathcal{T}_H$, which we presume to resolve all data functions of the underlying PDE. As an analytical tool, we also define the global fine grid by $\tau_h = \cup_{\Omega_m \in \mathcal{T}_H} \tau_h(\Omega_m)$, which is usually not required in practical computations. For simplicity, we require the local grids

of two subdomains $\Omega_m, \Omega'_m \in \mathcal{T}_H$ to match along the shared interface $\gamma_{m,m'} \in \mathring{\mathcal{T}}_H^\gamma$ and denote by $\tau_h^\gamma(\gamma_{m,m'})$ the corresponding set of all facets of τ_h which lie on $\gamma_{m,m'}$. Finally, we require that Γ does not cut any grid cells.

3. COUPLING LOCAL APPROXIMATION SPACES

3.1. Conforming approach. There are various ways to couple local reduced spaces such that we obtain a conforming approximation, such as the partition of unity method [BM97] or the generalized finite element method (GFEM) [BCO94, BBO04, BM97, BL11]. However, in this section we focus on the decomposition into interface spaces and intra-element spaces, where the coupling is performed via the coupling or interface modes spanning the interface space.

3.1.1. The multidomain problem and the Steklov-Poincaré interface equation. First, we introduce local Hilbert spaces $H_0^1(\Omega_m) \subset V^m \subset H^1(\Omega_m)$, $m = 1, \dots, M$, which are supposed to respect the boundary conditions on $\partial\Omega$, the local spaces $V_0^m := \{v \in V^m : v|_{\partial\Omega_m \setminus \partial\Omega} = 0\}$, and the trace space Λ associated with Γ . Moreover, we introduce local parameter-dependent bilinear and linear forms $a_m(\cdot, \cdot; \boldsymbol{\mu}) : V^m \times V^m \rightarrow \mathbb{R}$ and $f_m(\cdot; \boldsymbol{\mu}) \in V^{m'}$, $\boldsymbol{\mu} \in \mathcal{P}$, $m = 1, \dots, M$, and the inner product $(\cdot, \cdot)_{V^m} : V^m \times V^m \rightarrow \mathbb{R}$. We may then state the variational form (1) equivalently as follows (see for instance [QV05]): For any $\boldsymbol{\mu} \in \mathcal{P}$ find $u_m(\boldsymbol{\mu}) \in V^m$, $m = 1, \dots, M$ such that

$$(13a) \quad a_m(u_m(\boldsymbol{\mu}), v; \boldsymbol{\mu}) = f_m(v; \boldsymbol{\mu}) \quad \forall v \in V_0^m,$$

$$(13b) \quad u_m(\boldsymbol{\mu}) = u_{m'}(\boldsymbol{\mu}) \quad \text{on } \Gamma_{m,m'},$$

$$(13c) \quad \sum_{m=1}^M a_m(u_m(\boldsymbol{\mu}), \mathcal{E}_m \zeta; \boldsymbol{\mu}) = \sum_{m=1}^M f_m(\mathcal{E}_m \zeta; \boldsymbol{\mu}) \quad \forall \zeta \in \Lambda,$$

where $\mathcal{E}_m : \Lambda \rightarrow V^m$, $m = 1, \dots, M$ are linear and continuous extension operators.

The formulation (13) can then be used to derive an equation that solely acts on functions on the interface but nevertheless uniquely defines the solution $u(\boldsymbol{\mu})$ of (1). To that end, we introduce a parameter-dependent lifting operator $\mathcal{E}_{\Gamma \rightarrow \Omega}(\boldsymbol{\mu}) : \Lambda \rightarrow V$, where $\mathcal{E}_{\Gamma \rightarrow \Omega}(\boldsymbol{\mu})\zeta$ is defined as the minimizer of $\inf_{v(\boldsymbol{\mu}) \in V} a(v(\boldsymbol{\mu}), v(\boldsymbol{\mu}); \boldsymbol{\mu})$ subject to $v(\boldsymbol{\mu})|_\Gamma = \zeta$. Note that we then also have

$$(14) \quad a_m(\mathcal{E}_{\Gamma \rightarrow \Omega}(\boldsymbol{\mu})\zeta, v; \boldsymbol{\mu}) = 0 \quad \forall v \in V_0^m \quad \text{and} \quad \mathcal{E}(\boldsymbol{\mu})_{\Gamma \rightarrow \Omega} \zeta = \zeta \quad \text{on } \Gamma \cap \partial\Omega_m.$$

Then, we can rewrite the solution $u(\boldsymbol{\mu})$ as

$$(15) \quad u(\boldsymbol{\mu}) = \mathcal{E}_{\Gamma \rightarrow \Omega}(\boldsymbol{\mu})(u(\boldsymbol{\mu})|_\Gamma) + \sum_{m=1}^M u_m^f(\boldsymbol{\mu}),$$

where $u_m^f(\boldsymbol{\mu}) \in V_0^m$ solves

$$(16) \quad a_m(u_m^f(\boldsymbol{\mu}), v; \boldsymbol{\mu}) = f_m(v; \boldsymbol{\mu}) \quad \forall v \in V_0^m, \quad m = 1, \dots, M.$$

Inserting (15) into (13c) and choosing $\mathcal{E}_m = \mathcal{E}_{\Gamma \rightarrow \Omega_m}(\boldsymbol{\mu})$ yields the Steklov-Poincaré interface equation: Find $u(\boldsymbol{\mu})|_{\Gamma} \in \Lambda$ such that

$$(17) \quad \begin{aligned} & \sum_{m=1}^M a_m(\mathcal{E}_{\Gamma \rightarrow \Omega_m}(\boldsymbol{\mu})(u(\boldsymbol{\mu})|_{\Gamma}), \mathcal{E}_{\Gamma \rightarrow \Omega_m}(\boldsymbol{\mu})\zeta; \boldsymbol{\mu}) \\ &= \sum_{m=1}^M [f_m(\mathcal{E}_{\Gamma \rightarrow \Omega_m}(\boldsymbol{\mu})\zeta; \boldsymbol{\mu}) - a_m(u_m^f(\boldsymbol{\mu}), \mathcal{E}_{\Gamma \rightarrow \Omega_m}(\boldsymbol{\mu})\zeta; \boldsymbol{\mu})] \quad \forall \zeta \in \Lambda. \end{aligned}$$

Let us notice that the Steklov-Poincaré interface equation and its discrete, algebraic analogon, the Schur complement system, are at the base of iterative substructuring methods (see [QV05, TW05]), which have been combined with the reduced basis method in [MH14].

We may finally define a space associated with the interface V^{Γ} as $V^{\Gamma} = \{\mathcal{E}_{\Gamma \rightarrow \Omega}(\boldsymbol{\mu})\zeta \in V : \zeta \in \Lambda\}$ and obtain the decomposition $V = \left(\bigoplus_{m=1}^M V_0^m\right) \oplus V^{\Gamma}$. This decomposition is a -orthogonal thanks to (14).

While the computation of the (harmonic) lifting operators is inherently local (see (14)), the Steklov-Poincaré interface equation is posed on the whole interface Γ . To localize the latter we decompose V^{Γ} as we will describe next.

3.1.2. A conforming, localized reduced order approximation. First, we determine basis functions associated with the vertices $v \in \mathcal{T}_H^v$. One common approach [HL10, JBL11, BEOR17] is to require that a basis function $\psi^v \in V_h \cap [H_0^1(\bigcup_{v \subset \Omega_m} \bar{\Omega}_m)]^z$, $z = 1, \dots, d$ associated with some vertex v of the coarse mesh \mathcal{T}_H satisfies for all Ω_m , $m = 1, \dots, M$:

$$(18) \quad (\psi^v, w)_{V^m} = 0 \quad \forall w \in V_{h;0}^m \quad \text{and} \quad \psi^v(\mathbf{x}^v) = 1, \quad \psi^v(\mathbf{x}^{v'}) = 0, \quad v \neq v'.$$

Here, \mathbf{x}^v are the (global) coordinates of the vertex v and $V_{h;0}^m := \{v \in V_h^m : v = 0 \text{ on } \partial\Omega_m \setminus \Gamma_N\}$. To uniquely define ψ^v we need to prescribe the respective values on Γ . We may for instance require ψ^v to be linear on the respective edges or bilinear on the respective interfaces (see e. g. [BEOR17]). For multiscale problems in two space dimensions with a permeability $\kappa(\mathbf{x}_1, \mathbf{x}_2; \bar{\boldsymbol{\mu}})$ it has been suggested in [HW97] to prescribe

$$(19) \quad \psi^v(\mathbf{x}_1, \mathbf{x}_2^v) := \left(\int_{\mathbf{x}_1^{v'}}^{\mathbf{x}_1} \frac{ds}{\kappa(s, \mathbf{x}_2^v; \bar{\boldsymbol{\mu}})} \right) / \left(\int_{\mathbf{x}_1^{v'}}^{\mathbf{x}_1^v} \frac{ds}{\kappa(s, \mathbf{x}_2^v; \bar{\boldsymbol{\mu}})} \right)$$

on a horizontal edge $[\mathbf{x}_1^{v'}, \mathbf{x}_1^v] \times \{\mathbf{x}_2^v\}$ in a uniform rectangular coarse grid \mathcal{T}_H .

Next, we assume that we have given sets of discrete edge basis functions $\{\chi_k^e\}_{k=1}^{N_{h;0}^e} \in V_h|_e$ and discrete interface basis functions $\{\chi_k^\gamma\}_{k=1}^{N_{h;0}^\gamma} \in V_h|_\gamma$ defined on the respective edge $e \in \mathcal{T}_H^e$ or interface $\gamma \in \mathcal{T}_H^\gamma$. Here, we set $N_{h;0}^e := \dim(V_h|_{e \setminus \partial e})$ and $N_{h;0}^\gamma := \dim(V_h|_{\gamma \setminus \partial \gamma})$ as we require that χ_k^e and χ_k^γ are zero on the boundary of the edge and interface, respectively. Furthermore, we define $\Lambda_{N_{h;0}^e}^e := \text{span}\{\chi_1^e, \dots, \chi_{N_{h;0}^e}^e\}$ and $\Lambda_{N_{h;0}^\gamma}^\gamma := \text{span}\{\chi_1^\gamma, \dots, \chi_{N_{h;0}^\gamma}^\gamma\}$.

Similarly as for the vertices we may then define associated basis functions that have support on the union of subdomains that share the respective edge or interface:

Find $\psi_k^\gamma \in V_h \cap [H_0^1(\bigcup_{\gamma \in \overline{\Omega}_m} \overline{\Omega}_m)]^z$, $z = 1, \dots, d$, $\gamma \in \mathcal{T}_H^\gamma$, $k = 1, \dots, N_{h;0}^\gamma$ such that

$$(20) \quad (\psi_k^\gamma, w)_{V^m} = 0 \quad \forall w \in V_{h;0}^m \quad \text{and} \quad \psi_k^\gamma|_\gamma = \chi_k^\gamma.$$

Likewise, we find $\psi_k^e \in V_h \cap [H_0^1(\bigcup_{e \in \overline{\Omega}_m} \overline{\Omega}_m)]^z$, $z = 1, \dots, d$, $e \in \mathcal{T}_H^e$, $k = 1, \dots, N_{h;0}^e$ such that

$$(21) \quad (\psi_k^e, w)_{V^m} = 0 \quad \forall w \in V_{h;0}^m \quad \text{and} \quad \psi_k^e|_e = \chi_k^e.$$

Again, we need to provide the value of ψ_k^e on the interfaces sharing the edge $e \in \mathcal{T}_H^e$ in order to uniquely define ψ_k^e . Similarly to above we may require that ψ_k^e is linear on the respective interfaces as suggested for instance in [BEOR17] or define a function which takes into account also the coefficient function.

Note that if the interfaces are mutually disjoint, which is for instance the case if we associate the subdomains Ω_m , $m = 1, \dots, M$ with the components of a structure, only the basis functions ψ_k^γ , $k = 1, \dots, N_{h;0}^\gamma$ ($d = 3$) or ψ_k^e , $k = 1, \dots, N_{h;0}^e$ ($d = 2$) are needed. Here, the values of the basis functions on the boundary of the interfaces or edges are determined by the boundary conditions on $\partial\Omega$ (see for instance [HKP13b, HKP13a, EP13, SP16]).

For $N^\gamma \ll N_{h;0}^\gamma$ and $N^e \ll N_{h;0}^e$ may now define the reduced space associated with Γ as follows:

$$(22) \quad V_N^\Gamma := \bigoplus_{v \in \mathcal{T}_H^v} \text{span}\{\psi^v\} \oplus \bigoplus_{e \in \mathcal{T}_H^e} \text{span}\{\psi_1^e, \dots, \psi_{N^e}^e\} \oplus \bigoplus_{\gamma \in \mathcal{T}_H^\gamma} \text{span}\{\psi_1^\gamma, \dots, \psi_{N^\gamma}^\gamma\}.$$

Such reduced interface spaces are for instance employed in (adaptive) component mode synthesis (CMS) [HL10, JBL11], the static condensation reduced basis element (scrBE) method [HKP13b, HKP13a, EP13, SP16] for mutually disjoint interfaces, or in the ArbiLoMod [BEOR17]. Subspaces of V_Γ^N are considered in certain multiscale methods. For example in the MsFEM of Hou and Wu [HW97] the reduced space is spanned by the basis functions ψ^v , $v \in \mathcal{T}_H^v$. For further relations between CMS, MsFEM and GFEM we refer e.g. to [HL10].

Recall that the basis functions associated with the vertices, edges, and interfaces have all been computed w.r.t. an inner product that does not depend on the parameter (see (18), (20), (21)). Therefore, we finally assume that we have also given reduced spaces $V_{N;0}^m := \text{span}\{\zeta_1^m, \dots, \zeta_{N^m}^m\} \subset V_{h;0}^m$, $m = 1, \dots, M$, that will account for parameter variations. In detail, we obtain approximations $\tilde{\psi}_k^*(\boldsymbol{\mu})$, $*$ = v, e, γ by solving

$$(23) \quad \text{find } \tilde{b}_k^*(\boldsymbol{\mu}) \in V_{N;0}^m : \quad a_m(\psi_k^* + \tilde{b}_k^*(\boldsymbol{\mu}), w; \boldsymbol{\mu}) = 0 \quad \forall w \in V_{N;0}^m$$

and setting $\tilde{\psi}_k^*(\boldsymbol{\mu}) = \psi_k^* + \tilde{b}_k^*(\boldsymbol{\mu})$, $*$ = v, e, f . Finally, we define $\tilde{b}^m(\boldsymbol{\mu}) \in V_{N;0}^m$ as the solution of

$$(24) \quad \text{find } \tilde{b}^m(\boldsymbol{\mu}) \in V_{N;0}^m : \quad a_m(\tilde{b}^m(\boldsymbol{\mu}), w; \boldsymbol{\mu}) = f(w, \boldsymbol{\mu}) \quad \forall w \in V_{N;0}^m.$$

Note, that both $\tilde{b}_k^*(\boldsymbol{\mu})$, $*$ = v, e, γ and $\tilde{b}^m(\boldsymbol{\mu})$ can be interpreted as intra-element RB approximations. The corresponding reduced spaces $V_{N;0}^m$, $m = 1, \dots, M$ can for instance be constructed from solutions $b_k^*(\boldsymbol{\mu}), b^m(\boldsymbol{\mu}) \in V_{h;0}^m$, $*$ = v, e, f of

$$(25) \quad a_m(\psi_k^* + b_k^*(\boldsymbol{\mu}), w; \boldsymbol{\mu}) = 0 \quad \forall w \in V_{h;0}^m$$

and

$$(26) \quad a_m(b^m(\boldsymbol{\mu}), w; \boldsymbol{\mu}) = f(w, \boldsymbol{\mu}) \quad \forall w \in V_{h,0}^m,$$

respectively, via a standard greedy algorithm or a POD.² Let us also remark that for instance in the scRBE method for the approximation of each basis function ψ_k^* , $*$ = v, e, γ a different RB space is considered, to further reduce the size of problems (23), (24). Finally, we define the reduced spaces

$$(27) \quad V_N = \bigoplus_{m=1}^M V_{N;0}^m \oplus V_N^\Gamma$$

and

$$(28) \quad V_N^\Gamma(\boldsymbol{\mu}) := \bigoplus_{v \in \mathcal{T}_H^v} \text{span}\{\tilde{\psi}^v(\boldsymbol{\mu})\} \oplus \bigoplus_{e \in \mathcal{T}_H^e} \text{span}\{\tilde{\psi}_1^e(\boldsymbol{\mu}), \dots, \tilde{\psi}_{N^e}^e(\boldsymbol{\mu})\} \\ \oplus \bigoplus_{\gamma \in \mathcal{T}_H^\gamma} \text{span}\{\tilde{\psi}_1^\gamma(\boldsymbol{\mu}), \dots, \tilde{\psi}_{N^\gamma}^\gamma(\boldsymbol{\mu})\}.$$

The global reduced approximation $u_N(\boldsymbol{\mu})$ can then be computed by performing a Galerkin projection onto the reduced space $V_N^\Gamma(\boldsymbol{\mu})$ or a Petrov-Galerkin approximation using $V_N^\Gamma(\boldsymbol{\mu})$ as a trial and V_N^Γ as a test space (see e.g. [EP14, Sme15]). Instead of eliminating the volume degrees of freedom via (23), (24), $u_N(\boldsymbol{\mu})$ can also directly be determined by performing a Galerkin projection onto V_N (see for instance [BEOR17]). Similarly, for CMS and a fixed parameter a Galerkin projection onto V_N may be performed to compute the reduced solution; here, the reduced space $V_{N;0}^m$ is constructed from an eigenvalue problem and does not account for parameter variations (see e.g. [HL10]). Finally, in the reduced basis—domain decomposition—finite element (RDF) method [IQR16] the reduced space V_N is chosen as a direct sum of $\bigoplus_{m=1}^M V_{N;0}^m$ and standard FE spaces defined on the interface or on a (small) area around the interface. Here, the intra-element reduced spaces $V_{N;0}^m$ are constructed via a greedy algorithm considering a parametrized linear combination of standard Lagrange basis functions or Fourier modes as boundary conditions. Then, a Galerkin projection on V_N is performed to compute $u_N(\boldsymbol{\mu})$.

3.2. Non-conforming approach. With the term *non-conforming approach* we want to classify a set of alternative techniques to solve the reduced problem on the global computational domain. A first approach consists in considering a global system of equations given by local parametrized problems and additional equations ensuring the matching between the different subdomains through the use of Lagrange multipliers. This approach has been used for solving elliptic equation in [MR02, MR04] and Stokes equations in [LMR06, IQR12].

Another approach consists in coupling local FOM spaces by interior penalty bilinear forms, inspired by discontinuous Galerkin FEM. Here, we refer to the discontinuous Galerkin reduced basis element method [CHM11, APQ16, PGQ16] and the local reduced basis discontinuous Galerkin approach [KOH11]. A discontinuous Galerkin approach with local POD modes has been presented in [FIL18]. In the context of multiscale problems (cf. Example 2.2), the generalized multiscale discontinuous Galerkin method has been proposed in [CEL17a, CEL18b] and used

²Note that in actual practice one would construct the reduced bases only on a certain number $< M$ of reference domains; see for instance [HKP13b].

for solving the heat problem with phase change in [SVV18]. In this chapter we are going to present the localized reduced basis method (LRBMS) in Subsection 3.2.2 below. LRBMS has been introduced in [AHKO12] and analyzed in [OS14a, OS15] for elliptic and in [ORS17] for parabolic problems. Applications to the simulation of two phase flow in porous media have been addressed in [KFH⁺15] and to battery simulation with resolved electrodes in [OR17].

3.2.1. Non-conforming coupling based on Lagrange multipliers. We want to reformulate the problem (13), with the idea that exact coincidence of the traces of the discrete functions (equation (13b)) is generally too stringent, and may, in fact, lead to imposing $u_m = 0$ on the internal interfaces; thus, the gluing process can be done in a dual way through Lagrange multipliers. We assume that local basis functions are computed in each subdomain $\Omega_m, m = 1, \dots, M$ by solving local parametrized variational problems coming from the original problem (1) with proper boundary conditions along the boundaries which correspond to internal ones in the original domain. The choice of the boundary conditions is strongly related to the problem aimed to be solved. Thus, local reduced spaces are defined via these local solutions and denoted by $V_N^m, m = 1, \dots, M$. Possible ways to construct V_N^m are presented in section 4. If two or more subdomains are characterized by the same type of parameter and the same type of boundary conditions, the same local reduced space can be associated to those subdomains. For simplicity we consider different spaces for each different subdomain.

We define the following operator:

$$(29) \quad \mathcal{L}^{m,m'}(u(\boldsymbol{\mu}), \psi) = \int_{\Gamma_{m,m'}} (u(\boldsymbol{\mu})|_{\Omega_m} - u(\boldsymbol{\mu})|_{\Omega_{m'}})\psi ds = 0, \quad \forall \psi \in W_{m,m'},$$

where $m, m' \in \{1, \dots, M\}$, $\Gamma_{m,m'}$ is the interface between two adjacent sub-domains denoted with the indices m and m' respectively, and $W_{m,m'}$ is the Lagrange multiplier space defined on this interface. Typical choices for the latter are low-order polynomial spaces [MR02, IQR12] or spaces constructed from snapshots (and their derivatives) [MR04].

A basis for $W_{m,m'}$ can then for instance be provided by the characteristic Lagrange polynomials $\psi_q, q = 1, \dots, Q_{m,m'}$ associated with the $Q_{m,m'}$ nodes of $\Gamma_{m,m'}$. If we suppose that Ω has $M - 1$ internal interfaces, $\Gamma_{m,m+1}, m = 1, \dots, M - 1$, the reduced global problem of this approach reads: find $u_N(\boldsymbol{\mu}) \in V_N^1 \times \dots \times V_N^M, \lambda_N \in W_{m,m+1}, m = 1, \dots, M - 1$, such that

$$(30) \quad \begin{cases} a(u_N(\boldsymbol{\mu}), v_N, \boldsymbol{\mu}) + \sum_{i=1}^{M-1} \mathcal{L}^{m,m+1}(v_N, \lambda_N) = f(w, \boldsymbol{\mu}) \forall v_N \in V_N^1 \times \dots \times V_N^M, \\ \mathcal{L}^{m,m+1}(u_N(\boldsymbol{\mu}), \psi) = 0 & m = 1, \dots, M - 1, \forall \psi \in W_{m,m+1}. \end{cases}$$

3.2.2. Non-conforming coupling based on interior penalties. We demonstrate how to obtain a localized FOM by applying ideas from interior penalty (IP) DG schemes w.r.t. the domain decomposition \mathcal{T}_H in the context of the parametric multiscale Example 2.2. To define the localized FOM, we presume we are given a discretization on the full global grid τ_h (which is not used in actual computations), which we make precise by specifying the approximation space with an associated inner product and discrete variants of a and f . As a common ground for the analysis of conforming as well as non conforming schemes, we introduce the broken Sobolev space $H^s(\tau_h(\omega)) :=$

$\{v \in L^2(\omega) \mid v|_t \in H^s(t) \ \forall t \in \tau_h(\omega)\}$, for a given grid $\tau_h(\omega)$ of some domain $\omega \subseteq \Omega$ and $s \geq 1$, and associated broken gradient operator $\nabla_h : H^1(\tau_h(\omega)) \rightarrow L^2(\omega)^d$ by $(\nabla_h v)|_t := \nabla(v|_t)$ on all $t \in \tau_h$ for $v \in H^1(\tau_h(\omega))$.

Example 3.1 (Continuous Galerkin (CG) FEM). *The CG FEM scheme for the conforming approximation of Example 2.2 w.r.t. the full global grid τ_h is given by the conforming approximation space of order $k \geq 1$,*

$$V_h^{CG}(\tau_h) := \{v \in V \mid v|_t \in \mathbb{P}_k(t) \ \forall t \in \tau_h\} \subset V \subset H^1(\tau_h),$$

where $\mathbb{P}_k(\omega)$ for any $\omega \subset \Omega$ denotes the space of all polynomials defined on ω of degree at most $k \geq 0$; the bilinear form $(\cdot, \cdot)^{CG} : H^1(\tau_h) \times H^1(\tau_h) \rightarrow \mathbb{R}$, given by $(u, v)^{CG} := \int_{\Omega} \nabla_h u \cdot \nabla_h v \, dx$, as the inner product on $V_h^{CG}(\tau_h)$ (where we note that its restriction to $V \subset H^1(\tau_h)$ coincides with the V -inner product); and the discrete bilinear form $a_h^{CG}(\cdot, \cdot; \boldsymbol{\mu}) : H^1(\tau_h) \times H^1(\tau_h) \rightarrow \mathbb{R}$ and linear functional $f_h^{CG} : H^1(\tau_h) \rightarrow \mathbb{R}$, given by

$$a_h^{CG}(u, v; \boldsymbol{\mu}) := \int_{\Omega} (\kappa(\boldsymbol{\mu}) \nabla_h u) \cdot \nabla_h v \, dx \quad \text{and} \quad f_h^{CG}(v) := \int_{\Omega} qv \, dx$$

(again noting that their respective restriction to V coincide with a and f).

The definition of the non conforming scheme is more involved. We denote the set of faces of τ_h by τ_h^γ and to each face $\sigma \in \tau_h^\gamma$, we assign a unique normal $n_\sigma \in \mathbb{R}^d$ pointing away from t^+ , where the face may be either an inner face $\sigma \in \tau_h^\gamma$, given by the intersection of two grid elements $t^+, t^- \in \tau_h$, $\sigma = t^+ \cap t^-$, or a boundary face $\sigma \in \tau_h^\gamma$, given by $\sigma = t^+ \cap \partial\Omega$ for some $t^+ \in \tau_h$. Since functions in the broken Sobolev space are two-valued on grid faces, we introduce the mean $\langle \cdot \rangle$ and jump $[\cdot]$ on a boundary face by $\langle v \rangle := [v] := v|_{t^+}$ and by $\langle v \rangle := \frac{1}{2}(v|_{t^+} + v|_{t^-})$ and $[v] := v|_{t^+} - v|_{t^-}$, respectively, on any other face.

Considering the family of interior penalty discontinuous Galerkin (DG) schemes, we present the symmetric variant for ease of notation, and refer to the symmetric weighted variant [ESZ09], which is particularly well suited for multi-scale problems with highly varying or high-contrast coefficients.

Example 3.2 (Interior penalty (IP) discontinuous Galerkin (DG) FEM). *The symmetric IPDG FEM scheme for the non conforming approximation of Example 2.2 w.r.t. the full global grid τ_h is given by the non conforming approximation space of order $k \geq 1$,*

$$V_h^{DG}(\tau_h) := \{v \in L^2(\Omega) \mid v|_t \in \mathbb{P}_k(t) \ \forall t \in \tau_h\} \subset H^1(\tau_h);$$

the bilinear form $(\cdot, \cdot)^{DG} : H^1(\tau_h) \times H^1(\tau_h) \rightarrow \mathbb{R}$, given by

$$(u, v)^{DG} := (u, v)^{CG} + \sum_{\sigma \in \tau_h^\gamma} (u, v)_\sigma^p \quad \text{with} \quad (u, v)_\sigma^p := \int_{\sigma} h_\sigma^{-1} [u][v] \, ds,$$

as inner product on $V_h^{DG}(\tau_h)$, where h_σ is a positive number associated with each face $\sigma \in \tau_h^\gamma$, e.g., $h_\sigma := \text{diam}(\sigma)$ for $d \geq 2$ and $h_\sigma := \min\{\text{diam}(t^+), \text{diam}(t^-)\}$ for $d = 1$; and the linear functional $f_h^{DG} : H^1(\tau_h) \rightarrow \mathbb{R}$ given by $f_h^{DG}(v) := f_h^{CG}(v)$ and the discrete bilinear form $a_h^{DG}(\cdot, \cdot; \boldsymbol{\mu}) : H^2(\tau_h) \times H^2(\tau_h) \rightarrow \mathbb{R}$, given by

$$a_h^{DG}(u, v; \boldsymbol{\mu}) := a_h^{CG}(u, v; \boldsymbol{\mu}) + \sum_{\sigma \in \tau_h^\gamma} a_\sigma(u, v; \boldsymbol{\mu})$$

with the face bilinear form a_σ for any $\sigma \in \tau_h^\gamma$ given by

$$a_\sigma(v, u; \boldsymbol{\mu}) := a_\sigma^c(v, u; \boldsymbol{\mu}) + a_\sigma^c(u, v; \boldsymbol{\mu}) + (u, v)_\sigma^p w_\sigma$$

with $a_\sigma^c(u, v; \boldsymbol{\mu}) := \int_\sigma -\langle (\kappa(\boldsymbol{\mu})\nabla_h v) \cdot n_\sigma \rangle [u] \, ds$ and a user-dependent penalty weight $w_\sigma > 0$, such that a_h^{DG} is continuous and coercive w.r.t. the above inner product.

The main idea of an *IP localized FOM* is to consider the restriction of either of the above discretization schemes to each subdomain of the domain decomposition, and to again couple those with IP techniques along the interfaces of the subdomain. We thus choose $* \in \{\text{CG}, \text{DG}\}$ and obtain the localized FOM space in the sense of Definition 2.6 as a direct sum of subdomain spaces (with empty interface, edge and vertex spaces)

$$V_h := \bigoplus_{m=1}^M V_h^m, \quad \text{with} \quad V_h^m := \{v|_{\Omega_m} \mid v \in V^*\},$$

with associated inner product $(\cdot, \cdot)_{V_h} : V_h \times V_h \rightarrow \mathbb{R}$ given by

$$(u, v)_{V_h} := \sum_{m=1}^M (u|_{\Omega_m}, v|_{\Omega_m})^* + \sum_{\Gamma' \in \mathcal{T}_H^\gamma} \sum_{\sigma \in \tau_h^\gamma(\Gamma')} (u, v)_\sigma^p.$$

We also define the linear functional $f_h : V_h \rightarrow \mathbb{R}$ by $f_h := f_h^*$ and, in a similar manner as above, the non conforming bilinear form $a_h(\cdot, \cdot; \boldsymbol{\mu}) : V_h \times V_h \rightarrow \mathbb{R}$ by

$$a_h(u, v; \boldsymbol{\mu}) := \sum_{m=1}^M a_h^*(u|_{\Omega_m}, v|_{\Omega_m}; \boldsymbol{\mu}) + \sum_{\Gamma' \in \mathcal{T}_H^\gamma} \sum_{\sigma \in \tau_h^\gamma(\Gamma')} a_\sigma(u, v; \boldsymbol{\mu}).$$

We have thus fully specified a localized FOM in the sense of Definition 2.7 and comment on two special cases: for $* = \text{CG}$ and a trivial domain decomposition of a single subdomain, $\mathcal{T}_H = \{\Omega\}$, we obtain the above standard CG FEM while for $* = \text{DG}$ the resulting FOM coincides with the above standard symmetric IPDG FEM.

To make the coupling more precise, we may rearrange the above terms to obtain a localization of a_h w.r.t. the domain decomposition in the sense of

$$a_h(u, v; \boldsymbol{\mu}) = \sum_{m=1}^M a_h^m(u, v; \boldsymbol{\mu}) + \sum_{\Gamma' \in \mathcal{T}_H^\gamma} a_h^{\Gamma'}(u, v; \boldsymbol{\mu}),$$

with the subdomain and interface bilinear forms

$$\begin{aligned} a_h^m(u, v; \boldsymbol{\mu}) &:= a_h^*(u|_{\Omega_m}, v|_{\Omega_m}; \boldsymbol{\mu}) + \sum_{\Gamma' \in \mathcal{T}_H^\gamma \cap \Omega_m} \sum_{\sigma \in \tau_h^\gamma(\Gamma')} a_\sigma(u|_{\Omega_m}, v|_{\Omega_m}; \boldsymbol{\mu}), \\ a_h^{\Gamma'}(u, v; \boldsymbol{\mu}) &:= \sum_{\sigma \in \tau_h^\gamma(\Gamma')} \{a_\sigma(u|_{\Omega^+}, v|_{\Omega^-}; \boldsymbol{\mu}) + a_\sigma(u|_{\Omega^-}, v|_{\Omega^+}; \boldsymbol{\mu})\}, \end{aligned}$$

respectively, for all $1 \leq m \leq M$ and all $\Gamma' \in \mathcal{T}_H^\gamma$, with the subdomains $\Omega^+, \Omega^- \in \mathcal{T}_H$ sharing the interface Γ' .

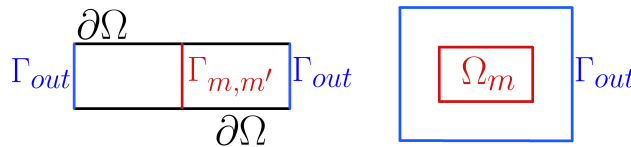


FIGURE 1. Illustration of possible decompositions of Ω_{out} with respect to $\Gamma_{m,m'}$ or Ω_m .

Now given a local reduced space $V_N^m \subset V_h^m$ for each subdomain we obtain the locally decomposed broken reduced space in the sense of (11) by

$$V_N = \bigoplus_{m=1}^M V_N^m \subset V_h.$$

Using the above decomposition of a_h into subdomain and interface contributions, we can readily observe that the locally decomposed ROM can be offline/online decomposed by local computations: namely by projection of the subdomain bilinear forms $a_h^m(\cdot, \cdot; \boldsymbol{\mu})$ onto $V_N^m \times V_N^m$ and the interface bilinear forms $a_h^{\Gamma'}(\cdot, \cdot; \boldsymbol{\mu})$ onto $V_N^m \times V_N^n$, with $1 \leq m, n \leq M$, such that $\Omega^+ = \Omega_m$ and $\Omega^- = \Omega_n$, respectively.

We thus obtain a sparse matrix representation of the resulting reduced system, with a sparsity pattern which coincides with the one from standard IPDG schemes.

4. PREPARATION OF LOCAL APPROXIMATION SPACES

Both, couplings that yield a conforming and non-conforming approximation require either reduced spaces $\Lambda_{N\gamma}^\gamma \subset V_h|_\gamma$ for interfaces and/or edges $\Lambda_{Ne}^\epsilon \subset V_h|_e$ (see subsection 3.1) or reduced spaces V_N^m (see subsection 3.2) or both. As the generation of edge basis functions can be done analogously to the construction of interface basis functions we restrict ourselves to the latter in order to simplify notation. To fix the setting we thus consider the task of finding a suitable reduced space either on a subdomain $\Omega_m \subsetneq \Omega_{out} \subset \Omega$ with $\text{dist}(\Gamma_{out}, \partial\Omega_m) \geq \rho > 0$, $\Gamma_{out} := \partial\Omega_{out} \setminus \partial\Omega$ or an interface $\Gamma_{m,m'} \subset \partial\Omega_m$, where $\text{dist}(\Gamma_{out}, \Gamma_{m,m'}) \geq \rho > 0$. Possible geometric configurations of the oversampling domain Ω_{out} are illustrated in Fig. 1.

We will first briefly discuss in subsection 4.1 reduced spaces that are spanned by *polynomials or solutions of “standard” eigenvalue problems* and are thus related to the spectral element method or hp-FEM. Subsequently, in subsection 4.2 we will present reduced spaces that are generated from local solutions of the PDE, are thus of *empirical* nature, and are optimal in the sense of Kolmogorov. We will also show how those optimal basis functions can be efficiently and accurately approximated by means of random sampling.

4.1. Polynomial-based local approximation spaces. Component mode synthesis (CMS) as introduced in [Hur65, BC68] relies on free vibration modes or eigenmodes of local, constrained eigenvalue problems [Hur65, BC68, Bou92, HL10, JBL11, HK14] for the approximation within subdomains. To couple the modes at the interfaces a reduced interface space spanned by eigenmodes is employed [Hur65, BC68, Bou92, HL10, JBL11, HK14].

A combination of domain decomposition and RB methods has first been considered in the reduced basis element method (RBEM) [MR02]. Here, inspired by the mortar spectral element method [BMP94], the Lagrange multiplier space $W_{m,m'}$ as

defined in Subsection 3.2 is chosen as a low-order polynomial space. The reduced basis hybrid method [IQR12] extends the RBEM by additionally considering a coarse FE discretization on the whole domain to account for continuity of normal stresses and also employs a low-order polynomial Lagrange multiplier space on the interface. For the scRBE method a reduced interface space spanned by the eigenvectors of a discrete generalized eigenvalue problem based on the Laplacian has been suggested in [HKP13b, HKP13a] and eigenmodes of a singular Sturm–Liouville eigenproblem have been used in [EP13]. Finally, in the RDF method [IQR16] a standard FE space is considered on the interface or on a (small) area around the interface.

4.2. Local approximation spaces based on empirical training. In this subsection we are concerned with local approximation spaces that are constructed from local solutions of the PDE; those approaches are often called *empirical*. Basis functions on the interfaces selected from local snapshots are for instance suggested in [EP13], where an empirical pairwise training procedure for interface reduction within the scRBE context is developed, and within a heterogeneous domain decomposition method in [MRH15]. Local approximation spaces that are optimal in the sense of Kolmogorov have been introduced for subdomains within the GFEM in [BL11] for parameter-independent PDEs and for interfaces within static condensation procedures [SP16] for parametrized PDEs. While the authors of [SP16] introduce and analyze a spectral greedy algorithm to deal with parameter variations, [TP18] suggests using a POD making use of the hierarchical approximate POD [HLR18]. Those optimal local spaces both allow for a rigorous *a priori* theory and yield a rapidly (and often exponentially) convergent approximation; in certain cases the superalgebraic convergence can be proved [BL11]. Recently, in [TP18, Tad16] the results in [BL11, BHL14, SP16] have been generalized from linear differential operators whose associated bilinear form is coercive to elliptic, inf-sup stable ones. In [BS18] it has been shown that those optimal local approximation spaces can be efficiently approximated by transferring methods from randomized numerical linear algebra [HMT11]; the local approximation approximation spaces in [BS18] are constructed from local solutions of the PDE with random boundary conditions. Local reduced spaces generated from random snapshots have also been suggested in [BEOR17, EP13] and methods from randomized linear algebra have been exploited in the FETI-2 λ domain decomposition method in [WV15] and in [CEGL16] for the generalized multiscale finite element method.

We will first present the optimal local approximation spaces as introduced in [BL11, SP16] for a fixed parameter $\mathcal{P} = \{\bar{\mu}\}$, subsequently discuss their approximation via random sampling, and conclude this subsection with the discussion of the general case $\mathcal{P} \neq \{\bar{\mu}\}$. To simplify notation we will omit $\bar{\mu}$ as long as it is fixed.

4.2.1. Optimal local approximation spaces for $\mathcal{P} = \{\bar{\mu}\}$. To enable maximum flexibility regarding the shape of Ω on the user’s side, we assume that we do not have any a priori knowledge of the shape of Ω when constructing the reduced order model. We thus know that the global solution u satisfies the considered PDE locally on Ω_{out} but suppose that the trace of u on $\partial\Omega_{out}$ is *unknown* to us. Therefore, we aim at approximating all local solutions u_{loc} of

$$(31) \quad a_{loc}(u_{loc}, v) = f_{loc}(v) \quad \forall v \in V_{loc},$$

with *arbitrary Dirichlet boundary conditions on Γ_{out}* . Here, the Hilbert space V_{loc} is defined such that $[H_0^1(\Omega_{out})]^z \subset V_{loc} \subset [H^1(\Omega_{out})]^z$, $z = 1, \dots, d$, respecting the

boundary conditions on $\partial\Omega$, and $a_{loc} : [H^1(\Omega_{out})]^z \times [H^1(\Omega_{out})]^z \rightarrow \mathbb{R}$, $f_{loc} : V_{loc} \rightarrow \mathbb{R}$ are local bilinear and linear forms. We will first restrict ourselves to the case $f_{loc} = 0$, $g_D = 0$, and $\partial\Omega_m \cap \Gamma_D = \emptyset$; the general case will be dealt with at the end of this subsection. We may then define the space of all local solutions of the PDE as

$$(32) \quad \mathcal{H} := \{w \in [H^1(\Omega_{out})]^z : w \text{ solves (31), } w = 0 \text{ on } \Gamma_D \cap \partial\Omega_{out}\}, \quad z = 1, \dots, d.$$

As suggested in [BL11, SP16] we introduce a transfer operator $\mathcal{T} : \mathcal{S} \rightarrow \mathcal{R}$ for Hilbert spaces \mathcal{S} and \mathcal{R} , where $\mathcal{S} = \{w|_{\Gamma_{out}} : w \in \mathcal{H}\}$. We define \mathcal{T} for interfaces or subdomains, respectively, for $w \in \mathcal{H}$ as

$$(33) \quad \mathcal{T}(w|_{\Gamma_{out}}) = (w - P_{\Omega_{out}}(w))|_{\Gamma_{m,m'}} \quad \text{or} \quad \mathcal{T}(w|_{\Gamma_{out}}) = (w - P_{\Omega_m}(w))|_{\Omega_m}$$

and set $\mathcal{R} = \{v|_{\Gamma_{m,m'}} : v = w - P_{\Omega_{out}}(w), w \in \mathcal{H}\}$ or $\mathcal{R} = \{(w - P_{\Omega_m}w)|_{\Omega_m} : w \in \mathcal{H}\}$. Here, P_D , $D \subset \Omega_{out}$, denotes an orthogonal projection onto the kernel of the bilinear form; for further details see [BS18, SP16]. In the case of heat conduction we would for instance subtract the mean value of the respective function on D . Note that subtracting this projection is necessary to prove compactness of the transfer operator \mathcal{T} . The key argument to show compactness of \mathcal{T} is Caccioppoli's inequality, which estimates the energy norm of a function in \mathcal{H} on Ω_m in terms of the L^2 -norm on Ω_{out} of the respective function. Using the Hilbert-Schmidt theorem and Theorem 2.2 in [Pin85, Chapter 4] it can then be shown that certain eigenfunctions of $\mathcal{T}^*\mathcal{T}$ span the optimal local approximation space, where $\mathcal{T}^* : \mathcal{R} \rightarrow \mathcal{S}$ denotes the adjoint operator of \mathcal{T} . As we aim at approximating \mathcal{H} and thus a whole set of functions, the concept of optimality of Kolmogorov [Kol36] is used: A subspace $\mathcal{R}_n \subset \mathcal{R}$ of dimension at most n for which holds

$$d_n(\mathcal{T}(\mathcal{S}); \mathcal{R}) = \sup_{\psi \in \mathcal{S}} \inf_{\zeta \in \mathcal{R}_n} \frac{\|\mathcal{T}\psi - \zeta\|_{\mathcal{R}}}{\|\psi\|_{\mathcal{S}}}$$

is called an optimal subspace for $d_n(\mathcal{T}(\mathcal{S}); \mathcal{R})$, where the Kolmogorov n -width $d_n(\mathcal{T}(\mathcal{S}); \mathcal{R})$ is defined as

$$d_n(\mathcal{T}(\mathcal{S}); \mathcal{R}) := \inf_{\substack{\mathcal{R}_n \subset \mathcal{R} \\ \dim(\mathcal{R}_n) = n}} \sup_{\psi \in \mathcal{S}} \inf_{\zeta \in \mathcal{R}_n} \frac{\|\mathcal{T}\psi - \zeta\|_{\mathcal{R}}}{\|\psi\|_{\mathcal{S}}}.$$

We summarize the findings about the optimal local approximation spaces in the following theorem.

Theorem 4.1 (Optimal local approximation spaces [BL11, SP16]). *The optimal approximation space for $d_n(\mathcal{T}(\mathcal{S}); \mathcal{R})$ is given by*

$$(34) \quad \mathcal{R}_n := \text{span}\{\chi_1^{sp}, \dots, \chi_n^{sp}\}, \quad \text{where } \chi_j^{sp} = \mathcal{T}\phi_j, \quad j = 1, \dots, n,$$

and λ_j are the largest n eigenvalues and ϕ_j the corresponding eigenfunctions that satisfy the transfer eigenvalue problem: Find $(\phi_j, \lambda_j) \in (\mathcal{S}, \mathbb{R}^+)$ such that

$$(35) \quad (\mathcal{T}\phi_j, \mathcal{T}w)_{\mathcal{R}} = \lambda_j(\phi_j, w)_{\mathcal{S}} \quad \forall w \in \mathcal{S}.$$

Moreover, we have:

$$(36) \quad d_n(\mathcal{T}(\mathcal{S}); \mathcal{R}) = \sup_{\xi \in \mathcal{S}} \inf_{\zeta \in \mathcal{R}_n} \frac{\|\mathcal{T}\xi - \zeta\|_{\mathcal{R}}}{\|\xi\|_{\mathcal{S}}} = \sqrt{\lambda_{n+1}}.$$

Remark 4.2. We emphasize that the optimal space \mathcal{R}_n is optimal in the sense of Kolmogorov for the approximation of the range of \mathcal{T} and not necessarily for the approximation of $u(\boldsymbol{\mu})$. Moreover, we remark that χ_i^{sp} are the left singular vectors and $\sqrt{\lambda_i}$ the singular values of \mathcal{T} .

Next, for $f_{loc} \neq 0$ but still $g_D = 0$ we solve the problem: Find $u_{loc}^f \in V_{loc}$ such that $a_{loc}(u_{loc}^f, v) = f_{loc}(v)$ for all $v \in V_{loc}$ and augment the space \mathcal{R}_n either with $u_{loc}^f|_{\Omega_m}$ or $u_{loc}^f|_{\Gamma_{m,m'}}$. To take non-homogeneous Dirichlet boundary conditions into account one can proceed for instance with a standard lifting approach, adjusting f_{loc} accordingly. Note that for homogeneous boundary conditions we proceed very similar to above, prescribing “arbitrary” boundary conditions on Γ_{out} and homogeneous boundary conditions on $\partial\Omega \cap \partial\Omega_{out}$. The optimal local approximation space for subdomains are then defined as

$$(37) \quad \mathcal{R}_n^+ := \text{span}\{\chi_1^{sp}, \dots, \chi_n^{sp}, u_{loc}^f|_{\Omega_m}\} \oplus \ker(a_m(\cdot, v))$$

and similarly for interfaces as

$$(38) \quad \mathcal{R}_n^+ := \text{span}\{\chi_1^{sp}, \dots, \chi_n^{sp}, u_{loc}^f|_{\Gamma_{m,m'}}\} \oplus \ker(a_m(\cdot, v))|_{\Gamma_{m,m'}},$$

respectively. Here, $\ker(a_m(\cdot, v))$ denotes the kernel of the mapping $a_m(\cdot, v) : [H^1(\Omega_m)]^z \rightarrow \mathbb{R}$, $z = 1, \dots, d$, $v \in V_0^m$ for the bilinear form a_m defined in subsection 3.1. In case $\partial\Omega_m \cap \Gamma_D \neq \emptyset$ all modifications in this subsection involving the kernel of the bilinear form are waived.

The result in (36) can be exploited to derive an *a priori* error bound for the approximation error between the solution $u(\bar{\boldsymbol{\mu}})$ of (1) still for a fixed reference parameter $\bar{\boldsymbol{\mu}}$ and the optimal static condensation approximation $u^n(\bar{\boldsymbol{\mu}})$ as stated in the following proposition:

Proposition 4.3 (*A priori error bound [SP16]*). Assume that the interfaces $\gamma \in \mathcal{T}_H^\gamma$ are mutually disjoint, that all interfaces have the same geometry, and that each Ω_m , $m = 1, \dots, M$ has exactly two interfaces. Let $u(\bar{\boldsymbol{\mu}})$ be the (exact) solution of (1) for a fixed parameter $\bar{\boldsymbol{\mu}}$. Moreover, let $u_{n+}(\bar{\boldsymbol{\mu}})$ be the static condensation approximation defined in subsection 3.1, where we employ the optimal interface space \mathcal{R}_n^+ for each $\gamma \in \mathcal{T}_H^\gamma$ and assume that the error due to the intra-element RB approximation is zero. Then, we have the following *a priori* error bound:

$$(39) \quad \frac{\|u(\bar{\boldsymbol{\mu}}) - u_{n+}(\bar{\boldsymbol{\mu}})\|_{\bar{\boldsymbol{\mu}}}}{\|u(\bar{\boldsymbol{\mu}})\|_{\bar{\boldsymbol{\mu}}}} \leq \#\gamma \max_{\gamma \in \mathcal{T}_H^\gamma} \left(C_\gamma \sqrt{\lambda_{n+1}^\gamma} \right),$$

where $\#\gamma$ denotes the number of interfaces in \mathcal{T}_H^γ and λ_{n+1}^γ is the $n+1$ -th eigenvalue of (35) for the interface $\gamma \in \mathcal{T}_H^\gamma$. The constant C_γ depends only on the subdomains that share the interface γ and neither on Ω nor on $u(\bar{\boldsymbol{\mu}})$.

To define reduced interface spaces $\Lambda_{N_\gamma}^\gamma$, $\gamma \in \mathcal{T}_H^\gamma$ and reduced spaces V_N^m , $m = 1, \dots, M$ we approximate (35) with finite elements. To that end, we introduce a conforming FE space $V_{h;loc} \subset V_{loc}$, the FE source space $S := \{v|_{\Gamma_{out}} : v \in V_h\}$ of dimension N_S , and the FE range space $R := \{(v - P_{\Omega_{out}}(v))|_{\Gamma_{m,m'}} : v \in V_h\}$ or $R := \{(v - P_{\Omega_m})|_{\Omega_m} : v \in V_h\}$ with $\dim(R) = N_R$. We may then define the discrete transfer operator $T : S \rightarrow R$ for $w \in \mathcal{H}_h = \{w \in V_h|_{\Omega_{out}} : a_{loc}(w, \varphi) = 0 \forall \varphi \in V_{h;loc}, w = 0 \text{ on } \Gamma_D \cap \partial\Omega_{out}\}$ as

$$(40) \quad T(w|_{\Gamma_{out}}) = (w - P_{\Omega_{out}}(w))|_{\Gamma_{m,m'}} \text{ or } T(w|_{\Gamma_{out}}) = (w - P_{\Omega_m}(w))|_{\Omega_m}.$$

In order to define a matrix form of the transfer operator we introduce DOF mappings $\mathbb{B}_{S \rightarrow V_h|_{\Omega_{out}}} \in \mathbb{R}^{\dim(V_h|_{\Omega_{out}}) \times N_S}$ and $\mathbb{B}_{V_h|_{\Omega_{out}} \rightarrow R} \in \mathbb{R}^{N_R \times \dim(V_h|_{\Omega_{out}})}$ that map the DOFs of S to the DOFs of $V_h|_{\Omega_{out}}$ and the DOFs of $V_h|_{\Omega_{out}}$ to the DOFs of R , respectively. Moreover, we introduce the stiffness matrix \mathbb{A}_{loc} obtained from the FE discretization of (31), where we assume that in the rows associated with the Dirichlet DOFs the non-diagonal entries are zero and the diagonal entries equal one. By denoting by ζ the FE coefficients of $\zeta \in S$ and by defining \mathbb{P}_D as the matrix of the orthogonal projection on the kernel of the bilinear form on $D \subset \Omega_{out}$, we obtain the following matrix representation $\mathbb{T} \in \mathbb{R}^{N_R \times N_S}$ of the transfer operator for subdomains

$$(41) \quad \mathbb{T} \zeta = (1 - \mathbb{P}_{\Omega_m}) \mathbb{B}_{V_h|_{\Omega_{out}} \rightarrow R} \mathbb{A}^{-1} \mathbb{B}_{S \rightarrow V_h|_{\Omega_{out}}} \zeta$$

and interfaces

$$(42) \quad \mathbb{T} \zeta = \mathbb{B}_{V_h|_{\Omega_{out}} \rightarrow R} (1 - \mathbb{P}_{\Omega_{out}}) \mathbb{A}^{-1} \mathbb{B}_{S \rightarrow V_h|_{\Omega_{out}}} \zeta.$$

Finally, we denote by \mathbb{M}_S the inner product matrix of S and by \mathbb{M}_R the inner product matrix of R . Then, the FE approximation of the transfer eigenvalue problem reads as follows: Find the eigenvectors $\zeta_j \in \mathbb{R}^{N_S}$ and the eigenvalues $\lambda_j \in \mathbb{R}_0^+$ such that

$$(43) \quad \mathbb{T}^t \mathbb{M}_R \mathbb{T} \zeta_j = \lambda_j \mathbb{M}_S \zeta_j.$$

The coefficients of the FE approximation of the basis functions $\{\chi_{h,1}^{sp}, \dots, \chi_{h,n}^{sp}\}$ of the discrete optimal local approximation space

$$(44) \quad R_n := \text{span}\{\chi_{h,1}^{sp}, \dots, \chi_{h,n}^{sp}\}$$

are then given by $\chi_{h,j}^{sp} = \mathbb{T} \zeta_j$, $j = 1, \dots, n$. Adding the representation of the right-hand side, the boundary conditions, and a basis of the kernel of the bilinear form yields the optimal spaces $\Lambda_{N\gamma}^\gamma$ and V_N^m .

Note that in actual practice we would not assemble the matrix \mathbb{T} . Instead one may solve the PDE locally N_S times prescribing the basis functions of S as Dirichlet boundary conditions on Γ_{out} and subsequently assemble and solve the transfer eigenvalue problem. Alternatively, one may pass \mathbb{T} implicitly to the Lanczos method. For instance, the implicitly restarted Lanczos method as implemented in ARPACK [LSY98] requires $\mathcal{O}(n)$ local solutions of the PDE in each iteration and applications of the adjoint T^* . In the next subsection we will show how methods from randomized linear algebra [HMT11, DM16, Mah11, MD09] can be used to compute an approximation of the optimal local approximation spaces. However, beforehand, we conclude this subsection with some numerical experiments on the transfer eigenvalues and thus via Proposition 4.3 on the convergence behavior of the relative approximation error.

To this end, we present the simplified model for a ship stiffener from [SP16]: We consider $\bar{\Omega}_{out} = \Omega_1 \cup \Omega_2$ and $\Gamma_{m,m'} = \Gamma_{1,2} = \bar{\Omega}_1 \cap \Omega_2$, where Ω_2 is depicted in Fig. 2, Ω_1 is just a shifted version of Ω_2 , and the part of Γ_{out} in Ω_2 is indicated in yellow in Fig. 2. We allow $E(\boldsymbol{\mu})$ to vary in the red areas of the subdomains between 1 and 20 and prescribe $E(\boldsymbol{\mu}) \equiv 1$ in the gray areas; we choose $\mathbf{G}(\boldsymbol{\mu}) = (0, 0, 0)^T$.

In detail, we consider $\Omega_1 = (-0.7, 0.7) \times (-0.05, 0.05) \times (-0.6, 0.6)$, $\Omega_2 = (0.7, 2.1) \times (-0.05, 0.05) \times (-0.6, 0.6)$ and $\Gamma_{out} = \{-0.7\} \times (-0.05, 0.05) \times (-0.6, 0.6) \cup \{2.1\} \times (-0.05, 0.05) \times (-0.6, 0.6)$. We employ a conforming linear FE space associated with the mesh depicted in Fig. 2, resulting in $N = 13125$ degrees of freedom per subdomain and an FE interface space of dimension $N_\Gamma = 375$. Finally, we equip

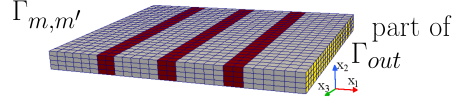


FIGURE 2. Mesh in the subdomain Ω_2 for the ship stiffener. The part of Γ_{out} in Ω_2 is indicated in yellow and on the opposite we have the interface $\Gamma_{m,m'}$. In the red shaded areas Young’s modulus may be varied between 1 and 20 and in the gray areas we consider $E(\boldsymbol{\mu}) \equiv 1$.

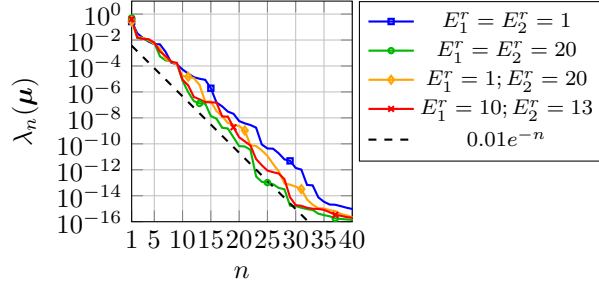


FIGURE 3. Eigenvalues $\lambda_n(\boldsymbol{\mu})$ for different Young’s modulus ratios E_i^r in Ω_i , $i = 1, 2$.

both S and R with a lifting inner product based on the lifting operator $\mathcal{E}_{\Gamma \rightarrow \Omega_m}(\bar{\boldsymbol{\mu}})$ defined in subsection 3.1.1; for further details we refer to [SP16].

We consider different values for Young’s modulus (ratios) E_i^r , $i = 1, 2$ in the red areas of the subdomains and observe in Fig. 3 for the ship stiffener application an exponential convergence of order $\approx e^{-n}$ of the eigenvalues $\lambda_n(\boldsymbol{\mu})$ and thus the static condensation approximation. We emphasize that we observe in Fig. 3 that the eigenvalues associated with the stiffened plate ($E_1^r = E_2^r = 20$) decay fastest, while we see the slowest decay for the non-stiffened plate ($E_1^r = E_2^r = 1$). This is consistent with the expectation that stiffening the plate decreases the deflection of the plate, eliminating the higher eigenmodes. Moreover, an inspection of the optimal interface modes reveals many “classical” mode shapes such as bending or torsional modes of beams and demonstrates again the physical significance of the optimal modes. Also for beams of different shapes, including an I-beam with a crack and thus an irregular domain, an exponential convergence of the transfer eigenvalues and the physical significance of the transfer eigenmodes can be observed; for further details see [SP16].

4.2.2. Randomized Training. In order to compute an efficient approximation R_n^{rand} of R_n the adaptive randomized range approximation algorithm 4.1 as suggested in [BS18] iteratively enhances the reduced space with applications of T to a random function until a certain convergence criterion is satisfied.

In detail, in each iteration in line 5 we draw a new random vector $\mathbf{r} \in \mathbb{R}^{N_S}$ whose entries are independent and identically distributed random variables with standard normal distribution. Then, we employ the mapping $D_S^{-1} : \mathbb{R}^{N_S} \rightarrow S$ to define a unique FE function in S whose coefficients are the components of \mathbf{r} .

Algorithm 4.1: Adaptive Randomized Range Approximation

Input : Operator T , target accuracy tol , number of test vectors n_t ,
maximum failure probability $\varepsilon_{\text{algofail}}$

Output : space R_n^{rand} with property $P(\|T - P_{R_n^{\text{rand}}}T\| \leq \text{tol}) > (1 - \varepsilon_{\text{algofail}})$

1 Initialize: $B \leftarrow \emptyset$, $M \leftarrow \{TD_S^{-1}\mathbf{r}_1, \dots, TD_S^{-1}\mathbf{r}_{n_t}\}$

2 Compute error estimator factors:

3 $\varepsilon_{\text{testfail}} \leftarrow \varepsilon_{\text{algofail}}/N_T$; $c_{\text{est}} \leftarrow \left[\sqrt{2\lambda_{\min}^{\text{M}_S}} \text{erf}^{-1}(\sqrt[n_t]{\varepsilon_{\text{testfail}}}) \right]^{-1}$

4 while $(\max_{t \in M} \|t\|_R) \cdot c_{\text{est}} > \text{tol}$ **do**

5 $B \leftarrow B \cup (TD_S^{-1}\mathbf{r})$

6 $B \leftarrow \text{orthonormalize}(B)$

7 **orthogonalize test vectors:** $M \leftarrow \{t - P_{\text{span}\{B\}}t \mid t \in M\}$

8 return $R_n^{\text{rand}} = \text{span}\{B\}$

Subsequently, we apply the transfer operator T to $D_S^{-1}\mathbf{r}$, meaning that we solve the PDE locally on Ω_{out} with random boundary conditions and restrict the solution to Ω_m or $\Gamma_{m,m'}$; the resulting function is added to the set of basis functions B . Finally, the basis B is orthonormalized. Note that the orthonormalization is numerically challenging, as the basis functions are nearly linear dependent when $\text{span}\{B\}$ is already a good approximation of the range of T ; in [BS18] using the numerically stable Gram-Schmidt with adaptive re-iteration from [BEOR14] is suggested. The main loop of the algorithm is terminated when the following a posteriori norm estimator is smaller than the desired tolerance tol .

Proposition 4.4 (A probabilistic a posteriori norm estimator [BS18]). *Let \mathbf{r}_i , $i = 1, \dots, n_t$ be n_t random normal test vectors and $\lambda_{\min}^{\text{M}_S}$ and $\lambda_{\max}^{\text{M}_S}$ the smallest and largest eigenvalues of the matrix of the inner product in S . Then, the a posteriori norm estimator*

$$(45) \quad \Delta(n_t, \varepsilon_{\text{testfail}}) := c_{\text{est}}(n_t, \varepsilon_{\text{testfail}}) \max_{i \in 1, \dots, n_t} \|(T - P_{R_n^{\text{rand}}}T) D_S^{-1} \mathbf{r}_i\|_R$$

satisfies

$$(46) \quad P\{\|T - P_{R_n^{\text{rand}}}T\| \leq \Delta(n_t, \varepsilon_{\text{testfail}})\} \geq (1 - \varepsilon_{\text{testfail}}),$$

where $c_{\text{est}}(n_t, \varepsilon_{\text{testfail}}) := 1/[(2\lambda_{\min}^{\text{M}_S})^{1/2} \text{erf}^{-1}(\sqrt[n_t]{\varepsilon_{\text{testfail}}})]$. Additionally, there holds

$$P\left\{\frac{\Delta(n_t, \varepsilon_{\text{testfail}})}{\|T - P_{R_n^{\text{rand}}}T\|} \leq c_{\text{eff}}(n_t, \varepsilon_{\text{testfail}})\right\} \geq 1 - \varepsilon_{\text{testfail}},$$

where the constant $c_{\text{eff}}(n_t, \varepsilon_{\text{testfail}})$ is defined as

$$c_{\text{eff}}(n_t, \varepsilon_{\text{testfail}}) := \left[Q^{-1}\left(\frac{N_T}{2}, \frac{\varepsilon_{\text{testfail}}}{n_t}\right) \frac{\lambda_{\max}^{\text{M}_S}}{\lambda_{\min}^{\text{M}_S}} (\text{erf}^{-1}(\sqrt[n_t]{\varepsilon_{\text{testfail}}}))^{-2} \right]^{1/2}$$

and Q^{-1} is the inverse of the upper normalized incomplete gamma function.

The constant $c_{\text{est}}(n_t, \varepsilon_{\text{testfail}})$ is calculated in line 3 using N_T , which denotes the rank of operator T . In practice N_T is unknown and an upper bound for N_T such as $\min(N_S, N_R)$ can be used instead. Note that the term $(\max_{t \in M} \|t\|_R) \cdot$

$c_{\text{est}}(n_t, \varepsilon_{\text{testfail}})$ is the norm estimator (45). The test vectors are reused for all iterations.

To finally analyze the failure probability of Algorithm 4.1 we first note that after N_T steps we have $R_n^{\text{rand}} = \text{range}(T)$ and thus $\|T - P_{R_n^{\text{rand}}}T\| = 0$, yielding the termination of Algorithm 4.1. Using the fact that the a posteriori error estimator defined in (45) is therefore executed at most N_T times combined with the probability for one estimate to fail in (46) and an union bound argument we infer that the failure probability for the whole algorithm is $\varepsilon_{\text{algofail}} \leq N_T \varepsilon_{\text{testfail}}$.

Remarkably, the convergence behavior of the reduced space R_n^{rand} is only slightly worse than the rate $\sqrt{\lambda_{n+1}}$, which is achieved by the optimal local approximation spaces defined in Theorem 4.1:

Proposition 4.5 (A priori error bound [BS18]). *Let $\lambda_{\max}^{\mathbb{M}_R}$ and $\lambda_{\min}^{\mathbb{M}_R}$ denote the largest and smallest eigenvalues of the inner product matrix \mathbb{M}_R and let R_n^{rand} be the outcome of Algorithm 4.1. Then, for $n \geq 4$ there holds*

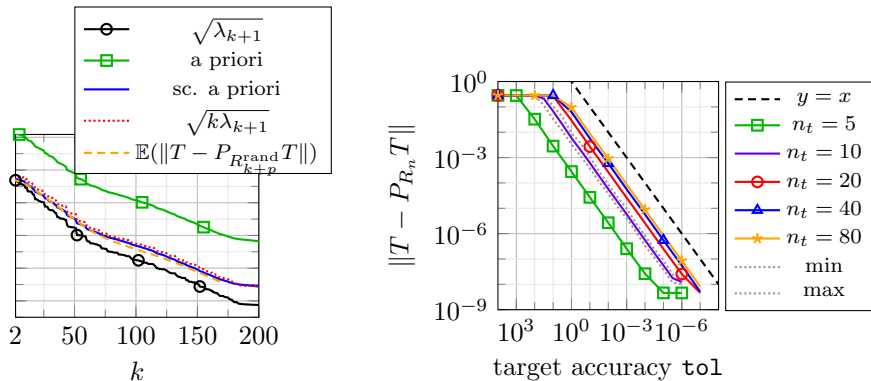
$$(47) \quad \mathbb{E}\|T - P_{R_n^{\text{rand}}}T\| \leq C_{R,S} \min_{\substack{k+p=n \\ k \geq 2, p \geq 2}} \left[\left(1 + \sqrt{\frac{k}{p-1}}\right) \sqrt{\lambda_{k+1}} + \frac{e\sqrt{n}}{p} \left(\sum_{j>k} \lambda_j\right)^{\frac{1}{2}} \right],$$

where $C_{R,S} = (\lambda_{\max}^{\mathbb{M}_R}/\lambda_{\min}^{\mathbb{M}_R})^{1/2}(\lambda_{\max}^{\mathbb{M}_S}\lambda_{\min}^{\mathbb{M}_S})^{1/2}$.

It can be observed in numerical experiments that the a priori bound in Proposition 4.5 is sharp in terms of the predicted convergence behavior as we will show now for a test case from [BS18]. Moreover, we will investigate the performance of Algorithm 4.1 also for a test case from [BS18]. To that end, let $\widehat{\Omega}_m = (-0.5, 0.5) \times (-0.25, 0.25) \times (-0.5, 0.5)$ and $\Omega_m = (-0.5, 0.5) \times (-0.5, 0.5) \times (-0.5, 0.5)$ be the subdomains on which we aim to construct a local approximation space, $\widehat{\Omega}_{out} = (-2, 2) \times (-0.25, 0.25) \times (-2, 2)$ and $\Omega_{out} = (-2, 2) \times (-0.5, 0.5) \times (-2, 2)$ the corresponding oversampling domains and $\widehat{\Gamma}_{out} = \{-2, 2\} \times (-0.25, 0.25) \times (-2, 2) \cup (-2, 2) \times (-0.25, 0.25) \times \{-2, 2\}$ and $\Gamma_{out} = \{-2, 2\} \times (-0.5, 0.5) \times (-2, 2) \cup (-2, 2) \times (-0.5, 0.5) \times \{-2, 2\}$ the respective outer boundaries. On $\partial\widehat{\Omega}_{out} \setminus \widehat{\Gamma}_{out}$ and $\partial\Omega_{out} \setminus \Gamma_{out}$ we prescribe homogeneous Neumann boundary conditions and we suppose that $\widehat{\Omega}_{out}$ and Ω_{out} do not border the Dirichlet boundary of Ω . For the FE discretization we use a regular mesh with hexahedral elements and a mesh size $h = 0.1$ in each space direction and a corresponding conforming FE space with linear FE resulting in $\dim(V_h|_{\widehat{\Omega}_{out}}) = 30258$, $\dim(R) = N_R = 2172$, $\dim(S) = N_S = 2880$ for $\widehat{\Omega}_{out}$ and $V_h|_{\Omega_{out}} = 55473$, $N_R = 3987$, and $N_S = 5280$ for Ω_{out} .³ We equip the source space S with the L^2 -inner product and the range space R with the energy inner product. Finally, for all results in this subsection we computed the statistics over 1000 samples.

Analyzing the convergence behavior of $\mathbb{E}(\|T - P_{R_{k+p}^{\text{rand}}}T\|)$ on $\widehat{\Omega}_{out}$ for a growing number of randomly generated basis functions k and a (fixed) oversampling parameter $p = 2$ in Fig. 4a we see that until $k \approx 75$ the a priori bound reproduces the convergence behavior of $\mathbb{E}(\|T - P_{R_{k+p}^{\text{rand}}}T\|)$ perfectly. We may thus conclude that

³Note that although in theory we should subtract the orthogonal projection on the six rigid body motions from the FE basis functions, in actual practice we avoid that by subtracting the orthogonal projection from the harmonic extensions only.


 (A) Convergence behavior on $\hat{\Omega}_{out}$.

 (B) Median for varying n_t on Ω_{out}

FIGURE 4. Comparison of the convergence behavior of $\sqrt{\lambda_{k+1}}$, $\sqrt{k\lambda_{k+1}}$, $\mathbb{E}(\|T - P_{R_{k+p}^{rand}}T\|)$, the a priori error bound (47), and the a priori error bound of (47) scaled with a constant such that its value for $k = 2$ equals the one of $\mathbb{E}(\|T - P_{R_{k+p}^{rand}}T\|)$ (sc. a priori) for increasing k for and $p = 2$ for the oversampling domain $\hat{\Omega}_{out}$ (a). Median of the projection error $\|T - P_{R_n^{rand}}T\|$ for a decreasing target accuracy \mathbf{tol} for a varying number of test vectors n_t and the minimal and maximal values for $n_t = 10$ on Ω_{out} (b).

the a priori bound in (47) seems to be sharp regarding the convergence behavior of $\mathbb{E}(\|T - P_{R_{k+p}^{rand}}T\|)$ in the basis size k . We also observe that the a priori bound is rather pessimistic as it overestimates $\mathbb{E}(\|T - P_{R_{k+p}^{rand}}T\|)$ by a factor of more than 100; this is mainly due to the square root of the conditions of the inner product matrices.

Regarding the performance of Algorithm 4.1 on Ω_{out} we first observe in Fig. 4b that the actual error $\|T - P_{R_n^{rand}}T\|$ lies below the target tolerance \mathbf{tol} for all 1000 samples for $n_t = 10$; which holds also true for all other considered values of n_t . Here, we prescribe $\varepsilon_{\text{algofail}} = 10^{-10}$ and use 3993 as an upper bound for N_T . We see in Fig. 4b that increasing the number of test vectors n_t from 5 to 10 or from 10 to 20 increases the ratio between the median of the actual error $\|T - P_{R_n^{rand}}T\|$ and the target accuracy \mathbf{tol} significantly — for the former by more than one magnitude — while an increase from $n_t = 40$ to $n_t = 80$ has hardly any influence; similar results have been obtained in [BS18] for heat conduction and a Helmholtz problem. This can be explained by the scaling of the effectivity of the employed a posteriori error estimator, which is of the order of 1000 for $n_t = 5$ and of the order of 10 for $n_t \geq 20$. Regarding the choice of n_t it seems that for the present test case a value of about 20 is in the sweet spot. We thus infer that for the present test case only very few local solutions in addition to the optimal amount are required, demonstrating that Algorithm 4.1 performs nearly optimally in terms of computational complexity for the current problem.

4.2.3. *The general setting $\mathcal{P} \neq \{\bar{\mu}\}$.* The processes in subsection 4.2.1 and 4.2.2 yield for every $\mu \in \mathcal{P}$ the local approximation space $R_n^+(\mu)$ for this specific

parameter $\boldsymbol{\mu} \in \mathcal{P}$. $R_n^+(\boldsymbol{\mu})$ can also be generated by some other process, where we require that there holds

$$(48) \quad \|T(\boldsymbol{\mu}) - P_{R_n(\boldsymbol{\mu})}T(\boldsymbol{\mu})\| \leq \frac{\varepsilon}{2C_1(\mathcal{T}_H, \boldsymbol{\mu})}$$

possibly only at high probability and that $R_n^+(\boldsymbol{\mu})$ is defined as the direct sum of $R_n(\boldsymbol{\mu})$, the kernel of the bilinear form, and representations of non-homogeneous Dirichlet boundary conditions and the right-hand side. We abuse notation in this subsection by omitting henceforth the remark that the estimate may only hold in a probabilistic sense. The constant $C_1(\mathcal{T}_H, \boldsymbol{\mu})$ has to be chosen in such a manner that if one uses the parameter-dependent spaces $R_n^+(\boldsymbol{\mu})$ to define $u^n(\boldsymbol{\mu})$, we have

$$(49) \quad \frac{\|u(\boldsymbol{\mu}) - u_{n+}(\boldsymbol{\mu})\|_{\boldsymbol{\mu}}}{\|u(\boldsymbol{\mu})\|_{\boldsymbol{\mu}}} \leq \frac{\varepsilon}{2}.$$

The spectral greedy algorithm as introduced in [SP16]⁴ constructs *one* (quasi-optimal) parameter-independent approximation space R_N which approximates those parameter-dependent spaces $R_n^+(\boldsymbol{\mu})$ with a given accuracy on a finite dimensional training set $\Xi \subset \mathcal{P}$. In the spectral greedy algorithm we exploit the fact that we expect that the local spaces $R_n^+(\boldsymbol{\mu})$, and in particular the spectral modes that correspond to the largest eigenvalues, are not affected too much by a variation in the parameter thanks to the expected very rapid decay of the higher eigenfunctions in the interior of Ω_{out} .

The spectral greedy as described in Algorithm 4.2 then proceeds as follows. After the initialization we compute for all $\boldsymbol{\mu} \in \Xi$ the parameter-dependent spaces $R_n^+(\boldsymbol{\mu})$ such that we have (48). Note that for a decomposition \mathcal{T}_H with mutually disjoint interfaces (also called ports), where each Ω_m , $m = 1, \dots, M$ has exactly two interfaces and all interfaces have the same geometry we have the following *a priori* error bound [SP16] for the error between $u(\boldsymbol{\mu})$ and the continuous port-reduced static condensation approximation $u_{n+}(\boldsymbol{\mu})$ corresponding to the *parameter-dependent* optimal interface space $\mathcal{R}_n^+(\boldsymbol{\mu})$:

$$(50) \quad \frac{\|u(\boldsymbol{\mu}) - u_{n+}(\boldsymbol{\mu})\|_{\boldsymbol{\mu}}}{\|u(\boldsymbol{\mu})\|_{\boldsymbol{\mu}}} \leq \#\gamma c_1(\boldsymbol{\mu})c_2(\boldsymbol{\mu}) \max_{\gamma \in \mathcal{T}_H^\gamma} \left(C_{\gamma,1}(\Omega_\gamma, \boldsymbol{\mu}) \sqrt{\lambda_{\gamma,n+1}(\boldsymbol{\mu})} \right).$$

Here, the constant $C_{\gamma,1}(\Omega_\gamma, \boldsymbol{\mu})$ depends only on the subdomains that share γ and not on Ω or on $u(\boldsymbol{\mu})$. Moreover, $c_1(\boldsymbol{\mu})$ and $c_2(\boldsymbol{\mu})$ are chosen such that we have $c_1(\boldsymbol{\mu})\|\cdot\|_{\bar{\boldsymbol{\mu}}} \leq \|\cdot\|_{\boldsymbol{\mu}} \leq c_2(\boldsymbol{\mu})\|\cdot\|_{\bar{\boldsymbol{\mu}}}$ for all $\boldsymbol{\mu} \in \mathcal{P}$ and a fixed reference parameter $\bar{\boldsymbol{\mu}} \in \mathcal{P}$. Choosing $C_1(\mathcal{T}_H, \boldsymbol{\mu}) = \#\gamma c_1(\boldsymbol{\mu})c_2(\boldsymbol{\mu}) \max_{\gamma \in \mathcal{T}_H^\gamma} C_{\gamma,1}(\Omega_\gamma, \boldsymbol{\mu})$ and $\sqrt{\lambda_{\gamma,n+1}(\boldsymbol{\mu})} \leq \varepsilon/2$ yields a reduced space $R_n^+(\boldsymbol{\mu})$ that satisfies the requirements stated in the beginning for every $\boldsymbol{\mu} \in \Xi$. Although precise estimates for $C_{\gamma,1}(\Omega_\gamma, \boldsymbol{\mu})$ can be obtained, setting $C_{\gamma,1}(\Omega_\gamma, \boldsymbol{\mu}) = 1$ yields in general good results as another value would just result in rescaling ε ; for further details see [SP16]. After having collected all functions on $\Gamma_{m,m'}$ or Ω_m that are essential to obtain a good approximation for all local solutions $u_{loc}(\boldsymbol{\mu})$ of the PDE evaluated on $\Gamma_{m,m'}$ or Ω_m , $\boldsymbol{\mu} \in \Xi$, we must select a suitable basis from those functions. This is realized in an iterative manner in Lines 5-14.

⁴For a generalization to a setting where the discrete parameter set describes different geometries such as a beam with or without a crack we refer to [Sme19].

Algorithm 4.2: spectral greedy [SP16]

Input : train sample $\Xi \subset \mathcal{P}$, tolerance ε
Output : set of chosen parameters Ξ_N , local approximation space R_N

```

1 Initialize  $N \leftarrow \dim(\ker(a_m(\cdot, v)))$ ,
    $\Xi_N \leftarrow \emptyset, R_N \leftarrow \ker(a_m(\cdot, v))$  or  $R_N \leftarrow \ker(a_m(\cdot, v))|_{\Gamma_{m,m'}}$ 
2 foreach  $\mu \in \Xi$  do
3    $\left[ \text{Compute } R_n^+(\mu) \text{ such that } \|T(\mu) - P_{R_n^+(\mu)}T(\mu)\| \leq \frac{\varepsilon}{2C_1(\mathcal{T}_H, \mu)} \right]$ 
4 while true do
5   if  $\max_{\mu \in \Xi} E(S(R_n^+(\mu)), R_N) \leq \varepsilon/(\varepsilon + 2C_2(\mathcal{T}_H, \mu)c_1(\mu)c_2(\mu))$  then
6      $\left[ \text{return} \right]$ 
7    $\mu^* \leftarrow \arg \max_{\mu \in \Xi} E(S(R_n^+(\mu)), R_N)$ 
8    $\Xi_{N+1} \leftarrow \Xi_N \cup \mu^*$ 
9    $\kappa \leftarrow \arg \sup_{\rho \in S(R_n^+(\mu^*))} \inf_{\zeta \in R_N} \|\rho - \zeta\|_R$ 
10   $R_{N+1} \leftarrow R_N + \text{span}\{\kappa\}$ 
11   $N \leftarrow N + 1$ 
12 return  $\Xi_N, R_N$ 

```

In each iteration we first identify in Line 7 the reduced space $R_n^+(\mu^*)$ that maximizes the deviation

$$E(S(R_n^+(\mu)), R_N) := \sup_{\xi \in S(R_n^+(\mu))} \inf_{\zeta \in R_N} \|\xi - \zeta\|_R, \quad \mu \in \Xi,$$

where possible choices of $S(R_n^+(\mu)) \subset R_n^+(\mu)$ will be discussed below. Subsequently, we determine in Line 9 the function $\kappa \in S(R_n^+(\mu^*))$ that is worst approximated by the space R_N and enhance R_N with the span of κ . The spectral greedy algorithm terminates if for all $\mu \in \Xi$ we have

$$(51) \quad \max_{\mu \in \Xi} E(S(R_n^+(\mu)), R_N) \leq \varepsilon/(\varepsilon + 2C_2(\mathcal{T}_H, \mu)c_1(\mu)c_2(\mu))$$

for a constant $C_2(\mathcal{T}_H, \mu)$, which can in general be chosen equal to one. We emphasize, that both $C_1(\mathcal{T}_H, \mu)$ and $C_2(\mathcal{T}_H, \mu)$ do in general only depend on the *number* of faces or subspaces on which the respective reduced space R_N is used and *not on the precise decomposition* of Ω ; see (50). A slight modification of the stopping criterion (51) and a different scaling of ε in the threshold for the a priori error bound in Line 3 allows to prove that after termination of the spectral greedy for a decomposition \mathcal{T}_H with mutually disjoint interfaces, where each Ω_m , $m = 1, \dots, M$ has exactly two interfaces and all interfaces have the same geometry we have [SP16]

$$(52) \quad \||u(\mu) - u_N(\mu)\||_{\mu} / \||u(\mu)\||_{\mu} \leq \varepsilon.$$

Here, $u_N(\mu)$ is the continuous port-reduced static condensation approximation corresponding to \mathcal{R}_N ; \mathcal{R}_N being the continuous outcome of the spectral greedy.

Choice of the subset $S(R_n^+(\mu))$ First, we emphasize that in contrast to the standard greedy as introduced in [VPRP03] we have an ordering of the basis functions in $R_n^+(\mu)$ in terms of their approximation properties thanks to the transfer eigenvalue problem; the sorting of the basis functions in terms of their approximation

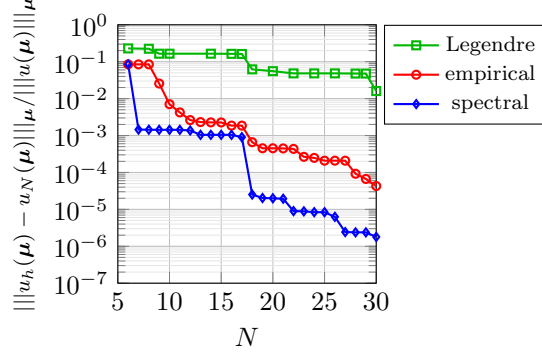


FIGURE 5. $\|u_h(\boldsymbol{\mu}) - u^N(\boldsymbol{\mu})\|_{\boldsymbol{\mu}} / \|u(\boldsymbol{\mu})\|_{\boldsymbol{\mu}}$ for the Legendre, empirical, and spectral interface basis functions for the solid beam.

properties is implicitly saved in their norms as $\|\chi_j^{sp}(\boldsymbol{\mu})\|_R^2 = \lambda_j(\boldsymbol{\mu})$, $j = 1, \dots, n$. To obtain local approximation spaces R_N that yield a (very) good approximation $u^N(\boldsymbol{\mu})$ already for moderate N it is therefore desirable that the spectral greedy algorithm selects the lower eigenmodes sooner rather than later during the `while`-loop. As suggested in [SP16] we thus propose to consider

$$(53) \quad S(R_n^+(\boldsymbol{\mu})) := \{\zeta(\boldsymbol{\mu}) \in R_n^+(\boldsymbol{\mu}) : \|\zeta(\boldsymbol{\mu})\|_{R_n^+(\boldsymbol{\mu})} \leq 1\}$$

$$\text{with } \|\zeta(\boldsymbol{\mu})\|_{R_n^+(\boldsymbol{\mu})} := \left(\sum_{i=1}^{n_+} (\zeta_i(\boldsymbol{\mu}))^2 \right)^{1/2}$$

where $\zeta(\boldsymbol{\mu}) = \sum_{i=1}^{n_+} \zeta_i(\boldsymbol{\mu}) \chi_i(\boldsymbol{\mu})$, $n_+ := \dim(R_n^+(\boldsymbol{\mu}))$ and here and henceforth $\{\chi_i(\boldsymbol{\mu})\}_{i=1}^{n_+}$ denotes the orthonormal basis of $R_n^+(\boldsymbol{\mu})$. Note that we are therefore considering a weighted norm in $R_n^+(\boldsymbol{\mu})$. The deviation $E(S(R_n^+(\boldsymbol{\mu})), R_N)$ can then be computed by solving the eigenvalue problem: Find $(\boldsymbol{\varrho}_j(\boldsymbol{\mu}), \sigma_j(\boldsymbol{\mu})) \in (\mathbb{R}^{n_+}, \mathbb{R}^+)$ such that

$$\mathbb{Z}(\boldsymbol{\mu}) \boldsymbol{\varrho}_j(\boldsymbol{\mu}) = \sigma_j(\boldsymbol{\mu}) \boldsymbol{\varrho}_j(\boldsymbol{\mu}),$$

$$\text{where } \mathbb{Z}_{i,l}(\boldsymbol{\mu}) := (\chi_l(\boldsymbol{\mu}) - \sum_{k=1}^N (\chi_l(\boldsymbol{\mu}), \chi_k)_R \chi_k, \chi_i(\boldsymbol{\mu}) - \sum_{k=1}^N (\chi_i(\boldsymbol{\mu}), \chi_k)_R \chi_k)_R$$

and χ_k denotes the orthonormal basis of R_N . We thus obtain $E(S(R_n^+(\boldsymbol{\mu})), R_N) = \sqrt{\sigma_1(\boldsymbol{\mu})}$, for all $\boldsymbol{\mu} \in \Xi$, and $\boldsymbol{\kappa} = \sum_{i=1}^{n_+} \boldsymbol{\varrho}_1(\boldsymbol{\mu}^*) \chi_i(\boldsymbol{\mu}^*)$ at each iteration.

Note that were we to consider the norm $\|\cdot\|_R$ in (53) the sorting of the spectral basis $\chi_i(\boldsymbol{\mu})$ of $R_n^+(\boldsymbol{\mu})$ in terms of approximation properties is neglected in the `while` loop of Algorithm 4.2; for further explanations see [SP16].

Finally, we compare in Fig. 5 the spectral modes generated by the spectral greedy algorithm 4.2 numerically with other interface modes, demonstrating the superior convergence of the former. In detail, we compare the relative error of the port-reduced static condensation approximation for interface spaces comprising

“Legendre polynomial”-type functions⁵ [EP13], empirical port modes constructed by a pairwise training algorithm⁶ [EP13, EP14], and the spectral modes. To that end, we consider a domain Ω which consists of two identical solid beams, each of whom is associated with a subdomain Ω_i , $i = 1, 2$. Here, we choose $\Omega_1 = (-0.5, 0.5) \times (-0.5, 0.5) \times (0, 5)$, $\Omega_2 = (-0.5, 0.5) \times (-0.5, 0.5) \times (5, 10)$ and $\Gamma_{out} = \Gamma_1 \cup \Gamma_2$, with $\Gamma_1 = (-0.5, 0.5) \times (-0.5, 0.5) \times \{0\}$ and $\Gamma_2 = (-0.5, 0.5) \times (-0.5, 0.5) \times \{10\}$. The underlying FE discretization has $N = 3348$ degrees of freedom per subdomain and $N_\Gamma = 108$ degrees of freedom per interface. We require $E(\boldsymbol{\mu})$ to be uniform within each subdomain, the constant varying in $[1, 10]$ and choose for $\mathbf{G}(\boldsymbol{\mu}) \in \mathbb{R}^3$ the admissible set of parameters to be $[-1, 1] \times [-1, 1] \times [-1, 1]$. Finally, we equip both S and R again with a lifting inner product. Within the spectral greedy we have considered 200 parameter values sampled from the uniform distribution over \mathcal{P} and $\varepsilon = 1 \cdot 10^{-6}$. On average the interface spaces $R_n^+(\boldsymbol{\mu})$ have had a size of 13.65 and the resulting parameter-independent port space R_N has a size of 56.

In the online stage we consider $E(\boldsymbol{\mu}) \equiv 1$ in both components, $\mathbf{G} = (0, 0, 0)^T$, and prescribe $\mathbf{g}_{D,1} = (0, 0, 0)^T$ at Γ_1 and $\mathbf{g}_{D,2} = (1, 1, 1)^T$ at Γ_2 . We observe that the Legendre modes perform by far the worst, demonstrating that including information on the solution manifold in the basis construction procedure can significantly improve the approximation behavior. We remark that the Legendre modes will perform even worse in the case of less regular behaviour on the interface, which further justifies the need for problem-specific local approximation spaces in the sense of model reduction. The empirical modes and spectral modes exhibit a comparable convergence until $N = 17$, but for $N > 17$ the relative error in the spectral approximation is one order of magnitude smaller than that of the empirical port mode approximation. This can be explained by the fact that thanks to its conception the pairwise training algorithm is able to identify and include the most significant modes, but (in contrast to the spectral greedy algorithm) might have difficulties to detect subtle modes that affect the shape of the function at the interface $\Gamma_{m,m'}$ only slightly. Note that the temporary stagnation of the relative error for $N = 7, \dots, 17$ for the spectral modes is due to the fact that the spectral greedy prepares the interface space for all possible boundary conditions and parameter configurations. Thus, for the boundary conditions considered here some spectral modes, as say a mode related to a twisting (torsion) of the beam, are not needed for the approximation.

5. A POSTERIORI ERROR ESTIMATION

5.1. Residual based a posteriori error estimation. A global residual based a posteriori error estimator for projection based model reduction is readily defined as

$$(54) \quad \Delta(u_N(\boldsymbol{\mu})) := \frac{1}{\alpha(\boldsymbol{\mu})} \|R(u_N(\boldsymbol{\mu}); \boldsymbol{\mu})\|_{V_h'}$$

where $R(u_N(\boldsymbol{\mu}); \boldsymbol{\mu}) \in V_h'$ is the global residual given as $\langle R(u_N(\boldsymbol{\mu}); \boldsymbol{\mu}), \varphi_h \rangle = f_h(\varphi_h; \boldsymbol{\mu}) - a_h(u_N(\boldsymbol{\mu}), \varphi_h; \boldsymbol{\mu})$ for all $\varphi_h \in V_h$. This error estimator is known to

⁵Note that each component of the displacement is the solution of a scalar singular Sturm-Liouville eigenproblem.

⁶Following the notation in [EP14] we have chosen $N_{\text{samples}} = 500$ and $\gamma = 3$ in the pairwise training algorithm.

be robust and efficient (cf. [HRS16, Proposition 4.4]), i.e. we have

$$(55) \quad \|u_h(\boldsymbol{\mu}) - u_N(\boldsymbol{\mu})\|_V \leq \Delta(u_N(\boldsymbol{\mu})) \leq \frac{\gamma(\boldsymbol{\mu})}{\alpha(\boldsymbol{\mu})} \|u_h(\boldsymbol{\mu}) - u_N(\boldsymbol{\mu})\|_V.$$

For localized model order reduction, however, we are merely interested in localized a posteriori error estimation. To this end, we first present abstract localized lower and upper bounds for the dual norm of a linear functional (see [BEOR17]).

Theorem 5.1 (Localized lower and upper bounds for functionals). *Let O_i , $1 \leq i \leq \tilde{M}$ be a collection of linear subspaces of V_h , and let $P_{O_i} : V_h \rightarrow O_i \subseteq V_h$ be mappings which satisfy $\sum_{i=1}^{\tilde{M}} P_{O_i} = \text{id}_{V_h}$. Moreover, assume that for $J \in \mathbb{N}$ there exists a partition $\dot{\bigcup}_{j=1}^J \Upsilon_j = \{1, \dots, \tilde{M}\}$ such that for arbitrary $1 \leq j \leq J$ and $i_1 \neq i_2 \in \Upsilon_j$ we have $O_{i_1} \perp O_{i_2}$.*

Defining the stability constant of this partition modulo V_N as

$$(56) \quad c_N := \sup_{\varphi \in V_h \setminus \{0\}} \frac{(\sum_{i=1}^{\tilde{M}} \inf_{\tilde{\varphi} \in V_N \cap O_i} \|P_{O_i}(\varphi) - \tilde{\varphi}\|^2)^{\frac{1}{2}}}{\|\varphi\|}$$

we have for any linear functional $f \in V_h'$ with $\langle f, \varphi \rangle = 0 \forall \varphi \in V_N$ the estimate

$$(57) \quad \frac{1}{\sqrt{J}} \left(\sum_{i=1}^{\tilde{M}} \|f\|_{O_i'}^2 \right)^{\frac{1}{2}} \leq \|f\|_{V_h'} \leq c_N \cdot \left(\sum_{i=1}^{\tilde{M}} \|f\|_{O_i'}^2 \right)^{\frac{1}{2}}.$$

Here, $\|f\|_{O_i'}$ denotes the norm of the restriction of f to O_i .

When grouping the spaces O_i so that in each group, all spaces are orthogonal to each other, J is the number of groups needed. Note that subtracting the projection onto V_N in (56) allows subtracting say the mean value of a function or the orthogonal projection onto the rigid body motions, if the respective functions are included in V_N . We may thus employ say Poincaré's inequality or Korn's inequality in subdomains that do not lie at Γ_D .

Applying both estimates to the residual $R(u_N(\boldsymbol{\mu}); \boldsymbol{\mu}) \in V_h'$, we obtain from (54) and Theorem 5.1 a robust and efficient, localized error estimate:

Corollary 5.2 (Localized residual based a posteriori error estimate). *Let the assumptions on the subspace collection O_i and the mappings P_i from Theorem 5.1 be satisfied. Then, the error estimator $\Delta_{loc}(u_N(\boldsymbol{\mu}))$ defined as*

$$(58) \quad \Delta_{loc}(u_N(\boldsymbol{\mu})) := \frac{1}{\alpha(\boldsymbol{\mu})} c_N \left(\sum_{i=1}^{\tilde{M}} \|R(u_N(\boldsymbol{\mu}); \boldsymbol{\mu})\|_{O_i'}^2 \right)^{\frac{1}{2}}$$

is robust and efficient, i.e.

$$(59) \quad \|u_h(\boldsymbol{\mu}) - u_N(\boldsymbol{\mu})\|_V \leq \Delta_{loc}(u_N(\boldsymbol{\mu})) \leq \frac{\gamma(\boldsymbol{\mu})\sqrt{J}c_N}{\alpha(\boldsymbol{\mu})} \|u_h(\boldsymbol{\mu}) - u_N(\boldsymbol{\mu})\|_V.$$

Online-offline decomposition of this error estimator can be done by applying the usual strategy for online-offline decomposition used with the standard RB error estimator (see e.g. [HRS16, Sec. 4.2.5] or a numerically more stable approach [BEOR14, CEL14a, SFDE15]) to every dual norm in $\Delta_{loc}(u_N(\boldsymbol{\mu}))$.

The a posteriori error estimator for the ArbiLoMod derived in [BEOR17] and the a posteriori error estimator for the scRBE method as suggested in [Sme15] both fit into the framework above as will be detailed below in Examples 5.3 and

5.4. In contrast, for instance the error estimators proposed in [HKP13b, HKP13a] for the scRBE method exploit matrix perturbation analysis at the system level to bound the Euclidean norm of the error between the coefficients of the static condensation solution and the coefficients of the static condensation solution using an RB approximation in the interior. To estimate the error caused by interface reduction in [EP13] a computationally tractable non-conforming approximation to the exact error is employed. To take into account the error due to the intra-element RB approximations ideas from [HKP13b] are used. It can also be noted that the error estimators in [HKP13b, HKP13a, EP13] are only valid under certain assumptions on the accuracy of the RB approximation. In [MRH15] a localized a posteriori error estimator for interface reduction and intra-element RB approximation is presented for the coupled Stokes-Darcy system. The a posteriori error estimator for the CMS method derived in [JBL11] employs the dual norms of residuals and eigenvalues of the eigenproblems used for the construction of the (local) basis functions. The error estimator in [JBL11] is however only partially local as it involves the residual for the port or interface space on the whole interface Γ . For localized a posteriori error estimation in the context of adaptive GMsFEM we refer to [CEL14b, CEL18a, CEL15, CEL17b].

Example 5.3 (Localized a posteriori error estimate for ArbiLoMod [BEOR17]). *Let us assume $V_h \subset V = H_0^1(\Omega)$, and choose O_i as subspaces of $H^1(\Omega_i)$ where $\tilde{\mathcal{T}}_H := \{\tilde{\Omega}_1, \dots, \tilde{\Omega}_{\tilde{M}}\}$ is an arbitrary overlapping decomposition of Ω , which may be chosen independently from \mathcal{T}_H . Assume that there is a partition of unity $p_i \in H^{1,\infty}(\tilde{\Omega}_i) \cap C(\tilde{\Omega}_i)$, $\sum_{i=1}^{\tilde{M}} p_i = 1$, such that $\|p_i\|_\infty \leq 1$ and $\|\nabla p_i\|_\infty \leq c_{\text{pu}} \text{diam}(\tilde{\Omega}_i)^{-1}$. The constant c_{pu} will depend on size of the overlap of the subdomains $\tilde{\Omega}_i$ with their neighbors in relation to their diameters.*

Moreover, we assume that there is a linear interpolation operator \mathcal{I} onto V_h such that \mathcal{I} is the identity on V_h with $\mathcal{I}(p_i V_h) \subseteq O_i$ and $\|\mathcal{I}(p_i v_h) - p_i v_h\|_V \leq c_I \|v_h\|_{\tilde{\Omega}_i,1}$ for all $v_h \in V_h$. We then can define mappings

$$P_{O_i}(v_h) := \mathcal{I}(p_i \cdot v_h).$$

which satisfy the assumptions of Theorem 5.1. In case V_h comes from a finite element discretization, a possible choice for \mathcal{I} is Lagrange interpolation.

If we now ensure that the partition of unity p_i is included in V_N , we can choose $\tilde{\varphi}$ in the definition of c_N as $\tilde{\varphi} := p_i \cdot |\tilde{\Omega}_i|^{-1} \int_{\tilde{\Omega}_i} \varphi$, which allows us to prove [BEOR17, Proposition 5.7] that c_N can be bounded by

$$c_N \leq \sqrt{4 + 2c_I^2 + 4(c_{\text{pu}}c_{\text{pc}})^2} \cdot \sqrt{c_{\text{ovlp}}}.$$

In this estimate $c_{\text{ovlp}} := \max_{x \in \Omega} \#\{i \in \Upsilon_E \mid x \in \Omega_i\}$ is the maximum number of estimator domains $\tilde{\Omega}_i$ overlapping in any point x of Ω , and c_{pc} is a Poincaré-inequality constant associated with $\tilde{\mathcal{T}}_H$. In particular, this result shows that the efficiency of (58) is independent from the number of subdomains in \mathcal{T}_H , provided that the partition of unity p_i is included in V_N .

Example 5.4 (scRBE method and interface reduction from [Sme15]). *We exemplify the a posteriori error estimator from Corollary 5.2 for the scRBE method, which*

is equally applicable when considering solely static condensation and no intra-element RB approximations.⁷ To simplify notations we define interface spaces $V_h^\gamma := \text{span}\{\psi_1^\gamma, \dots, \psi_{N_h^\gamma}^\gamma\}$, where $N_h^\gamma = \dim(V_h|_\gamma)$; for the definition of ψ_k^γ we refer to subsection 3.1. Recall that we then have the following space decomposition of the (global) finite element space V_h

$$(60) \quad V_h = \bigoplus_{m=1}^M V_{h;0}^m \oplus \left(\bigoplus_{\gamma \in \mathcal{T}_H^\gamma} V_h^\gamma \right).$$

We may thus uniquely rewrite every $\varphi \in V_h$ as

$$(61) \quad \varphi = \sum_{m=1}^M \varphi^m + \sum_{\gamma \in \mathcal{T}_H^\gamma} \varphi^\gamma$$

where $\varphi^m \in V_{h;0}^m$ and $\varphi^\gamma \in V_h^\gamma$, extending φ^m and φ^γ by zero. This allows us to define mappings $P_{V_{h;0}^m} : V_h \rightarrow V_{h;0}^m$, $\varphi \mapsto \varphi^m$ and $P_{V_h^\gamma} : V_h \rightarrow V_h^\gamma$, $\varphi \mapsto \varphi^\gamma$ as required in Theorem 5.1. Thanks to (20) we also obtain

$$V_{h;0}^m \perp V_{h;0}^{m'}, \quad m \neq m' \quad \text{and} \quad V_{h;0}^m \perp V_h^\gamma, \quad m = 1, \dots, \Omega, \gamma \in \mathcal{T}_H^\gamma.$$

It thus remains to verify that we can bound the constant c_N with V_N as defined in (27). To that end, we first note that thanks to (20) we have the following stability result [Sme15, Proposition 4.1]:

$$(62) \quad \|\varphi\|_V^2 = \sum_{m=1}^M \|\varphi^m\|_V^2 + \left\| \sum_{\gamma \in \mathcal{T}_H^\gamma} \varphi^\gamma \right\|_V^2.$$

We thus obtain

$$\begin{aligned} c_N &\leq \sup_{\varphi \in V_h \setminus \{0\}} \frac{\left(\sum_{m=1}^M \|\varphi^m\|_V^2 + \sum_{\gamma \in \mathcal{T}_H^\gamma} \inf_{\tilde{\varphi}^\gamma \in V_N^\gamma} \|\varphi^\gamma - \tilde{\varphi}^\gamma\|_V^2 \right)^{1/2}}{\|\varphi\|_V} \\ &\stackrel{(62)}{\leq} \sup_{\varphi \in V_h \setminus \{0\}} \frac{\left(\|\varphi\|_V^2 + \sum_{\gamma \in \mathcal{T}_H^\gamma} \inf_{\tilde{\varphi}^\gamma \in V_N^\gamma} \|\varphi^\gamma - \tilde{\varphi}^\gamma\|_V^2 \right)^{1/2}}{\|\varphi\|_V}, \end{aligned}$$

where $V_N^\gamma := \text{span}\{\psi_1^\gamma, \dots, \psi_{N_h^\gamma}^\gamma\}$. To show $\sum_{\gamma \in \mathcal{T}_H^\gamma} \inf_{\tilde{\varphi}^\gamma \in V_N^\gamma} \|\varphi^\gamma - \tilde{\varphi}^\gamma\|_V^2 \leq c \|\varphi\|_V$ for a constant c we choose $\tilde{\varphi}^\gamma$ such that $(\varphi^\gamma - \tilde{\varphi}^\gamma)|_\gamma$ equals the trace of φ minus the orthogonal projection on the kernel of the bilinear form; for further details see [BS18, SP16]. Then, we can use [SP16, Lemma B.4] to conclude boundedness of c_N and thus (59), the latter corresponding to [Sme15, Proposition 4.2 and Corollary 4.6].

Finally, we shortly discuss how to compute the dual norms of the residuals in (57). The dual norms of the residuals of the intra-element RB approximations can be computed by employing Riesz representations. The dual norms of the residuals in the interface space can be computed by means of conservative fluxes [HEML00],

⁷The error estimator in [Sme15] is derived for mutually disjoint interfaces. However, we conjecture that the estimator can be generalized to general decompositions of Ω .

which have been extended to interface reduction in [Sme15]. In detail, we compute the conservative flux $H_N^m(\boldsymbol{\mu})$ such that

$$(63) \quad \sum_{\gamma \in \overline{\Omega}_m} (H_N^m(\boldsymbol{\mu}), \psi^\gamma)_\gamma = f_m(\psi^\gamma; \boldsymbol{\mu}) - a_m(u_N(\boldsymbol{\mu}), \psi^\gamma; \boldsymbol{\mu}) \quad \forall \psi^\gamma \in \bigoplus_{\gamma \in \overline{\Omega}_m} V_h^\gamma,$$

where $(\cdot, \cdot)_\gamma$ denotes a suitable inner product on the interface γ . Note that thanks to our mutual disjoint interface assumption problem (63) decouples and we may compute the conservative flux separately for each interface γ . Moreover, by orthonormalizing the interface basis functions χ_k^γ defined in subsection 3.1 w.r.t the $(\cdot, \cdot)_\gamma$ inner product, the computation of $H_N^m(\boldsymbol{\mu})$ reduces to the assembling of the residual in (63). The computational costs thus scale linearly in $(N_h^\gamma - N^\gamma)$ and N^γ . For further details we refer to [Sme15].

5.2. Local flux reconstruction based error estimation. Following [OS15], we discuss local flux reconstruction based a posteriori error estimation of the full approximation error $u(\boldsymbol{\mu}) - u_N(\boldsymbol{\mu})$ (that is: the discretization as well as the model reduction error) in the context of non conforming approximations of elliptic multiscale problems such as Example 2.2. An extension to convection–diffusion–reaction problems based on [ESV10] is straightforward. This estimate was introduced in the IP localized non conforming setting of the LRBMS (compare Section 3.2.2).

Recalling the broken Sobolev space and broken gradient operator from Section 3.2.2, the key idea of flux reconstruction based error estimation is to observe that not only the approximate solution $u_N(\boldsymbol{\mu})$ is non conforming, but also the approximate diffusive flux $-\kappa(\boldsymbol{\mu})\nabla_h u_N(\boldsymbol{\mu})$, in the sense that it is not contained in $H_{\text{div}}(\Omega)$ (i.e., the space of functions in $L^2(\Omega)^d$ whose divergence exists in a weak sense and lies in $L^2(\Omega)$).

We may then obtain computable estimates by comparing these quantities with conforming reconstructions, as detailed further below.⁸ The respective reconstructed diffusive flux is locally conservative and is related to the conservative flux reconstruction to compute the dual norm of the residuals in the interface space in Example 5.4.

To begin with, we specify the parameter dependent (semi-)energy norm induced by the bilinear form a for a parameter $\bar{\boldsymbol{\mu}} \in \mathcal{P}$, $\|\cdot\|_{\bar{\boldsymbol{\mu}}} : H^1(\tau_h) \rightarrow \mathbb{R}$, $v \mapsto \|v\|_{\bar{\boldsymbol{\mu}}} := a(v, v; \bar{\boldsymbol{\mu}})^{\frac{1}{2}}$, (by using the broken gradient in the definition of a) and note that we can compare these semi norms for two parameters by means of the affine decomposition of a (compare (68)),

$$\underline{\Theta}_a(\boldsymbol{\mu}, \bar{\boldsymbol{\mu}})^{1/2} \|v\|_{\bar{\boldsymbol{\mu}}} \leq \|v\|_{\boldsymbol{\mu}} \leq \overline{\Theta}_a(\boldsymbol{\mu}, \bar{\boldsymbol{\mu}})^{\frac{1}{2}} \|v\|_{\bar{\boldsymbol{\mu}}},$$

with the equivalence constants given by $\underline{\Theta}_a(\boldsymbol{\mu}, \bar{\boldsymbol{\mu}}) := \min_{q=1}^{Q_a} \Theta_a^q(\boldsymbol{\mu}) \Theta_a^q(\bar{\boldsymbol{\mu}})^{-1}$ and $\overline{\Theta}_a(\boldsymbol{\mu}, \bar{\boldsymbol{\mu}}) := \max_{q=1}^{Q_a} \Theta_a^q(\boldsymbol{\mu}) \Theta_a^q(\bar{\boldsymbol{\mu}})^{-1}$, respectively. The first abstract result is the following discretization-agnostic lemma, which leaves the choice of the reconstructions, v and s , open. (We give estimates on the full V_h -norm at the end of this subsection.)

Lemma 5.5 (Abstract energy norm estimate (Lemma 4.1 in [OS15])). *For $\boldsymbol{\mu} \in \mathcal{P}$, let $u(\boldsymbol{\mu}) \in V$ denote the weak solution of (1) with the data functions κ and q as in*

⁸Note that all of the analysis holds for the FOM solution $u_h(\boldsymbol{\mu})$ as well as the ROM solution $u_N(\boldsymbol{\mu})$ (compare [OS15]), but we restrict the exposition to the latter. In particular, the presented estimates can thus also be used to steer grid adaptation of the FOM solution.

example 2.2. It then holds for arbitrary $v_N \in H^1(\tau_h)$ and $\bar{\boldsymbol{\mu}} \in \mathcal{P}$, that

$$\begin{aligned} & \| \|u(\boldsymbol{\mu}) - v_N\| \|_{\bar{\boldsymbol{\mu}}} \\ & \leq \Theta_a(\boldsymbol{\mu}, \bar{\boldsymbol{\mu}})^{-\frac{1}{2}} \left\{ \Theta_a(\boldsymbol{\mu}, \bar{\boldsymbol{\mu}})^{\frac{1}{2}} \inf_{v \in V} \| \|u(\boldsymbol{\mu}) - v\| \|_{\bar{\boldsymbol{\mu}}} \right. \\ & \quad \left. + \inf_{s \in H_{\text{div}}} \left(\sup_{\substack{\varphi \in V \\ |\varphi|_{a; \boldsymbol{\mu}} = 1}} \{ (q - \nabla \cdot s, \varphi)_{L^2(\Omega)} - (\kappa(\boldsymbol{\mu}) \nabla_h v_N + s, \nabla \varphi)_{L^2(\Omega)} \} \right) \right\} \\ & \leq \frac{\Theta_a(\boldsymbol{\mu}, \bar{\boldsymbol{\mu}})^{\frac{1}{2}}}{\Theta_a(\boldsymbol{\mu}, \bar{\boldsymbol{\mu}})} 2 \| \|u(\boldsymbol{\mu}) - v_N\| \|_{\bar{\boldsymbol{\mu}}}. \end{aligned}$$

To obtain a fully computable localizable estimate we need to specify the conforming reconstruction of the solution (v in the above lemma) and of the diffusive flux (s in the above lemma). We define both reconstructions w.r.t. the global fine grid τ_h and note, that their respective computations can be localized w.r.t. the domain decomposition to allow for offline/online decomposable localized estimates.

We reconstruct the non conforming solution $u_h(\boldsymbol{\mu}) \in V_h$ by means of its *Oswald interpolant* $I_{\text{OS}}[u_h(\boldsymbol{\mu})] \in V$. We define the corresponding Oswald interpolation operator $I_{\text{OS}} : V_h \rightarrow V_h \cap V$ by specifying its values on each Lagrange node ν of τ_h : given any $v_h \in V_h$, we set $I_{\text{OS}}[v_h](\nu) := v_h|_t(\nu)$ for any Lagrange node lying inside a grid element $t \in \tau_h$,

$$I_{\text{OS}}[v_h](\nu) := 0 \quad \text{for all boundary nodes and} \quad I_{\text{OS}}[v_h](\nu) := \frac{1}{|\tau_h^\nu|} \sum_{t \in \tau_h^\nu} v_h|_t(\nu)$$

for all nodes which are shared by multiple grid elements, which we collect in $\tau_h^\nu \subset \tau_h$.

The definition of the conforming reconstruction of the non conforming diffusive flux $-\kappa(\boldsymbol{\mu}) \nabla_h u_h(\boldsymbol{\mu}) \in L^2(\Omega)^d$ is more involved. Given $l \geq 0$, we define the l th order *Raviart-Thomas-Nédélec* space of vector valued functions by

$$RTN_h^l(\tau_h) := \{ s \in H_{\text{div}}(\Omega) \mid s|_t \in [\mathbb{P}_l(t)]^d + x \mathbb{P}_l(t) \quad \forall t \in \tau_h \}$$

and note that the DoFs of any $s_h \in RTN_h^l(\tau_h)$ are uniquely defined by specifying the moments of order up to $l-1$ of $s_h|_t$ on all elements $t \in \tau_h$ and the moments of order up to l of $s_h|_\sigma \cdot n_\sigma$ on all faces $\sigma \in \tau_h^\gamma$ (compare [BF91]). With these preliminaries we define the *diffusive flux reconstruction operator* $R_h^l : \mathcal{P} \rightarrow [V_h \rightarrow RTN_h^l(\tau_h)]$, given some $v_h \in V_h$ and some $\boldsymbol{\mu} \in \mathcal{P}$ by specifying the DoFs of $R_h^l[v_h; \boldsymbol{\mu}] \in RTN_h^l(\tau_h)$, such that

$$(64) \quad (R_h^l[v_h; \boldsymbol{\mu}] \cdot n_\sigma, r)_{L^2(\sigma)} = a_\sigma^c(v_h, r; \boldsymbol{\mu}) + (v_h, r)_\sigma^p \quad \text{for all } r \in \mathbb{P}_l(\sigma),$$

on all $\sigma \in \tau_h^\gamma$ and

$$(65) \quad (R_h^l[v_h; \boldsymbol{\mu}], \nabla r)_{L^2(t)} = -a^{\text{CG}}(R_h^l[v_h; \boldsymbol{\mu}]|_t, r; \boldsymbol{\mu}) - \sum_{\sigma \in \tau_h^\gamma \cap t} a_\sigma^c(r, v_h; \boldsymbol{\mu})$$

for all $\nabla r \in [\mathbb{P}_{l-1}(t)]^d$ with $r \in \mathbb{P}_l(t)$ on all $t \in \tau_h$. Given a FOM space V_h of polynomial order $k \geq 1$, we choose a $k-1$ st order reconstruction. With this definition, the reconstructed diffusive flux of a given a reduced solution $u_N(\boldsymbol{\mu})$ fulfills the following *local conservation* property, given that the constant function 1 is present in the local reduced spaces V_N^m :

$$(\nabla \cdot R_h^{k-1}[u_N(\boldsymbol{\mu}); \boldsymbol{\mu}], 1)_{L^2(\Omega_m)} = (q, 1)_{L^2(\Omega_m)}, \quad \text{for all } \Omega_m \in \mathcal{T}_H.$$

When inserting this diffusive flux reconstruction for s in lemma 5.5, this local conservation property is key to obtaining the following estimate.

Theorem 5.6 (Locally computable energy norm a posteriori estimate). *Let the domain decomposition \mathcal{T}_H from Definition 2.5 be such, that the Poincaré-inequality holds on each subdomain $\Omega_m \in \mathcal{T}_H$ with a constant $C_P^m > 0$,*

$$\|\varphi - \Pi_0^m \varphi\|_{L^2(\Omega_m)}^2 \leq C_P^m h_m^2 \|\nabla \varphi\|_{L^2(\Omega_m)}^2 \quad \text{for all } \varphi \in H^1(\Omega_m),$$

where $h_m := \text{diam}(\Omega_m)$ and where $\Pi_0^m \varphi$ denotes the mean value of φ over Ω_m . Let further $u(\boldsymbol{\mu}) \in V$ be the weak solution of (2) and $u_N(\boldsymbol{\mu}) \in V_N$ be the IP localized ROM solution, with $1 \in V_N^m$ for $1 \leq m \leq M$. It then holds for arbitrary $\bar{\boldsymbol{\mu}}, \hat{\boldsymbol{\mu}} \in \mathcal{P}$ that

$$\| |u(\boldsymbol{\mu}) - u_N(\boldsymbol{\mu})| |_{\bar{\boldsymbol{\mu}}} \leq \eta(\boldsymbol{\mu}; \bar{\boldsymbol{\mu}}; \hat{\boldsymbol{\mu}})$$

with the a posterior error estimator $\eta(\boldsymbol{\mu}; \bar{\boldsymbol{\mu}}; \hat{\boldsymbol{\mu}})$ given by

$$\begin{aligned} \eta(\boldsymbol{\mu}; \bar{\boldsymbol{\mu}}; \hat{\boldsymbol{\mu}}) := & \underline{\Theta}_a(\boldsymbol{\mu}, \bar{\boldsymbol{\mu}})^{-\frac{1}{2}} \left[\overline{\Theta}_a(\boldsymbol{\mu}, \bar{\boldsymbol{\mu}})^{\frac{1}{2}} \left(\sum_{\Omega_m \in \mathcal{T}_H} \eta_{\text{nc}}^{\Omega_m}(\boldsymbol{\mu}; \bar{\boldsymbol{\mu}})^2 \right)^{\frac{1}{2}} \right. \\ & \left. + \left(\sum_{\Omega_m \in \mathcal{T}_H} (\eta_r^{\Omega_m}(\boldsymbol{\mu}) + \underline{\Theta}_a(\boldsymbol{\mu}, \hat{\boldsymbol{\mu}})^{-1} \eta_{\text{df}}(\boldsymbol{\mu}; \hat{\boldsymbol{\mu}}))^2 \right)^{\frac{1}{2}} \right], \end{aligned}$$

and the local non conformity, residual and diffusive flux indicators given by

$$\begin{aligned} \eta_{\text{nc}}^{\Omega_m}(\boldsymbol{\mu}; \bar{\boldsymbol{\mu}}) &:= |(v_N(\boldsymbol{\mu}) - I_{\text{OS}}[v_N(\boldsymbol{\mu})])|_{\Omega_m}|_{\alpha; \bar{\boldsymbol{\mu}}}, \\ \eta_r^{\Omega_m}(\boldsymbol{\mu}) &:= \frac{C_P^m}{\kappa_{\Omega_m}}^{\frac{1}{2}} \|q - \nabla \cdot R_h^{k-1}[u_N(\boldsymbol{\mu}); \boldsymbol{\mu}]\|_{L^2(\Omega_m)} \quad \text{and} \\ (66) \quad \eta_{\text{df}}(\boldsymbol{\mu}; \hat{\boldsymbol{\mu}}) &:= \|\kappa(\hat{\boldsymbol{\mu}})^{-1} (\kappa(\boldsymbol{\mu}) \nabla_h u_N(\boldsymbol{\mu}) + R_h^{k-1}[u_N(\boldsymbol{\mu}); \boldsymbol{\mu}])\|_{L^2(\Omega_m)} \end{aligned}$$

respectively, where κ_{Ω_m} denotes the minimum eigenvalue of κ over Ω_m and \mathcal{P} .

We obtain an a posterior error estimate w.r.t. the V_h -norm or a full energy norm, $\| |\cdot| |_{\boldsymbol{\mu}} + (\sum_{\sigma \in \tau_h^\gamma} (\cdot, \cdot)_\sigma^p)^{\frac{1}{2}}$, by noting that $(u(\boldsymbol{\mu}), u(\boldsymbol{\mu}))_\sigma^p = 0$ for a weak solution $u(\boldsymbol{\mu})$ of sufficient regularity.

6. BASIS ENRICHMENT AND ONLINE ADAPTIVITY

Model order reduction is usually employed either (i) in the context of real-time decision making and embedded devices, or (ii) in the context of outer-loop applications, such as optimal control, inverse problems or Monte Carlo methods. In (i), one is usually interested in reduced spaces V_N of very low dimension to obtain ROMs as small as possible, at the possible expense of very involved offline computations. Here, localized model order reduction may help to reduce the latter, but we can usually not expect the resulting reduced space to be smaller than the one generated using traditional global model order reduction methods. In (ii), however, one is interested in a black-box-like approximation scheme which is queried for a huge amount of parameters, with a somehow “optimal” computational cost (including offline as well as online cost). Here, one may keep high-dimensional data throughout the computational process (offline as well as online), and it is in this context that localized model order reduction techniques may truly outperform other approaches. In the context of PDE constrained optimization this has been investigated e.g. in [OS17, OSS18, WFR19].

The localized a posteriori error estimation as discussed in Section 5 enables adaptive enrichment of the local reduced approximation spaces, whenever the quality of the reduced scheme is estimated to be insufficient – be it due to insufficient training due to lacking computational resources or due to limited knowledge about the range of possible parameters or due to other reasons altogether.

Let us thus assume that an initial (possibly empty) localized reduced approximation space V_N is given, compare Section 4. The goal of an adaptive enrichment is to enlarge the local solution spaces with additional modes that reflect non-local influences of the true solution such as channeling effect or singularities. Local adaptive basis enrichment can be employed both offline for the whole parameter range and/or online for a specific chosen parameter. Empirical training followed by offline enrichment is e.g. used in a Greedy manner for the basis construction in ArbiLoMod (cf. Example 5.3) in [BEOR17]. Adaptive enrichment for the GMsFEM is presented in [CEL14b, CEL18a] and online adaptive enrichment in [CEL15, CEL17b]. For the exposition in this section, we restrict to online enrichment as introduced [OS15], i.e. for local enrichment of the basis when a certain parameter is already chosen.

From a birds-eye perspective, we can think of an online adaptive reduced scheme as a p -adaptive FE scheme with problem adapted basis functions, where the local reduced bases are adapted during online enrichment.⁹ Thus, we can think of online enrichment in the usual Solve \rightarrow Estimate \rightarrow Mark \rightarrow Refine (SEMR) manner, well known in grid-adaptive discretization schemes. In the Estimate step we employ an a posteriori error estimate η that is localizable w.r.t. the domain decomposition, i.e. $\eta^2 \leq \sum_{m=1}^M \eta_m^2$, with appropriate local indicators η_m . Examples are given in Section 5. As such, most marking strategies from grid-adaptive schemes are applicable, and we give examples in Section 8.1. In this context, refinement is locally done by enriching the local reduced spaces, that is: by adding additional basis functions to the local reduced bases on selected subdomains. We thus presume we are given a parameter $\boldsymbol{\mu} \in \mathcal{P}$ and a reduced solution $u_N(\boldsymbol{\mu}) \in V_N$, the estimated error of which is above a given tolerance.

As an example, we detail the online enrichment procedure used in the context of the LRBMS (compare Section 3.2.2), using the a posteriori error estimation techniques from Section 5.2. Inspired by domain decomposition as well as numerical multiscale methods, we may then obtain a candidate for the next element of a local reduced basis by solving local corrector problems on a collection $\widetilde{\mathcal{T}}_H \subseteq \mathcal{T}_H$ of marked subdomains with $u_N(\boldsymbol{\mu})$ as boundary values. For each marked subdomain $\Omega_m \in \widetilde{\mathcal{T}}_H$, we denote by $\widetilde{\Omega}_m := \{\Omega_{m'} \in \mathcal{T}_H \mid \Omega_m \cap \Omega_{m'} \neq \emptyset\}$ an overlapping subdomain and by $V_h^{\widetilde{\Omega}_m} := \{v|_{\widetilde{\Omega}_m} \mid v \in V_h, v|_{\partial\widetilde{\Omega}_m} = 0\}$ the associated restricted FOM space, encoding zero Dirichlet boundary values. We are then looking for a local correction $\varphi^{\widetilde{\Omega}_m} \in V_h^{\widetilde{\Omega}_m}$, such that

$$(67) \quad a_h(\varphi^{\widetilde{\Omega}_m}, v_h; \boldsymbol{\mu}) = f_h(v_h; \boldsymbol{\mu}) - a_h(u_N(\boldsymbol{\mu})|_{\widetilde{\Omega}_m}, v_h; \boldsymbol{\mu}) \quad \text{for all } v_h \in V_h^{\widetilde{\Omega}_m},$$

where we understand all quantities to be implicitly extended to Ω by zero, if required, and note that $\varphi^{\widetilde{\Omega}_m}$ can be computed involving only quantities associated with $\widetilde{\Omega}_m$. Using this local correction on the overlapping subdomain, we obtain the next

⁹We would also like to mention the h -adaptive model order reduction approach from [Car15] which is based on a k -means clustering of the DoFs, but we restrict the exposition here to localization w.r.t. a domain decomposition.

Algorithm 6.1: Adaptive online enrichment in the context of the LRBMS.

Input : a marking strategy **MARK**, an orthonormalization procedure **ONB**, a localizable offline/online decomposable a posteriori error estimate $\eta(\boldsymbol{\mu})^2 \leq \sum_{m=1}^M \eta_m(\boldsymbol{\mu})^2$, local reduced bases Φ^m for $1 \leq m \leq M$, $\boldsymbol{\mu} \in \mathcal{P}$, $u_N(\boldsymbol{\mu})$, $\Delta_{\text{online}} > 0$

Output : Updated reduced solution

```

1  $\Phi^{m(0)} \leftarrow \Phi^m, \forall 1 \leq m \leq M$ 
2  $n \leftarrow 0$ 
3 while  $\eta(\boldsymbol{\mu}) > \Delta_{\text{online}}$  do
4   forall  $1 \leq m \leq M$  do
5      $\lfloor$  compute local error indicator  $\eta_m(\boldsymbol{\mu})$ 
6      $\widetilde{\mathcal{T}}_H \leftarrow \text{MARK}(\mathcal{T}_H, \{\eta_m(\boldsymbol{\mu})\}_{1 \leq m \leq M})$ 
7     forall  $\Omega_m \in \widetilde{\mathcal{T}}_H$  do
8        $\lfloor$  Solve (67) for  $\varphi^{\widetilde{\Omega}_m}$   $\Phi^{m(n+1)} \leftarrow \text{ONB}(\{\Phi^{m(n)}, (\varphi^{\widetilde{\Omega}_m} + u_N(\boldsymbol{\mu}))|_{\Omega_m}\})$ 
9       update all reduced quantities (system matrices, error estimates) w.r.t. the
        newly added basis elements
10       $\lfloor$  solve (12) for the reduced solution  $u_N(\boldsymbol{\mu})$  using the updated quantities
11 return  $u_N(\boldsymbol{\mu})$ 

```

element of the local reduced basis associated with Ω_m by an orthonormalization of $(\varphi^{\widetilde{\Omega}_m} + u_N(\boldsymbol{\mu}))|_{\Omega_m}$ with respect to the existing basis on V_N^m .

Given a marking strategy and an orthonormalization procedure, we summarize the adaptive online enrichment used in the context of the LRBMS in Algorithm 6.1.

7. COMPUTATIONAL ASPECTS

In this section we discuss the computational efficiency of localized model order reduction schemes in comparison to standard, non-localized techniques. Imposing a localization constraint on the reduced space naturally yields sub-optimal spaces in the sense of Kolmogorov N -width. However, this is mitigated by the sparse structure of the resulting reduced system matrices. In particular, for problems with large-dimensional parameter domains with localized influence of each parameter component on the solution, we can expect localized ROMs to show comparable or even better online efficiency in comparison to a standard ROM. In addition, localized model order reduction provides more flexibility to balance computational and storage requirements between the offline and online phase and has thus the potential to be optimized with respect to the specific needs. This is particularly favorable for large-scale or multiscale problems, where global snapshot computations are extremely costly or even prohibitive.

In the offline (and enrichment) phase of the localized schemes, only relatively small-dimensional local problems are solved instead of the computation of global solution snapshots. In comparison to a global reduction approach with a parallel solver for snapshot generation (e.g. a domain decomposition scheme), the preparation of the local reduced spaces via training (Section 4) can be performed almost communication-free, allowing the application of these schemes on parallel compute architecture without fast interconnect such as cloud environments. Via adaptive enrichment

of the approximation spaces – based on the solution of local correction problems (Section 6) – smaller and more efficient ROMs can be obtained. In comparison to domain-decomposition methods, where similar correction problems are solved, these correction problems are only solved in regions of the domain where the approximation space is insufficient. Thus, for problems with a localized effect of the parameterization, a significant reduction of the computational effort can be expected in the reduced basis generation process.

In the context of component-based localized model order reduction (e.g. CMS, scRBE, RBHM, RDF) large computational savings can be achieved by the preparation of local approximation spaces (components) w.r.t. arbitrary neighboring components (connected through so-called ports). In addition to parametric changes of the governing equations or computational domain, this allows the (non-parametric) recombination of components in arbitrary new configurations without requiring additional offline computations.

7.1. Online efficiency. In view of Definition 2.8, we can interpret the localized model order reduction methods introduced in Section 3 as standard projection based model reduction methods – such as the reduced basis method – subject to the constraint that the reduced space V_N admits a localizing decomposition of the form (11). As such, the usual offline/online decomposition methodology can be applied. To this end, let us assume that the bilinear form $a(\cdot, \cdot; \boldsymbol{\mu})$ and the source functional $f(\cdot; \boldsymbol{\mu})$ admit affine decompositions

$$(68) \quad a(v, w; \boldsymbol{\mu}) = \sum_{q=1}^{Q_a} \Theta_q^a(\boldsymbol{\mu}) a^q(v; w), \quad f(w; \boldsymbol{\mu}) = \sum_{q=1}^{Q_f} \Theta_q^f(\boldsymbol{\mu}) f^q(w),$$

for all $v, w \in V$, $\boldsymbol{\mu} \in \mathcal{P}$ with non-parametric bilinear forms $a^q : V \times V \rightarrow \mathbb{R}$, functionals $f^q \in V'$ and some parameter functionals $\Theta_q^a, \Theta_q^f : \mathcal{P} \rightarrow \mathbb{R}$. If the given problem is not of the form (68), we can employ empirical interpolation [BMNP04] to compute an approximate affine decomposition.

We begin by computing the reduced approximation space V_N using the methods outlined in Section 4. After that, a reduced model is assembled by computing matrix representations $\mathbb{A}^q \in \mathbb{R}^{N \times N}$ of a^q and vector representations $\mathbb{F}^q \in \mathbb{R}^N$ of f^q w.r.t. a given basis $\varphi_1, \dots, \varphi_N$ of V_N , i.e.

$$(69) \quad \mathbb{A}_{ij}^q := a^q(v_j, w_i), \quad \mathbb{F}_i^q := f^q(w_i).$$

After this computationally demanding offline phase, the coordinate representation $\mathbb{U}_N(\boldsymbol{\mu}) \in \mathbb{R}^N$ of the reduced solution $u_N(\boldsymbol{\mu})$ of (12) is quickly obtained for arbitrary new parameters $\boldsymbol{\mu}$ by solving

$$(70) \quad \sum_{q=1}^{Q_a} \Theta_q^a(\boldsymbol{\mu}) \mathbb{A}^q \cdot \mathbb{U}_N(\boldsymbol{\mu}) = \sum_{q=1}^{Q_f} \Theta_q^f(\boldsymbol{\mu}) \mathbb{F}^q$$

in the following online phase. The computational effort to determine $u_N(\boldsymbol{\mu})$ is of order

$$(71) \quad \mathcal{O}(Q_a N^2 + Q_f N) + \mathcal{O}(N^3)$$

for the assembly and solution of the dense equation system (70). In particular, we have obtained full offline/online splitting, i.e. the effort to obtain $\mathbb{U}_N(\boldsymbol{\mu})$ is independent of $\dim V_h$. From $\mathbb{U}_N(\boldsymbol{\mu})$ we can then either reconstruct $u_N(\boldsymbol{\mu})$ by linear combination with the reduced basis or evaluate arbitrary linear functionals of $u_N(\boldsymbol{\mu})$

by additionally computing vector representations of these functionals in the offline phase.

RB methods aim at constructing reduced spaces V_N which are near-optimal approximation spaces for the discrete solution manifold $\{u_h(\boldsymbol{\mu}) \mid \boldsymbol{\mu} \in \mathcal{P}\}$ in the sense of Kolmogorov, i.e. it should hold that

$$(72) \quad \sup_{\boldsymbol{\mu} \in \mathcal{P}} \inf_{v \in V_N} \|u_h(\boldsymbol{\mu}) - v\| \approx d_N := \inf_{\substack{W \subseteq V_h \\ \dim W = N}} \sup_{\boldsymbol{\mu} \in \mathcal{P}} \inf_{v \in W} \|u_h(\boldsymbol{\mu}) - v\|,$$

where d_N is the Kolmogorov N -width of the solution manifold. Localized RB methods aim at reducing the computational effort of the offline phase by replacing the computation of solution snapshots $u_h(\boldsymbol{\mu})$ of the global discrete full order model by solutions of smaller localized problems associated with the domain \mathcal{T}_H (see below). This comes at the expense of replacing the set of all N -dimensional subspaces of V_h by the smaller set of all N -dimensional subspaces of V_h of the form (11), i.e. we aim at constructing V_N with

$$(73) \quad \sup_{\boldsymbol{\mu} \in \mathcal{P}} \inf_{v \in V_N} \|u_h(\boldsymbol{\mu}) - v\| \approx d_N^{loc} := \inf_{\substack{W \subseteq V_h \\ \dim W = N \\ W \text{ satisf. (11)}}} \sup_{\boldsymbol{\mu} \in \mathcal{P}} \inf_{v \in W} \|u_h(\boldsymbol{\mu}) - v\|.$$

As $d_N^{loc} > d_N$, localized RB methods generally result in larger V_N to satisfy a given approximation error tolerance ε . Since we can represent any basis vector of a global RB approximation of (10) w.r.t. the localizing space decomposition (9) as a sum of $M^{tot} := M + \#\mathcal{T}_H^\gamma + \#\mathcal{T}_H^e + \#\mathcal{T}_H^v$ local vectors, we have the a priori bound $d_{M^{tot}, N}^{loc} < d_N$. In other words, if we denote by N (N^{glob}) the number of reduced basis vectors required for a localized (global) RB approximation for given ε and denoting by N^{loc} the maximum dimension of the local RB spaces $V_N^m, V_N^\gamma, V_N^e, V_N^v$, we have

$$(74) \quad N \leq N^{loc} M^{tot} \leq N^{glob} M^{tot} \leq C_{\mathcal{T}_H} M N^{glob}.$$

where the constant $C_{\mathcal{T}_H}$ only depends on the topology of the domain decomposition \mathcal{T}_H . Whether or not estimate (74) is sharp largely depends on the dependence of the solution $u(\boldsymbol{\mu})$ on the parameter $\boldsymbol{\mu}$. When a change in $\boldsymbol{\mu}$ equally affects the solution in all subdomains Ω_m , we expect that optimal local RB spaces will be of similar dimension N^{loc} and that $N^{loc} \approx N^{glob}$. On the other hand, it may be the case that the influence of $\boldsymbol{\mu}$ on $u(\boldsymbol{\mu})$ is weak in many Ω_m , in which case $N \ll N^{loc} M^{tot}$, or that each of the p components of $\boldsymbol{\mu} \in \mathbb{R}^p$ affects $u(\boldsymbol{\mu})$ on different subdomains, in which case $N^{loc} M^{tot} \ll N^{glob} M^{tot}$. Thus, the actual loss in online efficiency due to localization will strongly depend on the type of problem to be solved.

More importantly though, note that the localization of V_N results in a change of the structure of the reduced system matrices \mathbb{A}^q . While these matrices are dense for global RB approximations, localized RB schemes yield \mathbb{A}^q with a sparse block structure of $M^{tot} \times M^{tot}$ blocks of maximum dimension $N^{loc} \times N^{loc}$ and a maximum of C_{cup} blocks per row. C_{cup} depends on the specific localization method and on the topology of \mathcal{T}_H . For instance, for non-conforming methods, $C_{cup} - 1$ is given by the maximum number of interfaces of a given subdomain Ω_m , whereas for the ArbiLoMod with a quadrilateral mesh $C_{cup} = 25$.

Thus, estimate (74) has to be interpreted in relation to the fact that the computational complexity for solving (70) can be vastly reduced in comparison to (71) by exploiting the structure of the \mathbb{A}^q . In particular, the costs for assembling (70) can be reduced to $\mathcal{O}(C_{\mathcal{T}_H} C_{cup} (N^{loc})^2 M)$. For the solution of (70) direct or

block-preconditioned iterative solvers can be used. For the latter, the computational effort can be expected to increase sub-quadratically in the number of subdomains M . In the scRBE method, the volume degrees of freedom associated with the spaces V_N^m are eliminated from (70) using static condensation to improve computational efficiency.

7.2. Offline costs and parallelization. While the local RB spaces V_N^m , V_N^γ , V_N^e , V_N^v can be initialized by decomposing global solution snapshots $u_h(\boldsymbol{\mu})$ w.r.t. (9) (see [AHKO12]), the core element of localized RB methods is the construction of local RB spaces from local problems associated with the subdomains Ω_m as described in Section 4. This has various computational benefits:

First, we can expect a reduction of computational complexity as for most linear solvers we expect a super-linear increase in computational complexity for an increasing dimension of V_h , whereas the ratio of the dimensions of V_h and the local subspaces in (9) remains constant of order $1/M$ (for the volume spaces V_h^m and smaller for the spaces V_h^γ , V_h^e , V_h^v) as $h \rightarrow 0$. Thus, solving $\mathcal{O}(MN^{loc})$ training problems of size $\dim V_h/M$ is expected to be faster than solving N global problems. At the same time, we expect N^{loc} to decrease for $H \rightarrow h$. Thus smaller subdomains Ω_m will generally lead to shorter offline times at the expense of less-optimal spaces V_N . In particular, for the non-conforming schemes in Subsection 3.2.2 it is readily seen that for $H = h$ we have $V_N = V_h$ and that (12) and (10) are equivalent.

Even more important than a potential reduction of complexity is the possibility to choose H small enough such that each local training problem can be solved communication-free on a single compute node without the need for a high-performance interconnect. Also the problem setup and the computation of the reduced system (70) can be performed mostly communication-free: Instead of instantiating a global fine-scale compute mesh, each compute node can generate a local mesh from a geometry definition, solve training problems for a given local RB space and all coupling spaces to obtain corresponding block-entries in \mathbb{A}^q , \mathbb{F}^q . Only the local geometry and the resulting reduced-order quantities are communicated (see [BEOR17, Section 8]). This makes localized RB methods attractive for cloud-based environments, where large computational resources can be dynamically made available, but communication speed is limited.

Depending on the problem structure, the use of online enrichment (Section 6) can yield smaller, problem adapted reduced spaces V_N . Similar to the training of V_N , online enrichment is based on the solution of small independent local problems, that can easily be parallelized. As typically only some fraction of the subspaces of V_N undergo enrichment, less computational resources need to be allocated during an online-enrichment phase. It has to be noted, however, that online enrichment leads to a propagation of snapshot data through the computational domain as the value of the current solution $u_N(\boldsymbol{\mu})$ at the boundary of the enrichment-problem domain enters the problem definition. Thus, to perform online-enrichment, (boundary values of) reduced basis vectors have to be communicated between compute nodes and the entire reduced basis has to be kept available.

8. APPLICATIONS AND NUMERICAL EXPERIMENTS

8.1. Multiscale problems. We demonstrate the IP localized RB methods from Section 3.2.2 in the context of parametric multiscale problems, such as Example 2.2, with a focus on online adaptivity as in Section 6 (using the a posteriori error

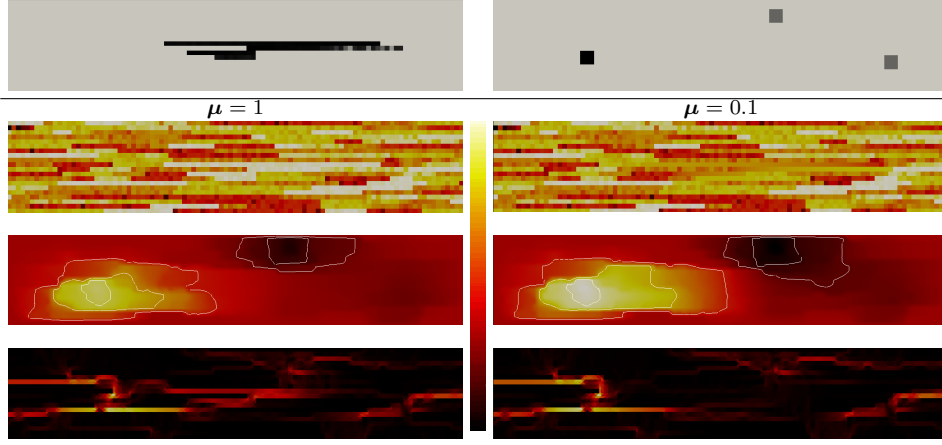


FIGURE 6. Data functions and sample solutions of the experiment in Section 8.1. First row: location of the channel function λ_c (left) and plot of the force f (right) modeling one source (black: $2 \cdot 10^3$) and two sinks (dark gray: $-1 \cdot 10^3$, zero elsewhere). Second to fourth row: both plots in each row share the same color map (middle) with different ranges per row, for parameters $\mu = 1$ (left column) and $\mu = 0.1$ (right column). From top to bottom: logarithmic plot of $\lambda(\mu)\kappa_\varepsilon$ (dark: $1.41 \cdot 10^{-3}$, light: $1.41 \cdot 10^3$), plot of the pressure $u_h(\mu)$ (IP localized FOM solution of (2), dark: $-3.92 \cdot 10^{-1}$, light: $7.61 \cdot 10^{-1}$, isolines at 10%, 20%, 45%, 75% and 95%) and plot of the magnitude of the reconstructed diffusive flux $R_h^0[u_h(\mu); \mu]$ (defined in (64) and (65), dark: $3.10 \cdot 10^{-6}$, light: $3.01 \cdot 10^2$). Note the presence of high-conductivity channels in the permeability (second row left, light regions) throughout large parts of the domain. The parameter dependency models a removal of one such channel in the middle right of the domain (second row right), well visible in the reconstructed Darcy velocity fields (bottom).

estimate from Section 5.2), rather than offline training. These experiments were first published in the context of the online adaptive LRBMS in [OS15]. We consider a multiplicative splitting of the parameter dependency and the multiscale nature of the data functions, in the sense that $\kappa(\mu) := \lambda(\mu)\kappa_\varepsilon$, with a parametric total mobility $\lambda : \mathcal{P} \rightarrow L^\infty(\Omega)$ and a highly heterogeneous permeability field $\kappa_\varepsilon \in L^\infty(\Omega)^{d \times d}$. To be more precise, we consider (2) on $\Omega = [0, 5] \times [0, 1]$ with $f(x, y) = 2 \cdot 10^3$ if $(x, y) \in [0.95, 1.10] \times [0.30, 0.45]$, $f(x, y) = -1 \cdot 10^3$ if $(x, y) \in [3.00, 3.15] \times [0.75, 0.90]$ or $(x, y) \in [4.25, 4.40] \times [0.25, 0.40]$ and 0 everywhere else, $\lambda(x, y; \mu) = 1 + (1 - \mu)\lambda_c(x, y)$, homogeneous Dirichlet boundary values and a parameter space $\mathcal{P} = [0.1, 1]$. On each $t \in \tau_h$, $\kappa_\varepsilon|_t$ is the corresponding 0th entry of the permeability tensor used in the first model of the 10th SPE Comparative Solution Project (which is given by 100×20 constant tensors, see [SPE01]) and λ_c models a channel, as depicted in Fig. 6, top left.

The right hand side f models a strong source in the middle left of the domain and two sinks in the top and right middle of the domain, as is visible in the structure of

the solutions (see Fig. 6, third row). The role of the parameter μ is to toggle the existence of the channel λ_c . Thus $\lambda(1)\kappa_\varepsilon = \kappa_\varepsilon$ while $\mu = 0.1$ models the removal of a large conductivity region near the center of the domain (see the second row in Fig. 6). This missing channel has a visible impact on the structure of the pressure distribution as well as the reconstructed velocities, as we observe in the last two rows of Fig. 6. With a contrast of 10^6 in the diffusion tensor and an ε of about $|\Omega|/2,000$ this setup is a challenging heterogeneous multi-scale problem.

We used several software packages for this numerical experiment and refer to [OS15] for a full list and instructions on how to reproduce these results. We would like to mention that all grid-related structures (such as data functions, operators, functionals, products, norms) were implemented in a DUNE-based C++ discretization (which is by now contained in the DUNE extension modules¹⁰ and the generic discretization toolbox `dune-gdt`¹¹), while we used `pyMOR` [MRS16] for everything related to model reduction (such as Gram-Schmidt, Greedy). We consider a domain decomposition of $|\mathcal{T}_H| = 25 \times 5$ squares, each refined such that the full global grid would consist of $|\tau_h| = 1,014,000$ elements. For the IP localized FOM, following Section 3.2.2, we choose on each subdomain $\Omega_m \in \mathcal{T}_H$ the DG space (1st order), product and bilinear form from example 3.2. For error estimation, we employed the flux reconstruction ansatz from Section 5.2 using a zero order diffusive flux reconstruction (compare Theorem 5.6).

The sole purpose of these experiments is to demonstrate the capabilities of localized RB methods regarding online enrichment. We thus initialize the local reduced spaces V_N^m on each subdomain a priori by orthonormalized Lagrangian shape functions of order up to one, thus obtaining a reduced space with poor approximation properties (comparable to a standard DG space w.r.t. the domain decomposition). Since we employ the a posteriori error estimate η on the full approximation error (including the discretization as well as the model reduction error) from Theorem 5.6, and since we omit grid-refinement in these experiments, the estimated discretization error over all parameters of 1.66 is a lower bound for the overall approximation error, and we thus choose a tolerance of $\Delta_{\text{online}} = 2$ for the online enrichment in Algorithm 6.1.

We compare two different strategies, corresponding to the two plots in Fig. 7. In both cases, we simulate an outer-loop application in the online part by randomly choosing ten parameters $\mathcal{P}_{\text{online}} \subset \mathcal{P}$ which are subsequently processed. For each parameter, the local reduced spaces are enriched according to Algorithm 6.1 and the respective marking strategy, until the estimated error is below the specified tolerance. Note that the evaluation of the localizable a posteriori error estimate can be fully offline/online decomposed and that after each enrichment only information from a subdomain and its neighbors are required to locally update the offline/online decomposed data.

In the first experiment, we use a uniform marking strategy, which results in an unconditional enrichment on each subdomain (comparable to domain decomposition methods). As we observe in Fig. 7 (top), however, it takes 129 enrichment steps to lower the estimated error below the desired tolerance for the first online parameter μ_0 . After this extensive enrichment it takes 12 steps for μ_1 and none or one enrichment steps to reach the desired tolerance for the other online parameters.

¹⁰<https://github.com/dune-community/dune-xt-common/>

¹¹<https://github.com/dune-community/dune-gdt/>

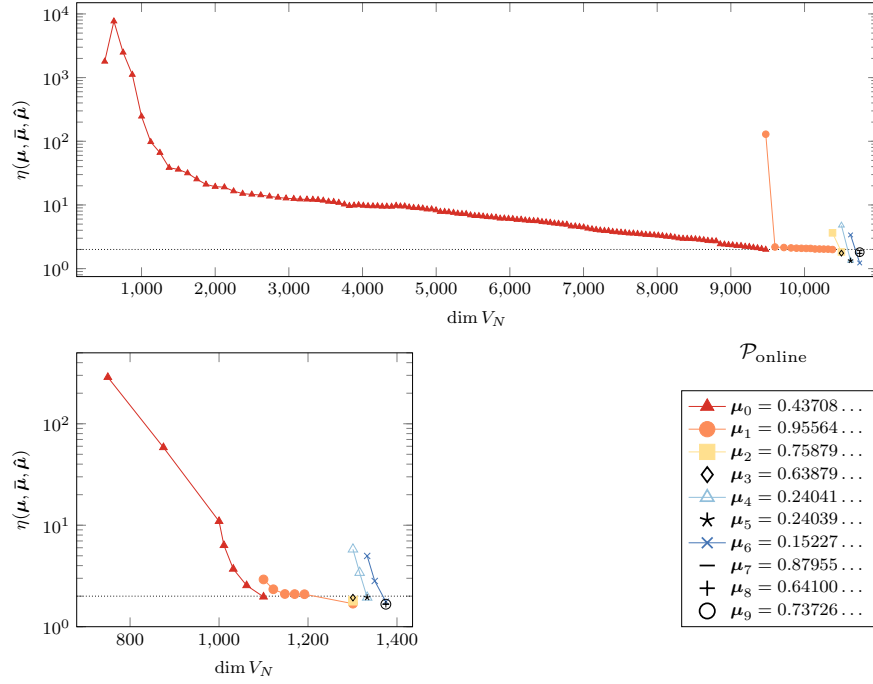


FIGURE 7. Estimated error evolution during the adaptive online phase for the experiment in Section 8.1 with $|\mathcal{T}_H| = 125$, $k_H = 1$, $\Delta_{\text{online}} = 2$ (dotted line), $\bar{\mu} = \hat{\mu} = 0.1$, for different on-line and offline strategies: no global snapshot (greedy search disabled, $N_{\text{greedy}} = 0$) during the offline phase, uniform marking during the online phase (top) and two global snapshots (greedy search on $\mathcal{P}_{\text{train}} = \{0.1, 1\}$, $N_{\text{greedy}} = 2$) and combined uniform marking while $\eta(\mu, \bar{\mu}, \hat{\mu}) > \theta_{\text{uni}} \Delta_{\text{online}}$ with $\theta_{\text{uni}} = 10$, Dörfler marking with $\theta_{\text{doerf}} = 0.85$ and age-based marking with $N_{\text{age}} = 4$ (bottom left); note the different scales. With each strategy the local reduced bases are enriched according to Algorithm 6.1 while subsequently processing the online parameters μ_0, \dots, μ_9 (bottom right).

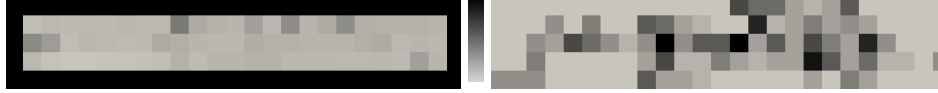


FIGURE 8. Spatial distribution of the final sizes of the local reduced bases on each subdomain, after the adaptive online phase for the experiment in Section 8.1 with $\Omega = [0, 5] \times [0, 1]$, $|\mathcal{T}_H| = 25 \times 5$ for the two strategies shown in Fig. 7: no global snapshot with uniform enrichment (left, light: 24, dark: 148) and two global snapshots with adaptive enrichment (right, light: 9, dark: 20). Note the pronounced structure (right) reflecting the spatial structure of the data functions (compare Fig. 6).

The resulting coarse reduced space is of size 10,749 (with an average of 86 basis functions per subdomain), which is clearly not optimal. Although each subdomain was marked for enrichment, the sizes of the final local reduced bases differ since the local Gram Schmidt basis extension may reject updates (if the added basis function is locally not linearly independent). As we observe in Fig. 8 (left) this is indeed the case with local basis sizes ranging between 24 and 148. Obviously, a straightforward domain decomposition ansatz without suitable training is not feasible for this setup. This is not surprising since the data functions exhibit strong multiscale features and non-local high-conductivity channels connecting domain boundaries, see Fig. 6.

To remedy the situation we allow for two global snapshots during the offline phase (for parameters $\mu \in \{0.1, 1\}$) and use an adaptive marking strategy which combines uniform marking, Dörfler marking and age-based marking (see the caption of Fig. 7) in the online phase. This strategy employs uniform marking until a saturation condition is reached, and afterwards uses a Dörfler marking combined with a marking based on counting how often a subdomain has not been marked. With two global solution snapshots incorporated in the basis the situation improves significantly, as we observe in Fig. 7 (bottom left). In total we observe only two enrichment steps with uniform marking (see the first two steps for μ_0), which indicates that further offline training would be beneficial. The number of elements marked range between 11 and 110 (over all online parameters and all but the first two enrichment steps) with a mean of 29 and a median of 22. Of these marked elements only once have 87 out of 110 elements been marked due to their age (see the last step for μ_1). Overall we could reach a significantly lower overall basis size than in the previous setup (1,375 vs. 10,749) and the sizes of the final local bases range between only nine and 20 (compared to 24 to 148 above). We also observe in Fig. 8 (right) that the spatial distribution of the basis sizes follows the spatial structure of the data functions (compare Fig. 6), which nicely shows the localization qualities of our error estimator.

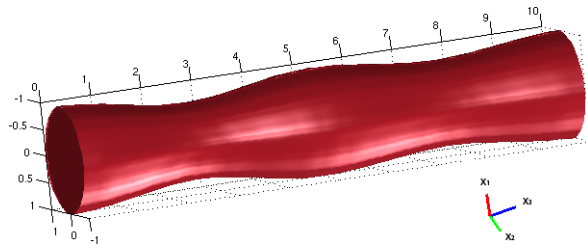


FIGURE 9. Computational domain ($\mu_1 = 7, \mu_2 = 10$).

8.2. Fluid dynamics. Flow simulations in pipelined channels have a growing interest in many biological and industrial applications. The localized model order reduction approaches presented in this chapter are suitable for the study of internal flows in hierarchical parametrized geometries. In particular, the non-conforming approach introduced in Section 3.2 has applications in the analysis of the blood flow in specific compartments of the circulatory system that can be represented as a combination of few deformed vessels from a reference one.

We want to solve the Stokes equation defined in (3), with $\delta = 0$, in a computational domain Ω composed by two stenosed blocks Ω_{μ_1} and Ω_{μ_2} (Fig. 9), by imposing

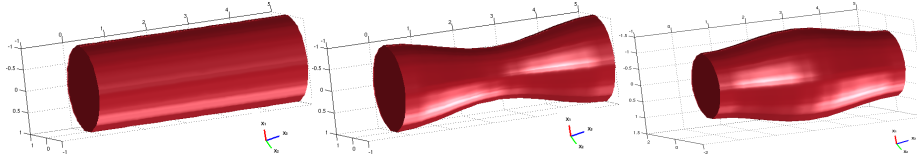


FIGURE 10. Reference pipe and two deformed pipes ($\mu = -5, \mu = 5$): stenosis and aneurysm configuration.

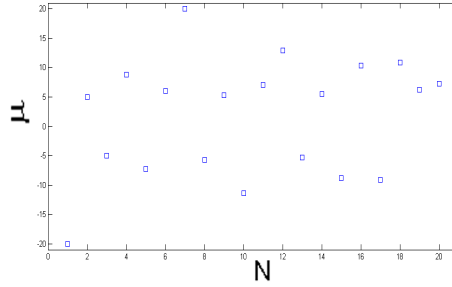


FIGURE 11. Distribution of the selected parameter values by the greedy algorithm used to generate the basis functions in a single block.

non-homogeneous BCs $\sigma_n^{in} = [0, 5]^T$ in the inlet surface ($x_1 = 10$), non-homogeneous BCs $\sigma_n^{in} = [0, -1]^T$ in the outlet surface ($x_1 = 0$) and homogeneous Dirichlet BC on the remaining boundaries of the domain. Here, the Taylor-Hood Finite Element Method has been used to compute the basis functions, \mathbb{P}_2 elements for velocity and supremizer, \mathbb{P}_1 for pressure, respectively and consequently $\mathbb{P}_1(\Gamma_{m,m'})$ for the Lagrange multipliers space. Fig. 11 shows the distribution of the parameter values selected by the greedy algorithm, by applying the offline stage of the reduced basis method to the single stenosis block. By taking into account that the range $[-5, 5]$ is not admitted, we can see that the higher concentration of values is in the intervals $[-10, -5]$ and $[5, 10]$ in correspondence to larger deformation of the pipe.

The geometry of a single stenosis is obtained by the deformation of a reference pipe through a parameter that represents the contraction in the middle of the pipe. The deformed domain Ω_μ is mapped from the straight reference pipe $\hat{\Omega}$ of length $L = 5$ and radius $r = 1$ through the following coordinate transformation $T_\mu : \hat{\Omega} \rightarrow \Omega_\mu$ such

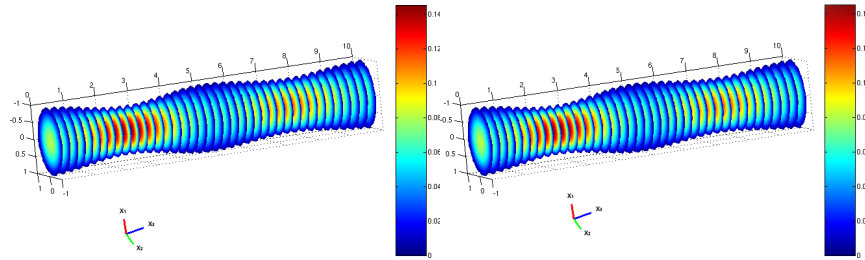


FIGURE 12. Representative solutions of velocity using RBHM (with $N_1 = 7, N_2 = 19$) (left) and using FEM as a global solution (right), $\mu_1 = 7, \mu_2 = 10$.

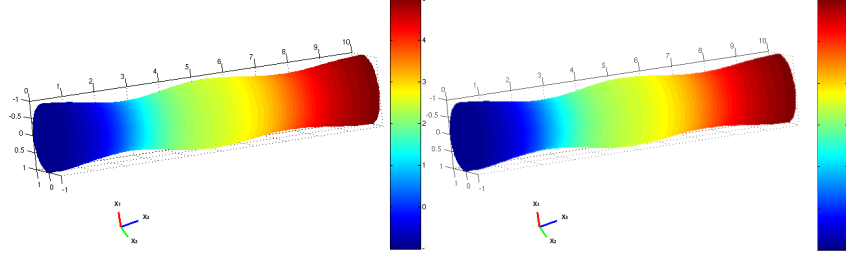


FIGURE 13. Representative solutions pressure using RBHM (with $N_1 = N_2 = 19$) (left) and using FEM as a global solution (right), $\mu_1 = 7, \mu_2 = 10$.

as $\mathbf{x} = T_\mu(\hat{\mathbf{x}})$ and $x_1 = \hat{x}_1 + \frac{\hat{x}_1}{\mu}(\cos(\frac{2\pi\hat{x}_3}{L}) - 1)$, $x_2 = \hat{x}_2 + \frac{\hat{x}_2}{\mu}(\cos(\frac{2\pi\hat{x}_3}{L}) - 1)$, $x_3 = \hat{x}_3$. The range of the parameter μ is $[-20, -5] \cup [5, 20]$, Fig. 10 shows the reference pipe and some representative deformations of the geometry. In order to compute the basis functions, we consider a parametrized Stokes problem for each subdomain. For the first subdomain, we compute the reduced basis imposing zero Dirichlet condition on the wall, Neumann boundary conditions given by imposing $\sigma_n = \sigma \cdot \mathbf{n} = \nu \frac{\partial \mathbf{u}}{\partial \mathbf{n}} - p \mathbf{n}$ to be $\sigma_n^{in} = [0, 5]^T$ on Γ_{in} and $\sigma_n^{out} = \mathbf{0}$ on the internal interface. For the second subdomain, we compute the reduced basis imposing zero Dirichlet condition on the wall, Neumann boundary conditions imposing $\sigma_n^{in} = \mathbf{0}$ on the internal interface and $\sigma_n^{out} = [0, -1]^T$ on the outflow interface Γ_{out} .

Moreover, we enrich the local RB spaces by a coarse finite element solution of the problem computed in the global domain. This strategy ensures not only the continuity of the velocity, but also the one of the normal stress along the internal interface. For this reason this method is called reduced basis hybrid method. Coarse and fine grids have been chosen in order to deal with respectively 155 and 2714 nodes in a single block domain. Fig. 12 shows a representative flow solution in Ω , found with the reduced basis hybrid method, to be compared with the finite element solution. The same comparison, regarding the pressure solutions, is shown in Fig. 13.

9. FURTHER PERSPECTIVES

9.1. Parabolic problems. Most of the techniques presented in this chapter so far can be extended or even directly applied to parabolic problems. For instance, local approximation spaces that are optimal in the sense of Kolmogorov are proposed in [Sch19] and the LRBMS for parabolic problems is presented in [ORS17, OR17]. To facilitate an adaptive construction of the local reduced space or online-adaptivity, a suitable, localized a posteriori error estimator is key. Therefore, we present in this subsection an abstract framework for a posteriori error estimation for approximations of scalar parabolic evolution equations, based on elliptic reconstruction techniques. For further reading and the application to localized model reduction we refer to [GLV11, ORS17].

Definition 9.1 (Parameterized parabolic problem in variational form). *Let a Gelfand triple of suitable Hilbert spaces $V \subset H = H' \subset V'$, an end time $T_{end} > 0$, initial data $u_0 \in V$ and right hand side $f \in H$ be given. For a parameter $\boldsymbol{\mu} \in \mathcal{P}$ find*

$u(\cdot; \boldsymbol{\mu}) \in L^2(0, T_{end}; V)$ with $\partial_t u(\cdot; \boldsymbol{\mu}) \in L^2(0, T_{end}; V')$, such that $u(0; \boldsymbol{\mu}) = u_0$ and

$$(75) \quad \langle \partial_t u(t; \boldsymbol{\mu}), q \rangle + a(u(t; \boldsymbol{\mu}), v; \boldsymbol{\mu}) = f(v; \boldsymbol{\mu}) \quad \text{for all } v \in V.$$

Depending on the error we want to quantify, the space V in (75) can be either a analytical function space as in (1) or an already discretized function space V_h . We drop the parameter dependency in this section to simplify the notation.

Definition 9.2 (Approximations of the parabolic problem). *Let $\tilde{V} \subseteq H$ be a finite dimensional approximation space for V , not necessarily contained in V . Potential candidates for \tilde{V} are conforming or non-conforming localized model reduction spaces V_N as discussed above, but also finite element or finite volume spaces fit into this setting. Denote by (\cdot, \cdot) , $\|\cdot\|$ the H -inner product and the norm induced by it.*

Let $f \in H$, and let $a_h : (V + \tilde{V}) \times (V + \tilde{V}) \rightarrow \mathbb{R}$ be a discrete bilinear form which coincides with a on $V \times V$ and is thus continuous and coercive on V . Let further $\|\cdot\|$ be a norm over $V + \tilde{V}$, which coincides with the square root of the symmetric part of a_h over V .

Our goal is to bound the error $e(t) := u(t) - \tilde{u}(t)$ between the analytical (or discrete) solution $u \in L^2(0, T_{end}; V)$, $\partial_t u \in L^2(0, T_{end}; V')$ of (75), where the duality pairing $\langle \partial_t u(t), v \rangle$ is induced by the H -scalar product via the Gelfand triple and the \tilde{V} -Galerkin approximation $\tilde{u} \in L^2(0, T_{end}; \tilde{V})$, $\partial_t \tilde{u} \in L^2(0, T_{end}; \tilde{V})$, solution of

$$(76) \quad (\partial_t \tilde{u}(t), \tilde{v}) + a_h(\tilde{u}(t), \tilde{v}) = (f, \tilde{v}) \quad \text{for all } \tilde{v} \in \tilde{V}.$$

Definition 9.3 (Elliptic reconstruction). *Denote by $\tilde{\Pi}$ the H -orthogonal projection onto \tilde{V} . For $\tilde{v} \in \tilde{V}$, define the elliptic reconstruction $\mathcal{R}_{\text{ell}}(\tilde{v}) \in V$ of \tilde{v} to be the unique solution of the variational problem*

$$(77) \quad a_h(\mathcal{R}_{\text{ell}}(\tilde{v}), v) = (A_h(\tilde{v}) - \tilde{\Pi}(f) + f, v) \quad \text{for all } v \in V,$$

where $A_h(\tilde{v}) \in \tilde{V}$ is the H -inner product Riesz representative of the functional $a_h(\tilde{v}, \cdot)$, i.e., $(A_h(\tilde{v}), \tilde{v}') = a_h(\tilde{v}, \tilde{v}')$ for all $\tilde{v}' \in \tilde{V}$. Note that $\mathcal{R}_{\text{ell}}(\tilde{v})$ is well-defined, due to the coercivity of a_h on V .

From the definition it is clear that \tilde{v} is the \tilde{V} -Galerkin approximation of the elliptic reconstruction $\mathcal{R}_{\text{ell}}(\tilde{v})$.

Let us assume that for each t we have a decomposition $\tilde{u}(t) =: \tilde{u}^c(t) + \tilde{u}^d(t)$ (not necessarily unique) where $\tilde{u}^c(t) \in V$, $\tilde{u}^d(t) \in \tilde{V}$ are the conforming and non-conforming parts of $\tilde{u}(t)$. We consider the following error quantities:

$$\begin{aligned} \rho(t) &:= u(t) - \mathcal{R}_{\text{ell}}(\tilde{u}(t)), & \varepsilon(t) &:= \mathcal{R}_{\text{ell}}(\tilde{u}(t)) - \tilde{u}(t), \\ e^c(t) &:= u(t) - \tilde{u}^c(t), & \varepsilon^c(t) &:= \mathcal{R}_{\text{ell}}(\tilde{u}(t)) - \tilde{u}^c(t). \end{aligned}$$

Theorem 9.4 (Abstract semi-discrete error estimate). *Let $C := (2\gamma_h^2 + 1)^{1/2}$, where γ_h denotes the continuity constant of a_h on V w.r.t. $\|\cdot\|$, then*

$$\begin{aligned} \|e\|_{L^2(0, T_{end}; \|\cdot\|)} &\leq \|e^c(0)\| + \sqrt{3} \|\partial_t \tilde{u}^d\|_{L^2(0, T_{end}; \|\cdot\|_{V, -1})} \\ &\quad + (C + 1) \cdot \|\varepsilon\|_{L^2(0, T_{end}; \|\cdot\|)} + C \cdot \|\tilde{u}^d\|_{L^2(0, T_{end}; \|\cdot\|)}. \end{aligned}$$

Note that $\varepsilon(t)$ denotes the approximation error of the coercive variational problem (77). Hence, this error contribution can be controlled by invoking any (localized) a posteriori error estimate for coercive variational problem as e.g. presented in Section 5.

It is straightforward to modify the estimate in Theorem 9.4 for semi-discrete solutions $\tilde{u}(t)$ to take the time discretization error into account:

Corollary 9.5. *Let $\tilde{u} \in L^2(0, T_{end}, \tilde{V})$, $\partial_t \tilde{u} \in L^2(0, T_{end}, \tilde{V})$ be an arbitrary discrete approximation of $u(t)$, not necessarily satisfying (76). Let $\mathcal{R}_T[\tilde{p}](t) \in \tilde{V}$ denote the \tilde{V} -Riesz representative w.r.t. the H -inner product of the time-stepping residual of $\tilde{u}(t)$, i.e.*

$$(\mathcal{R}_T[\tilde{u}](t), \tilde{v}) = (\partial_t \tilde{u}(t), \tilde{v}) + a_h(\tilde{u}(t), \tilde{v}) - (f, \tilde{q}) \quad \forall \tilde{v} \in \tilde{V}.$$

Then, with $C := (3\gamma_h^2 + 2)^{1/2}$, the following error estimate holds:

$$\begin{aligned} \|e\|_{L^2(0, T_{end}; \|\cdot\|_{V, -1})} &\leq \|e^c(0)\| + 2\|\partial_t \tilde{u}^d\|_{L^2(0, T_{end}; \|\cdot\|_{V, -1})} \\ &\quad + (C + 1) \cdot \|\varepsilon\|_{L^2(0, T_{end}; \|\cdot\|_{V, -1})} + C \cdot \|\tilde{u}^d\|_{L^2(0, T_{end}; \|\cdot\|_{V, -1})} \\ &\quad + 2C_{H, V}^b \cdot \|\mathcal{R}_T[\tilde{u}]\|_{L^2(0, T_{end}; H)}. \end{aligned}$$

9.2. Non-affine parameter dependence and non-linear problems. A key ingredient towards model order reduction for nonlinear problems is the empirical interpolation method (EIM) introduced in [BMNP04] and further developed in [DHO12], [CS10, MPPY15].

In the context of localized model order reduction empirical interpolation has been employed in, e.g., [CEGG14, PY15, OR17]. Based on the concept of empirical operator interpolation from [DHO12] localization strategies can be employed as follows. To present the main ideas, let us assume the simple situation that

$$V_h = \bigoplus_{m=1}^M V_h^m$$

and that we have a localized decomposition as follows

$$a_h(u_h(\boldsymbol{\mu}), v_h; \boldsymbol{\mu}) = \sum_{m=1}^M a_h^m(u_h^m(\boldsymbol{\mu}), v_h^m; \boldsymbol{\mu}),$$

with $a_h(u_h(\boldsymbol{\mu}), \cdot; \boldsymbol{\mu}) \in (V_h)'$. The strategy will then rely on an empirical operator interpolation of the local volume operators $a_h^m(u_h^m(\boldsymbol{\mu}), \cdot; \boldsymbol{\mu}) \in (V_h^m)'$ and will thus only involve localized computations in the construction of the interpolation operator. As an example, the interpolation of the local volume operator will be of the form

$$\mathcal{I}_L^m[a_h^m(u_h^m(\boldsymbol{\mu}), \cdot; \boldsymbol{\mu})] = \sum_{l=1}^L \mathcal{S}_l^m(a_h^m(u_h^m(\boldsymbol{\mu}), \cdot; \boldsymbol{\mu})) q_l^m$$

for a local collateral basis $\{q_l^m\}_{l=1}^L \subset (V_h^m)'$ and corresponding interpolation functionals $\{\mathcal{S}_l^m\}_{l=1}^L \subset \Sigma_h^{m''}$ from a suitable local dictionary $\Sigma_h^{m''} \subset (V_h^m)''$, the choice of which is crucial to ensure the accuracy as well as an online-efficient evaluation of the interpolant. Note that due to the isomorphism between V_h^m and its bi-dual, the local dictionary of interpolation functionals $\Sigma_h^{m''}$ can be identified with a dictionary of functions $\Sigma_h^m \subset V_h^m$, such that $\mathcal{S}_l^m(a_h^m(u_h^m(\boldsymbol{\mu}), \cdot; \boldsymbol{\mu})) = a_h^m(u_h^m(\boldsymbol{\mu}), \sigma_l^m; \boldsymbol{\mu})$, where $\sigma_l^m \in \Sigma_h^m$ corresponds to $\mathcal{S}_l^m \in \Sigma_h^{m''}$. An online-efficient evaluation of the interpolated operator $\mathcal{I}_L^m[a_h^m(u_h^m(\boldsymbol{\mu}), \cdot; \boldsymbol{\mu})]$ can be ensured by choosing the local dictionary Σ_h^m such that the computational complexity of the evaluation $a_h^m(u_h^m(\boldsymbol{\mu}), \sigma^m; \boldsymbol{\mu})$ for $\sigma^m \in \Sigma_h^m$ does not depend on the dimension of V_h^m . The choice of Σ_h^m thus depends on the underlying discretization: possible choices in the context of finite element schemes include the finite element basis of V_h^m . Other

choices of Σ_h^m are conceivable and could improve the interpolation quality, which is subject to further investigation.

REFERENCES

- [AB12] A. Abdulle and Y. Bai. Reduced basis finite element heterogeneous multiscale method for high-order discretizations of elliptic homogenization problems. *Journal of Computational Physics*, 231(21):7014 – 7036, 2012.
- [Abd05] A. Abdulle. On a priori error analysis of fully discrete heterogeneous multiscale FEM. *Multiscale Model. Simul.*, 4(2):447–459, 2005.
- [Abd15] P. Abdulle, A. and Henning. A reduced basis localized orthogonal decomposition. *J. Comput. Phys.*, 295:379–401, 2015.
- [AH02] J. Aarnes and T. Y. Hou. Multiscale domain decomposition methods for elliptic problems with high aspect ratios. *Acta Math. Appl. Sin. Engl. Ser.*, 18(1):63–76, 2002.
- [AHKO12] F. Albrecht, B. Haasdonk, S. Kaulmann, and M. Ohlberger. The localized reduced basis multiscale method. *Proceedings of Algoritmy 2012, Conference on Scientific Computing, Vysoke Tatry, Podbanske, September 9-14, 2012*, pages 393–403, 2012.
- [APQ16] P.F. Antonietti, P. Pacciarini, and A. Quarteroni. A discontinuous Galerkin reduced basis element method for elliptic problems. *ESAIM Math. Model. Numer. Anal.*, 50(2):337–360, 2016.
- [BBO04] I. Babuška, U. Banerjee, and J. Osborn. Generalized finite element methods — main ideas, results and perspective. *Int. J. Comput. Methods*, 1(1):67–103, 2004.
- [BC68] M. Bampton and R. Craig. Coupling of substructures for dynamic analyses. *AIAA Journal*, 6(7):1313–1319, 1968.
- [BCO94] I. Babuška, G. Caloz, and J. E. Osborn. Special finite element methods for a class of second order elliptic problems with rough coefficients. *SIAM J. Numer. Anal.*, 31(4):945–981, 1994.
- [BCOW17] P. Benner, A. Cohen, M. Ohlberger, and K. Willcox, editors. *Model reduction and approximation*, volume 15 of *Computational Science & Engineering*. Society for Industrial and Applied Mathematics (SIAM), Philadelphia, PA, 2017. Theory and algorithms.
- [BEOR14] A. Buhr, C. Engwer, M. Ohlberger, and S. Rave. A numerically stable a posteriori error estimator for reduced basis approximations of elliptic equations. In X. Oliver E. Onate and A. Huerta, editors, *Proceedings of the 11th World Congress on Computational Mechanics*, pages 4094–4102. CIMNE, Barcelona, 2014.
- [BEOR17] A. Buhr, C. Engwer, M. Ohlberger, and S. Rave. ArbiLoMod, a simulation technique designed for arbitrary local modifications. *SIAM J. Sci. Comput.*, 39(4):A1435–A1465, 2017.
- [BF91] F. Brezzi and M. Fortin. *Mixed and hybrid finite element methods*. Springer-Verlag New York, Inc., 1991.
- [BGW15] P. Benner, S. Gugercin, and K. Willcox. A survey of projection-based model reduction methods for parametric dynamical systems. *SIAM Rev.*, 57(4):483–531, 2015.
- [BHL14] I. Babuška, X. Huang, and R. Lipton. Machine computation using the exponentially convergent multiscale spectral generalized finite element method. *ESAIM Math. Model. Numer. Anal.*, 48(2):493–515, 2014.
- [BL11] I. Babuška and R. Lipton. Optimal local approximation spaces for generalized finite element methods with application to multiscale problems. *Multiscale Model. Simul.*, 9(1):373–406, 2011.
- [BM97] I. Babuška and J. M. Melenk. The partition of unity method. *Internat. J. Numer. Methods Engrg.*, 40(4):727–758, 1997.
- [BMNP04] M. Barrault, Y. Maday, N. C. Nguyen, and A. T. Patera. An ‘empirical interpolation’ method: application to efficient reduced-basis discretization of partial differential equations. *C. R. Math. Acad. Sci. Paris*, 339(9):667–672, 2004.
- [BMP94] C. Bernardi, Y. Maday, and A. T. Patera. A new nonconforming approach to domain decomposition: the mortar element method. In *Nonlinear partial differential equations and their applications. Collège de France Seminar, Vol. XI (Paris, 1989–1991)*, volume 299 of *Pitman Res. Notes Math. Ser.*, pages 13–51. Longman Sci. Tech., Harlow, 1994.

- [Bou92] F. Bourquin. Component mode synthesis and eigenvalues of second order operators: discretization and algorithm. *RAIRO Modél. Math. Anal. Numér.*, 26(3):385–423, 1992.
- [BS18] A. Buhr and K. Smetana. Randomized Local Model Order Reduction. *SIAM J. Sci. Comput.*, 40(4):A2120–A2151, 2018.
- [CA10] F. Chinesta and E. Ammar, A. and Cueto. Recent advances and new challenges in the use of the proper generalized decomposition for solving multidimensional models. *Arch. Comput. Methods Eng.*, 17(4):327–350, 2010.
- [Car15] K. Carlberg. Adaptive h -refinement for reduced-order models. *Internat. J. Numer. Methods Engrg.*, 102(5):1192–1210, 2015.
- [CEGG14] V. M. Calo, Y. Efendiev, J. Galvis, and M. Ghommem. Multiscale empirical interpolation for solving nonlinear PDEs. *J. Comput. Phys.*, 278:204–220, 2014.
- [CEGL16] V. M. Calo, Y. Efendiev, J. Galvis, and G. Li. Randomized oversampling for generalized multiscale finite element methods. *Multiscale Model. Simul.*, 14(1):482–501, 2016.
- [CEL14a] F. Casenave, A. Ern, and T. Lelièvre. Accurate and online-efficient evaluation of the a posteriori error bound in the reduced basis method. *ESAIM Math. Model. Numer. Anal.*, 48:207–229, 2014.
- [CEL14b] E. T. Chung, Y. Efendiev, and G. Li. An adaptive GMsFEM for high-contrast flow problems. *Journal of Computational Physics*, 273:54–76, Sep 2014.
- [CEL15] E. T. Chung, Y. Efendiev, and W. T. Leung. Residual-driven online generalized multiscale finite element methods. *J. Comput. Phys.*, 302:176–190, 2015.
- [CEL17a] E. T. Chung, Y. Efendiev, and W. T. Leung. An online generalized multiscale discontinuous Galerkin method (GMsDGM) for flows in heterogeneous media. *Commun. Comput. Phys.*, 21(2):401–422, 2017.
- [CEL17b] E. T. Chung, Y. Efendiev, and W. T. Leung. An online generalized multiscale discontinuous Galerkin method (GMsDGM) for flows in heterogeneous media. *Commun. Comput. Phys.*, 21(2):401–422, 2017.
- [CEL18a] E. T. Chung, Y. Efendiev, and W. T. Leung. An adaptive generalized multiscale discontinuous Galerkin method for high-contrast flow problems. *Multiscale Model. Simul.*, 16(3):1227–1257, 2018.
- [CEL18b] E. T. Chung, Y. Efendiev, and Wing T. Leung. An adaptive generalized multiscale discontinuous Galerkin method for high-contrast flow problems. *Multiscale Model. Simul.*, 16(3):1227–1257, 2018.
- [CHM11] Y. Chen, J. S. Hesthaven, and Y. Maday. A seamless reduced basis element method for 2D Maxwell’s problem: an introduction. In *Spectral and high order methods for partial differential equations*, volume 76 of *Lect. Notes Comput. Sci. Eng.*, pages 141–152. Springer, Heidelberg, 2011.
- [CKL14] Francisco Chinesta, Roland Keunings, and Adrien Leygue. *The proper generalized decomposition for advanced numerical simulations. A primer*. SpringerBriefs in Applied Sciences and Technology. Springer, Cham, 2014.
- [CLC11] F. Chinesta, P. Ladeveze, and E. Cueto. A short review on model order reduction based on proper generalized decomposition. *Arch. Comput. Methods Eng.*, 18(4):395–404, 2011.
- [CS10] S. Chaturantabut and D. C. Sorensen. Nonlinear model reduction via discrete empirical interpolation. *SIAM J. Sci. Comput.*, 32(5):2737–2764, 2010.
- [DHO12] M. Drohmann, B. Haasdonk, and M. Ohlberger. Reduced basis approximation for nonlinear parametrized evolution equations based on empirical operator interpolation. *SIAM J. Sci. Comput.*, 34(2):A937–A969, 2012.
- [DM16] P. Drineas and M. W. Mahoney. RandNLA: Randomized Numerical Linear Algebra. *Commun. ACM*, 59(6):80–90, 2016.
- [EE03] W. E and B. Engquist. The heterogeneous multiscale methods. *Commun. Math. Sci.*, 1(1):87–132, 2003.
- [EE05] W. E and B. Engquist. The heterogeneous multi-scale method for homogenization problems. In *Multiscale methods in science and engineering*, volume 44 of *Lect. Notes Comput. Sci. Eng.*, pages 89–110. Springer, Berlin, 2005.
- [EGH13] Y. Efendiev, J. Galvis, and T.Y. Hou. Generalized multiscale finite element methods (GMsFEM). *Journal of Computational Physics*, January 2013.

- [EH09] Y. Efendiev and T. Y. Hou. *Multiscale finite element methods*, volume 4 of *Surveys and Tutorials in the Applied Mathematical Sciences*. Springer, New York, 2009. Theory and applications.
- [EHG04] Y. Efendiev, T. Hou, and V. Ginting. Multiscale finite element methods for nonlinear problems and their applications. *Commun. Math. Sci.*, 2(4):553–589, 2004.
- [EP13] J. L. Eftang and A. T. Patera. Port reduction in parametrized component static condensation: approximation and a posteriori error estimation. *Internat. J. Numer. Methods Engrg.*, 96(5):269–302, 2013.
- [EP14] J.L. Eftang and A.T. Patera. A port-reduced static condensation reduced basis element method for large component-synthesized structures: approximation and *A posteriori* error estimation. *Advanced Modeling and Simulation in Engineering Sciences*, 1(3), 2014.
- [ESV10] A. Ern, A. F. Stephansen, and M. Vohralík. Guaranteed and robust discontinuous galerkin a posteriori error estimates for convection–diffusion–reaction problems. *J. Comput. Appl. Math.*, 234(1):114–130, 2010.
- [ESZ09] A. Ern, A. F. Stephansen, and P. Zunino. A discontinuous galerkin method with weighted averages for advection–diffusion equations with locally small and anisotropic diffusivity. *IMA J. Numer. Anal.*, 29(2):235–256, 2009.
- [FIL18] A. Ferrero, A. Iollo, and F. Larocca. Global and local POD models for the prediction of compressible flows with DG methods. *Internat. J. Numer. Methods Engrg.*, 116(5):332–357, 2018.
- [GE10] J. Galvis and Y. Efendiev. Domain decomposition preconditioners for multiscale flows in high-contrast media. *Multiscale Model. Simul.*, 8(4):1461–1483, 2010.
- [GL17] M. J. Gander and A. Loneland. SHEM: an optimal coarse space for RAS and its multiscale approximation. In *Domain decomposition methods in science and engineering XXIII*, volume 116 of *Lect. Notes Comput. Sci. Eng.*, pages 313–321. Springer, Cham, 2017.
- [GLS07] I. G. Graham, P. O. Lechner, and R. Scheichl. Domain decomposition for multiscale PDEs. *Numer. Math.*, 106(4):589–626, 2007.
- [GLV11] Emmanuil H. Georgoulis, Omar Lakkis, and Juha M. Virtanen. A posteriori error control for discontinuous Galerkin methods for parabolic problems. *SIAM J. Numer. Anal.*, 49(2):427–458, 2011.
- [HEML00] T.J.R. Hughes, G. Engel, L. Mazzei, and M.G. Larson. The continuous Galerkin method is locally conservative. *J. Comput. Phys.*, 163(2):467–488, 2000.
- [HFMQ98] T. J. R. Hughes, G. R. Feijóo, L. Mazzei, and J.-B. Quincy. The variational multiscale method - a paradigm for computational mechanics. *Comput. Methods Appl. Mech. Engrg.*, 166(1-2):3–24, 1998.
- [HK14] U. Hetmaniuk and A. Klawonn. Error estimates for a two-dimensional special finite element method based on component mode synthesis. *Electron. Trans. Numer. Anal.*, 41:109–132, 2014.
- [HKKR18] A. Heinlein, A. Klawonn, J. Knepper, and O. Rheinbach. Multiscale coarse spaces for overlapping Schwarz methods based on the ACMS space in 2D. *Electron. Trans. Numer. Anal.*, 48:156–182, 2018.
- [HKP13a] D. B. P. Huynh, D. J. Knezevic, and A. T. Patera. A Static Condensation Reduced Basis Element Method: Complex Problems. *Comput. Methods Appl. Mech. Engrg.*, 259:197–216, 2013.
- [HKP13b] D. B. P. Huynh, D. J. Knezevic, and A. T. Patera. A static condensation reduced basis element method: approximation and *a posteriori* error estimation. *ESAIM Math. Model. Numer. Anal.*, 47(1):213–251, 2013.
- [HL10] U. Hetmaniuk and R. B. Lehoucq. A special finite element method based on component mode synthesis. *ESAIM Math. Model. Numer. Anal.*, 44(3):401–420, 2010.
- [HLR18] C. Himpe, T. Leibner, and S. Rave. Hierarchical approximate proper orthogonal decomposition. *SIAM J. Sci. Comput.*, 40(5):A3267–A3292, 2018.
- [HMP14] P. Henning, A. Malqvist, and D. Peterseim. A localized orthogonal decomposition method for semi-linear elliptic problems. *ESAIM Math. Model. Numer. Anal.*, 48(5):1331–1349, 2014.

- [HMT11] N. Halko, P. Martinsson, and J. A. Tropp. Finding structure with randomness: Probabilistic algorithms for constructing approximate matrix decompositions. *SIAM Rev.*, 53(2):217–288, 2011.
- [HNC18] A. Huerta, E. Nadal, and F. Chinesta. Proper generalized decomposition solutions within a domain decomposition strategy. *Internat. J. Numer. Methods Engrg.*, 113(13):1972–1994, 2018.
- [HOS14] P. Henning, M. Ohlberger, and B. Schweizer. An adaptive multiscale finite element method. *Multiscale Model. Simul.*, 12(3):1078–1107, 2014.
- [HRS16] J. S. Hesthaven, G. Rozza, and B. Stamm. *Certified reduced basis methods for parametrized partial differential equations*. SpringerBriefs in Mathematics. Springer, Cham; BCAM Basque Center for Applied Mathematics, Bilbao, 2016. BCAM Springer-Briefs.
- [Hug95] T. J. R. Hughes. Multiscale phenomena: Green’s functions, the Dirichlet-to-Neumann formulation, subgrid scale models, bubbles and the origins of stabilized methods. *Comput. Methods Appl. Mech. Engrg.*, 127(1-4):387–401, 1995.
- [Hur65] W. C. Hurty. Dynamic analysis of structural systems using component modes. *AIAA journal*, 3(4):678–685, 1965.
- [HW97] T. Y. Hou and X. Wu. A multiscale finite element method for elliptic problems in composite materials and porous media. *J. Comput. Phys.*, 134(1):169–189, 1997.
- [IQR12] L. Iapichino, A. Quarteroni, and G. Rozza. A reduced basis hybrid method for the coupling of parametrized domains represented by fluidic networks. *Comput. Methods Appl. Mech. Engrg.*, 221/222:63–82, 2012.
- [IQR16] L. Iapichino, A. Quarteroni, and G. Rozza. Reduced basis method and domain decomposition for elliptic problems in networks and complex parametrized geometries. *Comput. Math. Appl.*, 71(1):408–430, 2016.
- [JBL11] H. Jakobsson, F. Bengzon, and M. G. Larson. Adaptive component mode synthesis in linear elasticity. *Internat. J. Numer. Methods Engrg.*, 86(7):829–844, 2011.
- [KFH⁺15] S. Kaulmann, B. Flemisch, B. Haasdonk, K.-A. Lie, and M. Ohlberger. The localized reduced basis multiscale method for two-phase flows in porous media. *Internat. J. Numer. Methods Engrg.*, 102(5):1018–1040, 2015.
- [KOH11] S. Kaulmann, M. Ohlberger, and B. Haasdonk. A new local reduced basis discontinuous Galerkin approach for heterogeneous multiscale problems. *C. R. Math. Acad. Sci. Paris*, 349(23-24):1233–1238, 2011.
- [Kol36] A. Kolmogoroff. Über die beste Annäherung von Funktionen einer gegebenen Funktionenklasse. *Ann. of Math. (2)*, 37(1):107–110, 1936.
- [KPY17] R. Kornhuber, J. Podlesny, and H. Yserentant. Direct and iterative methods for numerical homogenization. In *Domain decomposition methods in science and engineering XXIII*, volume 116 of *Lect. Notes Comput. Sci. Eng.*, pages 217–225. Springer, Cham, 2017.
- [KPY18] R. Kornhuber, D. Peterseim, and H. Yserentant. An analysis of a class of variational multiscale methods based on subspace decomposition. *Math. Comp.*, 87(314):2765–2774, 2018.
- [KRR16] A. Klawonn, P. Radtke, and O. Rheinbach. A comparison of adaptive coarse spaces for iterative substructuring in two dimensions. *Electron. Trans. Numer. Anal.*, 45:75–106, 2016.
- [KY16] R. Kornhuber and H. Yserentant. Numerical homogenization of elliptic multiscale problems by subspace decomposition. *Multiscale Model. Simul.*, 14(3):1017–1036, 2016.
- [LM05] M. G. Larson and A. Malqvist. Adaptive variational multiscale methods based on a posteriori error estimation: duality techniques for elliptic problems. In *Multiscale methods in science and engineering*, volume 44 of *Lect. Notes Comput. Sci. Eng.*, pages 181–193. Springer, Berlin, 2005.
- [LMR06] A. E. Løvgren, Y. Maday, and E. M. Rønquist. A reduced basis element method for the steady stokes problem. *ESAIM Math. Model. Numer. Anal.*, 40(3):529–552, 2006.
- [LSY98] R. B. Lehoucq, D. C. Sorensen, and C. Yang. *ARPACK users’ guide*, volume 6 of *Software, Environments, and Tools*. Society for Industrial and Applied Mathematics (SIAM), Philadelphia, PA, 1998. Solution of large-scale eigenvalue problems with implicitly restarted Arnoldi methods.

- [Mah11] M. W. Mahoney. Randomized algorithms for matrices and data. *Found. Trends Mach. Learn.*, 3(2):123–224, February 2011.
- [MD09] M. W. Mahoney and P. Drineas. CUR matrix decompositions for improved data analysis. *PNAS; Proceedings of the National Academy of Sciences*, 106(3):697–702, 2009.
- [MH14] I. Maier and B. Haasdonk. A Dirichlet–Neumann reduced basis method for homogeneous domain decomposition problems. *Appl. Numer. Math.*, 78:31–48, 2014.
- [MMPY15] Y. Maday, O. Mula, A. T. Patera, and M. Yano. The generalized empirical interpolation method: stability theory on Hilbert spaces with an application to the Stokes equation. *Comput. Methods Appl. Mech. Engrg.*, 287:310–334, 2015.
- [MP14] A. Malqvist and D. Peterseim. Localization of elliptic multiscale problems. *Math. Comp.*, 83(290):2583–2603, 2014.
- [MR02] Y. Maday and E. M. Rønquist. A reduced-basis element method. *Journal of scientific computing*, 17(1-4):447–459, 2002.
- [MR04] Y. Maday and E. M. Rønquist. The reduced basis element method: application to a thermal fin problem. *SIAM J. Sci. Comput.*, 26(1):240–258 (electronic), 2004.
- [MRH15] I. Martini, G. Rozza, and B. Haasdonk. Reduced basis approximation and a-posteriori error estimation for the coupled Stokes–Darcy system. *Adv. Comput. Math.*, 41(5):1131–1157, 2015.
- [MRS16] R. Milk, S. Rave, and F. Schindler. pyMOR—generic algorithms and interfaces for model order reduction. *SIAM J. Sci. Comput.*, 38(5):S194–S216, 2016.
- [MS07] J. Mandel and B. Sousedik. Adaptive selection of face coarse degrees of freedom in the BDDC and the FETI–DP iterative substructuring methods. *Comput. Methods Appl. Mech. Engrg.*, 196(8):1389–1399, 2007.
- [Ohl05] M. Ohlberger. A posteriori error estimates for the heterogeneous multiscale finite element method for elliptic homogenization problems. *Multiscale Model. Simul.*, 4(1):88–114, 2005.
- [OR17] M. Ohlberger and S. Rave. Localized reduced basis approximation of a nonlinear finite volume battery model with resolved electrode geometry. In *Model Reduction of Parametrized Systems*, volume 17 of *MS&A. Model. Simul. Appl.*, pages 201–212. Springer, 2017.
- [ORS17] M. Ohlberger, S. Rave, and F. Schindler. True error control for the localized reduced basis method for parabolic problems. In *Model reduction of parametrized systems*, volume 17 of *MS&A. Model. Simul. Appl.*, pages 169–182. Springer, Cham, 2017.
- [OS14a] M. Ohlberger and F. Schindler. A-posteriori error estimates for the localized reduced basis multi-scale method. In *Finite volumes for complex applications VII. Methods and theoretical aspects*, volume 77 of *Springer Proc. Math. Stat.*, pages 421–429. Springer, Cham, 2014.
- [OS14b] M. Ohlberger and K. Smetana. A dimensional reduction approach based on the application of reduced basis methods in the framework of hierarchical model reduction. *SIAM J. Sci. Comput.*, 36(2):A714–A736, 2014.
- [OS15] M. Ohlberger and F. Schindler. Error control for the localized reduced basis multiscale method with adaptive on-line enrichment. *SIAM J. Sci. Comput.*, 37(6):A2865–A2895, 2015.
- [OS17] M. Ohlberger and F. Schindler. Non-conforming localized model reduction with online enrichment: towards optimal complexity in PDE constrained optimization. In *Finite volumes for complex applications VIII—hyperbolic, elliptic and parabolic problems*, volume 200 of *Springer Proc. Math. Stat.*, pages 357–365. 2017.
- [OSS18] M. Ohlberger, M. Schaefer, and F. Schindler. *Localized Model Reduction in PDE Constrained Optimization*, pages 143–163. Springer International Publishing, Cham, 2018.
- [PEV10] S. Perotto, A. Ern, and A. Veneziani. Hierarchical local model reduction for elliptic problems: a domain decomposition approach. *Multiscale Model. Simul.*, 8(4):1102–1127, 2010.
- [PGQ16] P. Pacciarini, P. Gervasio, and A. Quarteroni. Spectral based discontinuous Galerkin reduced basis element method for parametrized Stokes problems. *Comput. Math. Appl.*, 72(8):1977–1987, 2016.
- [Pin85] A. Pinkus. *n-widths in approximation theory*, volume 7. Springer-Verlag, Berlin, 1985.

- [PY15] M. Presho and S. Ye. Reduced-order multiscale modeling of nonlinear p -Laplacian flows in high-contrast media. *Comput. Geosci.*, 19(4):921–932, 2015.
- [QN16] A. Quarteroni, A. Manzoni and F. Negri. *Reduced basis methods for partial differential equations*, volume 92 of *Unitext*. Springer, Cham, 2016. An introduction, La Matematica per il 3+2.
- [QV05] A. Quarteroni and A. Valli. *Domain decomposition methods for partial differential equations*. Numerical Mathematics and Scientific Computation. The Clarendon Press, Oxford University Press, New York, reprint, 2005.
- [Sch19] J. Schlei. Optimal local approximation spaces for parabolic problems. Master’s thesis, University of Mnster, 2019.
- [SDH⁺14] N. Spillane, V. Dolean, P. Hauret, F. Nataf, C. Pechstein, and R. Scheichl. Achieving robustness through coarse space enrichment in the two level Schwarz framework. In *Domain decomposition methods in science and engineering XXI*, volume 98 of *Lect. Notes Comput. Sci. Eng.*, pages 447–455. Springer, Cham, 2014.
- [SFDE15] A. Sommer, O. Farle, and R. Dyczij-Edlinger. A New Method for Accurate and Efficient Residual Computation in Adaptive Model-Order Reduction. *IEEE Transactions on Magnetics*, 51(3):1–4, 2015.
- [Sme15] K. Smetana. A new certification framework for the port reduced static condensation reduced basis element method. *Comput. Methods Appl. Mech. Engrg.*, 283:352–383, 2015.
- [Sme19] K. Smetana. Static condensation optimal port/interface reduction and error estimation for structural health monitoring. In B. Haasdonk J. Fehr, editor, *IUTAM Symposium on Model Order Reduction of Coupled Systems, Stuttgart, Germany, May 22-25, 2018: MORCOS 2018*, 2019.
- [SO17] K. Smetana and M. Ohlberger. Hierarchical model reduction of nonlinear partial differential equations based on the adaptive empirical projection method and reduced basis techniques. *ESAIM Math. Model. Numer. Anal.*, 51(2):641–677, 2017.
- [SP16] K. Smetana and A. T. Patera. Optimal local approximation spaces for component-based static condensation procedures. *SIAM J. Sci. Comput.*, 38(5):A3318–A3356, 2016.
- [SPE01] Society of Petroleum Engineers, SPE Comparative Solution Project, <http://www.spe.org/web/csp/index.html>, 2001.
- [SVV18] S. Stepanov, M. Vasilyeva, and V. I. Vasil’ev. Generalized multiscale discontinuous Galerkin method for solving the heat problem with phase change. *J. Comput. Appl. Math.*, 340:645–652, 2018.
- [Tad16] T. Taddei. *Model order reduction methods for data assimilation; state estimation and structural health monitoring*. PhD thesis, Massachusetts Institute of Technology, 2016.
- [TP18] T. Taddei and A. T. Patera. A localization strategy for data assimilation; application to state estimation and parameter estimation. *SIAM J. Sci. Comput.*, 40(2):B611–B636, 2018.
- [TW05] A. Toselli and O. Widlund. *Domain decomposition methods—algorithms and theory*, volume 34 of *Springer Series in Computational Mathematics*. Springer-Verlag, Berlin, 2005.
- [VB81] M. Vogelius and I. Babuka. On a dimensional reduction method. I. The optimal selection of basis functions. *Math. Comp.*, 37(155):31–46, 1981.
- [VPRP03] K. Veroy, C. Prud’homme, D. V. Rovas, and A. T. Patera. A posteriori error bounds for reduced-basis approximation of parametrized noncoercive and nonlinear elliptic partial differential equations. In *Proceedings of the 16th AIAA Computational Fluid Dynamics Conference*, volume 3847, 2003.
- [WFR19] S. Wu Fung and L. Ruthotto. A multiscale method for model order reduction in PDE parameter estimation. *J. Comput. Appl. Math.*, 350:19–34, 2019.
- [WV15] W. Wang and M. N. Vouvakis. Randomized computations in domain decomposition methods. In *2015 IEEE International Symposium on Antennas and Propagation USNC/URSI National Radio Science Meeting*, pages 177–178, July 2015.

MATHEMATICS MÜNSTER, EINSTEINSTR. 62, D-48149 MÜNSTER, GERMANY

DEPARTMENT OF MATHEMATICS AND COMPUTER SCIENCE, TU EINDHOVEN, EINDHOVEN, THE NETHERLANDS

MATHEMATICS MÜNSTER, EINSTEINSTR. 62, D-48149 MÜNSTER, GERMANY

MATHEMATICS MÜNSTER, EINSTEINSTR. 62, D-48149 MÜNSTER, GERMANY

MATHEMATICS MÜNSTER, EINSTEINSTR. 62, D-48149 MÜNSTER, GERMANY

UNIVERSITY OF TWENTE, FACULTY OF ELECTRICAL ENGINEERING, MATHEMATICS & COMPUTER SCIENCE, ZILVERLING, P.O. BOX 217, 7500 AE ENSCHEDE, THE NETHERLANDS